

AD-A265 853



WL-TR-93-2032

A NOVEL TEST METHOD FOR FUEL THERMAL STABILITY

Michael A. Serio
David S. Pines
Erik Kroo
Kim S. Knight
Peter R. Solomon

ADVANCED FUEL RESEARCH, INC.
87 Church Street
East Hartford, CT 06108

February 1993

Final Report for Period 13 April 1992 - 13 January 1993

Approved for public release; distribution is unlimited.

Aero Propulsion and Power Directorate
Wright Laboratory
Air Force Materiel Command
Wright-Patterson AFB, OH 45433-7650



DTIC
ELECTE
JUN 16 1993
S A D

93 6 15 18

397251

93-13490




84P8


NOTICE

When Government drawings, specifications, or other data are used for any purpose other than in connection with a definitely Government-related procurement, the United States Government incurs no responsibility or any obligation whatsoever. The fact that the Government may have formulated or in any way supplied the said drawings, specifications, or other data, is not to be regarded by implication, or otherwise in any manner construed, as licensing the holder, or any other person or corporation; or as conveying any rights or permission to manufacture, use, or sell any patented invention that may in any way be related thereto.


This report is releasable to the National Technical Information Service (NTIS). At NTIS, it will be available to the general public, including foreign nations.

This technical report has been reviewed and is approved for publication.


ELLEN STEWARD, Project Engineer
Fuels Branch
Fuels and Lubrication Division
Aero Propulsion and Power Directorate


CHARLES L. DELANEY, Chief
Fuels Branch
Fuels and Lubrication Division
Aero Propulsion and Power Directorate

FOR THE COMMANDER


LEO S. HAROOTYAN, JR.
Chief, Fuels & Lubrication Division
Aero Propulsion & Power Directorate

If your address has changed, if you wish to be removed from our mailing list, or if the addressee is no longer employed by your organization, please notify WL/POSE, WPAFB OH 45433-7103 to help us maintain a current mailing list.

Copies of this report should not be returned unless return is required by security considerations, contractual obligations, or notice on a specific document.

REPORT DOCUMENTATION PAGE			Form Approved OMB No. 0704-0188	
Public reporting burden for this collection of information is estimated to average 1 hour per response, including the time for reviewing instructions, searching existing data sources, gathering and maintaining the data needed, and completing and reviewing the collection of information. Send comments regarding this burden estimate or any other aspect of this collection of information, including suggestions for reducing this burden, to Washington Headquarters Services, Directorate for Information Operations and Reports, 1215 Jefferson Davis Highway, Suite 1204, Arlington, VA 22202-4302, and to the Office of Management and Budget, Paperwork Reduction Project (0704-0188), Washington, DC 20503.				
1. AGENCY USE ONLY (Leave blank)	2. REPORT DATE February 1993	3. REPORT TYPE AND DATES COVERED Final Report 13 April 1992 - 13 January 1993		
4. TITLE AND SUBTITLE A Novel Test Method for Fuel Thermal Stability		5. FUNDING NUMBERS C - F33615-92-C-2213 PE - 6502F PR - 3005 TA - 02 WU - OU		
6. AUTHOR(S) M.A. Serio, D.S. Pines, E. Kroo, K. Knight, P.R. Solomon, R. Malhotra*, M. Coglia*, S. Smedley*, S. Young*, M. Williams* * SRI International, Menlo Park, CA 94025				
7. PERFORMING ORGANIZATION NAME(S) AND ADDRESS(ES) Advanced Fuel Research, Inc. 87 Church Street East Hartford, CT 06108		8. PERFORMING ORGANIZATION REPORT NUMBER 526021		
9. SPONSORING/MONITORING AGENCY NAME(S) AND ADDRESS(ES) Aero Propulsion and Power Directorate Wright Laboratory Air Force Materiel Command Wright Patterson AFB, OH 45433-7650		10. SPONSORING/MONITORING AGENCY REPORT NUMBER WL-TR-93-2032		
11. SUPPLEMENTARY NOTES				
12a. DISTRIBUTION/AVAILABILITY STATEMENT Approved for public release; distribution is unlimited.		12b. DISTRIBUTION CODE		
13. ABSTRACT (Maximum 200 words) The object of this work was to demonstrate that an FT-IR fiber optic probe and a quartz crystal microbalance (QCM) probe could be used to measure deposit formation from thermal stressing of jet fuels in a high-temperature, high pressure flow system. These probes were designed, constructed and tested in an existing Fuel Stability Test System (FSTS) which had an FT-IR Attenuated Total Reflectance (ATR) circle cell monitoring the stressed fuel after cooling to ambient temperature. A Shell Jet A and a Sun Jet A-1 fuel were tested. It was demonstrated that both the FT-IR fiber optic probe and the QCM probe could successfully differentiate between a "stable" and an "unstable" fuel. The results from the QCM probe tests indicate that the drop in frequency for this particular probe results from viscosity dampening and not the mass of the film. The changes in the bulk fuel composition from thermal stressing were measured with the ATR circle cell, and were found to be significantly different from the changes in the deposit layer composition measured by the fiber-optic probe. The potential applications include an instrument for development and evaluation of thermally stable fuels or supercritical fuels, and development of on-board fuel stability monitors.				
14. SUBJECT TERMS Thermal Stability, Aviation Fuels, Stability Tests, FT-IR Diagnostics, Fiber Optics, Quartz Crystal Microbalance		15. NUMBER OF PAGES 83		16. PRICE CODE
17. SECURITY CLASSIFICATION OF REPORT Unclassified	18. SECURITY CLASSIFICATION OF THIS PAGE Unclassified	19. SECURITY CLASSIFICATION OF ABSTRACT Unclassified	20. LIMITATION OF ABSTRACT UL	

Table of Contents

LIST OF FIGURES iii

LIST OF TABLES vi

ACKNOWLEDGEMENTS vii

1. EXECUTIVE SUMMARY 1

 1.1. The Problem 1

 1.2. The Innovations 1

 1.3. Phase I Accomplishments 1

 1.4. Phase II Proposal 2

 1.5. Expected Results 3

2. IDENTIFICATION OF THE PROBLEM AND OPPORTUNITY 4

 2.1. The Problem 4

 2.2. The Innovations and Opportunity for Solution 4

3. PHASE I OBJECTIVES 5

4. PHASE I RESULTS 6

 4.1. Task 1 - Design and Construction of On-Line FT-IR Deposit Monitors 6

 4.2. Task 2 - Design and Construction of a QCM Deposit Probe 12

 4.3. Task 3 - Integration and Testing of On-Line Diagnostics 18

 4.4. Task 4 - Demonstration of the Advanced FSTS Over a Range
 of Fuel Stressing Conditions 38

5. CONCLUSIONS 63

 5.1. Technical Feasibility 63

 5.2. Technical, Economic and Social Benefits 63

 5.3. Estimated Cost of Approach Relative to Benefits 63

6. REFERENCES 64

APPENDIX A - Description of QCM Device 67

APPENDIX B - Raw Data from Attenuated Total Reflectance (ATR) Circle Cell 71

DTIC QUALITY INSPECTED &

By	
Distribution/	
Availability Codes	
Dist	Avail and/or Special
A-1	

<u>Figure</u>	<u>List of Figures</u>	<u>Page</u>
4.1-1.	The Schematic of the Fiber Optic Probe Designed for the Jet Fuel Thermal Stability Studies	7
4.1-2.	a) Internal Reflection of Radiation Transmitted from Air into a Cladded Fiber. b) Ray-Focussing of a Paraboloidal Reflector	7
4.1-3.	Schematic of FT-IR Deposit Monitor System with Multiple Path Optical Bench	11
4.1-4.	Detail of Fiber Optic Coupler	13
4.2-1.	Quartz Crystal Oscillator with Probe Attached	16
4.2-2.	Quartz Crystal Mass Detector and Reactor Vessel	17
4.2-3.	Typical Time-Temperature Plot for SRI QCM Test Cell	19
4.2-4.	Change in Frequency with Time for a Blank (air) Run and a Run with Shell Fuel Heated to 400 °C	19
4.2-5.	Ratio of Frequency Changes for Blank (air) and Shell Fuel Runs using Data from Fig. 4.2-4	20
4.2-6.	Ratio of Frequency Changes with Time for Repeat Blank (air) and Shell Fuel Runs . . .	20
4.3-1.	Schematic of First Generation Fuel Stability Test System (FSTS)	21
4.3-2.	Modified Reactor for Jet-Fuel Thermal Stress Measurements	23
4.3-3.	Temperature Profile for a) Wall and b) Jet Fuel for Experiments done at Different Control Temperatures	24
4.3-4.	a) Absorption Coefficient of Sapphire at Different Temperatures. b) Infrared Transmission of Sapphire at Different Temperatures	29
4.3-5.	Infrared F-O/ATR Spectra in Air at Different Temperatures, using 15° Sapphire Sensor	29
4.3-6.	Spectra for Various Optical Configurations (In air)	29
4.3-7.	Infrared Spectra from F-O/ATR Spectroscopy Compared with Aldrich Library Spectra. a) Benzene; b) Toluene	31
4.3-8.	Infrared Spectra from F-O/ATR Spectroscopy Compared with Aldrich Library Spectra. a) o-Cresol; b) Benzylmethylamine	32
4.3-9.	a) Tetralin Infrared Spectra from F-O/ATR Spectroscopy Compared with Aldrich Library Spectra; b) Absorption Bands from Harmonic Overtones of Benzene and Toluene	33

4.3-10.	The Transmission Spectra of o-Cresol from F-O/ATR Spectroscopy in a Non-Isothermal Experiment	34
4.3-11.	The Absorbance Spectra of Tetralin from F-O/ATR Spectroscopy in a Non-Isothermal Experiment	34
4.3-12.	Outline Drawing of the QCM Flow Cell Mounting Configuration	36
4.3-13.	QCM Frequency Data from an Overnight Test Run at Ambient Temperatures	37
4.3-14.	Data from a Test Run with Heated Air Flowing Over the QCM Probe	37
4.4-1.	Shell Fuel Sapphire FT-IR/ATR Absorption Spectra After Thermal Stressing to Various Temperatures	40
4.4-2.	Sun Fuel Sapphire FT-IR/ATR Absorption Spectra After Thermal Stressing to Various Temperatures	40
4.4-3.	Shell Fuel Sapphire FT-IR/ATR Absorption Spectra for Aliphatic Region After Thermal Stressing to Various Temperatures	41
4.4-4.	Sun Fuel Sapphire FT-IR/ATR Absorption Spectra for Aliphatic Region After Thermal Stressing to Various Temperatures	41
4.4-5.	Curve Resolving of the Shell Fuels CH, CH ₂ and CH ₃ Peaks	42
4.4-6.	Sapphire FT-IR/ATR Absorbance Data for Two Fuels Stressed to Various Temperatures. a) CH; b) CH ₂ ; c) CH ₃	43
4.4-7.	Percent Change in CH ₂ /CH ₃ Absorbance Ratios for Shell and Sun Fuels Stressed to Various Temperatures	45
4.4-8.	Comparison of Sapphire FT-IR/ATR Absorbance Spectra in Air after Exposing Fiber to Shell Fuel Stressed at Temperatures up to 500 °C	46
4.4-9.	Comparison of Sapphire FT-IR/ATR Absorbance Spectra in Air after Exposing Fiber to Sun Fuel Stressed at Temperatures up to 500 °C	46
4.4-10.	Absorption Spectra (at temperature) from Sapphire FT-IR/ATR Spectroscopy of Shell Fuel Stressed to Various Temperatures	48
4.4-11.	Absorption Spectra (at temperature) from Sapphire FT-IR/ATR Spectroscopy of Sun Fuel Stressed to Various Temperatures	48
4.4-12.	Comparison of Percent Change in CH ₂ /CH ₃ Ratio from Absorbance Spectra (at temperature) from Sapphire FT-IR/ATR Spectroscopy of Shell and Sun Fuels	49
4.4-13.	Comparison of Changes in Aromatic/Aliphatic Ratio from Absorbance Spectra (at Temperature) from Sapphire FT-IR/ATR Spectroscopy of Shell and Sun Fuels	49
4.4-14.	FT-IR/ATR Absorption Spectra from Circle Cell for Unstressed Fuels	50

4.4-15.	FT-IR/ATR Absorption Spectra from Circle Cell for Fuels Stressed at 500 °C	51
4.4-16.	FT-IR/ATR Absorption Data for CH ₂ /CH ₃ Ratio Data from Circle Cell for Shell and Sun Fuels Stressed to Various Temperatures	53
4.4-17.	FT-IR/ATR Absorption Data from Circle Cell Subtraction Spectra for Height of R ₂ C=CH ₂ Absorbance (890 cm ⁻¹) for Stable (Sun) and Unstable (Shell) Fuels	54
4.4-18.	FT-IR/ATR Absorption Data from Circle Cell Subtraction Spectra for Height of RCH=CH ₂ Absorbance (910 cm ⁻¹) for Stable (Sun) and Unstable (Shell) Fuels	54
4.4-19.	FT-IR/ATR Absorption Data for Height of Aromatic C-H (690 cm ⁻¹) Absorbance from Circle Cell Subtraction Spectra for Stable (Sun) and Unstable (Shell) Fuels Stressed to Various Temperatures	55
4.4-20.	FT-IR/ATR Absorption Data for Height of OH (3300 cm ⁻¹) Absorbance from Circle Cell Subtraction Spectra for Stable (Sun) and Unstable (Shell) Fuels Stressed to Various Temperatures	55
4.4-21.	FT-IR/ATR Absorption Data for Slope of Baseline at 5000 cm ⁻¹ Absorbance from Circle Cell Subtraction Spectra for Stable (Sun) and Unstable (Shell) Fuels Stressed to Various Temperatures	56
4.4-22.	QCM Data from a Run with Deaerated Shell Jet-A Fuel	57
4.4-23.	QCM Data from a Run with Aerated Shell Jet-A Fuel	57
4.4-24.	At Room Temperature, Resonant Frequency of the QCM does not Change with or Without the Deposit	59
4.4-25.	QCM Data from a Run with Aerated Sun Jet A-1 Fuel	60
4.4-26.	Reduction in Resonant Frequencies of the QCM Probe Resulting from Contact with Heated Shell Jet-A Fuel	60
4.4-27.	Reduction in Resonant Frequencies of the QCM Probe Resulting from Contact with Heated Sun Jet A-1 Fuel	61
A-1.	Schematic of QCM Detector Drive Circuit	69
B-1.	Raw FT-IR/ATR Absorbance Spectra from Circle Cell for Shell Fuel Stressed to Various Temperatures	72
B-2.	Raw FT-IR/ATR Absorbance Spectra from Circle Cell for Sun Fuel Stressed to Various Temperatures	73
B-3.	FT-IR/ATR Subtraction Spectra from Circle Cell for Shell Fuel Stressed to Various Temperatures	74
B-4.	FT-IR/ATR Subtraction Spectra from Circle Cell for Sun Fuel Stressed to Various Temperatures	75

<u>Table</u>	<u>List of Tables</u>	<u>Page</u>
4.1-1	Characteristics of IR Fiber Materials	9
4.2-1	Variation of Drive Voltage and Resonant Frequency with Medium, Temperature, and Time	15
4.3-1	Typical Properties of Sapphire	26
4.3-2	Important IR Bands in Sapphire Fiber Optics	28

ACKNOWLEDGEMENTS

The authors gratefully acknowledge the support of this work by the U.S. Air Force under Contract No. F33615-92-C-2231. The authors also wish to thank the Project Officer, Ellen Steward, for her help and support. Dr. Anthony Bonanno, of Advanced Fuel Research, Inc., assisted with the interpretation of the FT-IR spectra. The authors also wish to acknowledge helpful discussions with Prof. Eric Suuberg of Brown University. The preparation of the manuscript and figures was ably performed by Lisa A. Zapasnik and Lori Bellone.

1. EXECUTIVE SUMMARY

1.1. The Problem

The fuel is utilized as a primary heat sink on most aircraft. Consequently, the development of advanced high speed aircraft will require fuels which have very high thermal stability. The thermal stability of fuels has been a topic of many studies (1-48). While empirical evidence has been obtained about the effects of various contaminants and environmental parameters on fuel performance for a given fuel, relatively little is known about the mechanisms involved.

In the practical applications of fuels in advanced aircraft, the most important consideration is to know under what circumstances the fuel will degrade to the extent that a deposit is formed. A lot of effort has been devoted to the development of additives to enhance fuel stability. However, the testing of these additives and the formulation of thermally stable fuels have been hindered by the lack of a reliable instrument and test method to evaluate these fuels.

1.2. The Innovations

The first innovation is the application of Fourier-Transform Infrared (FT-IR) spectroscopy to the characterization of aviation fuel thermal stability. The mid-IR wavelengths (1-20 μm) contain a wealth of information about chemical bonds. Improvements in FT-IR design have led to spectrometers that are rugged, relatively inexpensive for the number of measurements performed, (<\$30,000), and sensitive. The use of FT-IR spectroscopy for monitoring and control of industrial process streams has become a realistic option for the first time. Advanced Fuel Research, Inc. (AFR) has been a pioneer in the application of FT-IR spectroscopy as an in situ diagnostic tool for hydrocarbon systems (49-60).

The second innovation is the use of Fiber-Optic (F-O) Attenuated Total Reflectance (ATR) spectroscopy. The use of fiber optics has provided the possibility of transmitting the IR light through a process stream under hostile operating conditions (high temperature, high pressure). ATR spectroscopy provides the possibility of analyses of highly absorbing materials, such as liquid hydrocarbon streams or surface deposit layers, by providing a reproducible, short path length. ATR spectroscopy is based on the fact that a light beam reflecting at a surface with a high refractive index actually penetrates a short distance into an adjoining medium with a low refractive index. A fiber optic with its cladding removed can serve as the IRE under the right circumstances.

The third innovation is the use of a quartz crystal microbalance (QCM) detector which has the potential to provide real-time data on fuel deposit formation. The detector is based on a piezoelectric device that was first designed and built by Robinson and Smedley (61) and is known as the Smedley Viscometer. While other QCM devices have been tested (31-33), this is the first system where the sensitive quartz piezoelectric crystals are remote from the fluid. This provides the opportunity to make tests at elevated temperatures and to test the effect of probe surface composition.

1.3 Phase I Accomplishments

The Phase I program demonstrated the feasibility of using an in situ FT-IR fiber optic probe and a quartz crystal microbalance (QCM) to monitor the growth of deposits and their composition in a high-temperature, high pressure flow system. The specific accomplishments of this program can be summarized as follows:

- Designed, constructed, and tested an on-line high-temperature FT-IR probe for monitoring the amount and composition of surface deposits.
- Designed, constructed, and tested a high-temperature quartz crystal microbalance (QCM) probe for the formation and growth of a surface deposit.
- Designed, constructed, and tested a multiple path FT-IR optical bench that could sequentially monitor the fiber optic probe, an ATR circle cell, and a transmission cell.
- Modified an existing fuel stability test system to incorporate the FT-IR fiber-optic probe and the QCM probe.
- Demonstrated that both the FT-IR fiber optic probe and the QCM probe could successfully differentiate between a "stable" and an "unstable" fuel. The results from the QCM probe tests indicate that the drop in frequency for this particular probe results from viscosity dampening and not the mass of the film.
- Measured the composition of the initial deposit and its changing composition with increased thermal stressing by the FT-IR fiber optic probe. Confirmed previous work which indicated that the initial deposits are highly aliphatic.
- Measured the changes in the bulk fuel composition from thermal stressing with the ATR circle cell, which were found to be significantly different from the changes in the deposit layer composition measured by the fiber-optic probe.

1.4 Phase II Proposal

The overall objective of the combined Phase I and Phase II programs is to develop a prototype instrument that uses FT-IR/F-O/ATR spectroscopy, a quartz crystal microbalance, and other advanced diagnostics to measure the growth and composition of jet fuel surface deposits. The Phase I program demonstrated the proof-of-concept. In Phase II, the measurement techniques will be refined and a prototype system will be constructed and delivered to the Air Force which is suitable for research or quality assurance applications. The work in the Phase II program will be divided into 8 tasks:

Task 1 - Design and Construct Improved FT-IR Fiber-Optic Probe - The design of the probe will be improved to allow a higher throughput of IR light, a more uniform temperature in the deposit region and a greater ease in removal and cleaning.

Task 2 - Test and Calibrate Improved FT-IR Fiber Optic Probe - A series of calibration experiments will be done with a standard set of jet fuels to calibrate the FT-IR probe and software will be developed to allow reliable real-time recognition of deposit formation and composition.

Task 3 - Design and Construct Improved QCM Probe - The QCM probe design and electronics will be improved to allow more stable operation and greater sensitivity for deposit detection.

Task 4 - Test and Calibrate Improved QCM Probe - The QCM probe will be tested and calibrated using the same set of jet fuels and software will be developed to allow reliable real-time measurement of deposit formation rates.

Task 5 - Evaluation of Other Diagnostics - An assessment will be made of other diagnostics (Near-IR, Raman, etc.) which could be incorporated into the Advanced Fuel Stability Test System (FSTS).

Task 6 - Design and Construct Prototype Test System - An advanced FSTS will be designed and built which incorporates an FT-IR fiber optic probe, a QCM detector and other advanced diagnostics as determined in Task 5. This will include the software required for the user interface to allow the system to be operated by nontechnical personal.

Task 7 - Testing of Prototype for Advanced FSTS - The complete system would be tested on a standard set of fuels for which thermal stability measurements have been made on similar scale (e.g., JFTOT) and larger scale test systems.

Task 8 - System Assessment/Applications Development - Complete assessment of capabilities of system for evaluation of aviation fuel thermal stability. Document system capabilities and operation in a user's manual. Make assessment of system capabilities for other applications such as : 1) evaluation of supercritical aviation fuels; 2) evaluation of gasolines; 3) development of on-board fuel monitors. Deliver prototype for the advanced FSTS to the Air Force.

1.5. Expected Results

If carried through Phases II and III, this program will result in an instrument package, including software, for monitoring of jet fuel thermal stability. The program is designed to produce an instrument that will have direct application to process development activities for thermally stable fuels and supercritical fuels for hypersonic aircraft. However, the same instrument would have applications in a much wider market such as the production of gasoline which does not clog fuel injectors and the assessment of heat exchanger fouling in the petrochemical industry. The technology developed under this program could also lead to the development of on-line monitors of fuel stability which can be installed on board an aircraft.

2. IDENTIFICATION OF THE PROBLEM AND OPPORTUNITY

2.1. The Problem

The fuel is utilized as a primary heat sink on most aircraft. Consequently, the development of advanced high speed aircraft using hydrocarbon fuels will require fuels which have very high thermal stability. In addition, the expected transition to fuels from new sources will require a more fundamental understanding of thermal stability, so that fuel specifications can be determined and fuel performance predicted. The thermal stability of fuels has been a topic of study for many years (1-48). Several techniques, e.g., adjustment of fuel physical and chemical properties, exclusion of oxygen, addition of chelating agents, etc., have been considered to enhance fuel stability. While empirical evidence has been obtained about the effects of various contaminants and environmental parameters on fuel performance for a given fuel, relatively little is known about the mechanisms involved.

In the practical applications of fuels in advanced aircraft, the most important consideration is to know under what circumstances the fuel will degrade to the extent that a deposit is formed. A lot of effort has been devoted to the development of additives to enhance fuel stability. However, the testing of these additives and the formulation of thermally stable fuels have been hindered by the lack of a reliable instrument and test method to evaluate these fuels.

2.2. The Innovations and Opportunity for Solution

This program involved three innovations that were used to investigate the potential for a fuel thermal stability test system based on advanced diagnostics. The first innovation is the application of Fourier-Transform Infrared (FT-IR) diagnostics to the characterization of aviation fuel thermal stability. The mid-IR wavelengths (1-20 μm) contain a wealth of information about chemical bonds for these fuels. Improvements in FT-IR design have led to spectrometers that are rugged, relatively inexpensive for the number of measurements performed, (<\$30,000), and sensitive. The use of FT-IR spectroscopy for monitoring and control of industrial process streams has become a realistic option for the first time. Advanced Fuel Research, Inc. (AFR) has been a pioneer in the application of FT-IR spectroscopy as an in-situ diagnostic tool for hydrocarbon systems (49-60).

The second innovation is the use of Fiber-Optic (F-O) Attenuated Total Reflectance (ATR) spectroscopy. The use of fiber optics has provided the possibility of transmitting the IR light through a process stream under hostile operating conditions (high temperature, high pressure). ATR spectroscopy provides the possibility of analyses of highly absorbing materials, such as liquid hydrocarbon streams, by providing a reproducible, short path length. ATR spectroscopy is based on the fact that a light beam reflecting at a surface with a high refractive index actually penetrates a short distance into an adjoining medium with a low refractive index. The use of suitable high refractive index crystals (internal reflection elements or IRE) will allow an IR beam inside the IRE to be used to analyze the composition of a liquid or a deposit layer adjoining its surface. A fiber optic with its cladding removed can serve as the IRE under the right circumstances.

The third innovation is the use of a quartz crystal microbalance (QCM) detector which has the potential to provide real time data on fuel deposit formation. The detector is based on a piezoelectric device that was first designed and built by Robinson and Smedley (61) and is known as the Smedley Viscometer. While other QCM devices have been tested (31-33), this is the first system where the sensitive quartz piezoelectric crystals are remote from the fluid. This provides the opportunity to make tests at elevated temperatures and to test the effect of probe surface composition.

3. PHASE I OBJECTIVES

The overall objective of Phase I was to demonstrate that the FT-IR fiber-optic ATR and the QCM probe can make measurements at high temperature and high pressure conditions in a flow system which directly monitor the growth of the deposits from thermal stressing of jet fuels and provide information on their composition. This was accomplished in four tasks with the following specific objectives.

Task 1 - Design and construction of an on-line FT-IR monitor based on a fiber-optic ATR probe for making composition and mass measurements.

Task 2 - Design and construction of a quartz crystal microbalance (QCM) for doing on-line monitoring of deposit formation and growth.

Task 3 - Installation and testing of the on-line diagnostics developed in Tasks 1 and 2 on a previously developed Fuel Stability Test System (FSTS).

Task 4 - Demonstration of the ability of the improved FSTS to monitor surface deposits formed from jet fuel by doing experiments over a wide range of stressing conditions.

4. PHASE I RESULTS

4.1 Task 1 - Design and Construction of On-Line FT-IR Deposit Monitors

Objective

Design and construction of an on-line FT-IR monitor based on an ATR fiber-optic probe for making composition and mass measurements.

Methodology

A fiber optic probe to monitor the thermal stability of jet fuel was constructed by selecting a combination of fiber materials that have low transmission loss and can withstand the high temperature and pressure conditions. System interfaces were successfully designed that transmit infrared radiation into the reactor and allow the ATR results to be collected and analyzed with a personal computer.

Optical fibers that have been used for transmitting infrared rays were surveyed. The fibers considered for use in the jet fuel thermal stability system should have a low transmission loss and meet the temperature requirements. Since experiments are performed at high liquid temperatures, the sensor fiber and the spectrometer (the infrared beam source) must be separated to avoid thermal damage to the spectrometer and detector. A transmitting fiber is, therefore, required to bring the infrared light into and out of the sensor fiber. In this case, the requirement for the sensor fiber would be thermal resistance, and that for the transmitting fiber would be low transmission loss. The sensing and transmitting fibers can be of different materials with suitable coupling.

In the actual system, several interface problems are encountered. In order to allow the infrared radiation to be totally transmitted through the fibers, it must be reflected at a certain range of angles in the fibers. This requires a technique to focus the collimated infrared rays from the spectrometer onto a fiber end at certain angles. For the interface between the transmitting and sensing fibers, a specially designed coupler was obtained from Foster-Miller, Inc., (Waltham MA).

Results

Probe Design - To minimize the fabrication cost of the fiber optic probe, the materials were standard size commercial stainless steel tubing and Swagelok fittings. Figure 4.1-1 is a schematic of the probe design. Since the sapphire fibers used were between 12 and 15 inches long, the length of the reactor was made to be 9½ inches which allowed enough infrared absorbance to occur, and also enabled the sapphire fiber to be coupled to the zirconium fluoride transmitting fiber without causing the latter fiber to be too close to the hot zone. The reactor material was 316 stainless steel tubing of 1/4 inch O.D. x 0.035 inch wall thickness. A quartz sleeve with a 0.118 inch internal diameter was inserted into the tube. The quartz insert provided an inert surface which would not affect the results of the thermal stability test. Attached to the stainless steel tube were 1/4 inch x 1/16 inch reducing unions. The reducing unions were modified by drilling a 1/16 inch port through the Swagelok hex body. The jet fuel entered and exited through these ports. The 0.25 mm fiber optic sensor was sealed into the reactor using an Altech 100/0.3-VG1 (15% graphite/85% Vespel) reducing ferrule.

The reactor tube was heated directly using an AC power supply. Three thermocouples were used to monitor the tube's outside wall temperature with the control thermocouple located 5 1/2 inches from the fuel inlet.

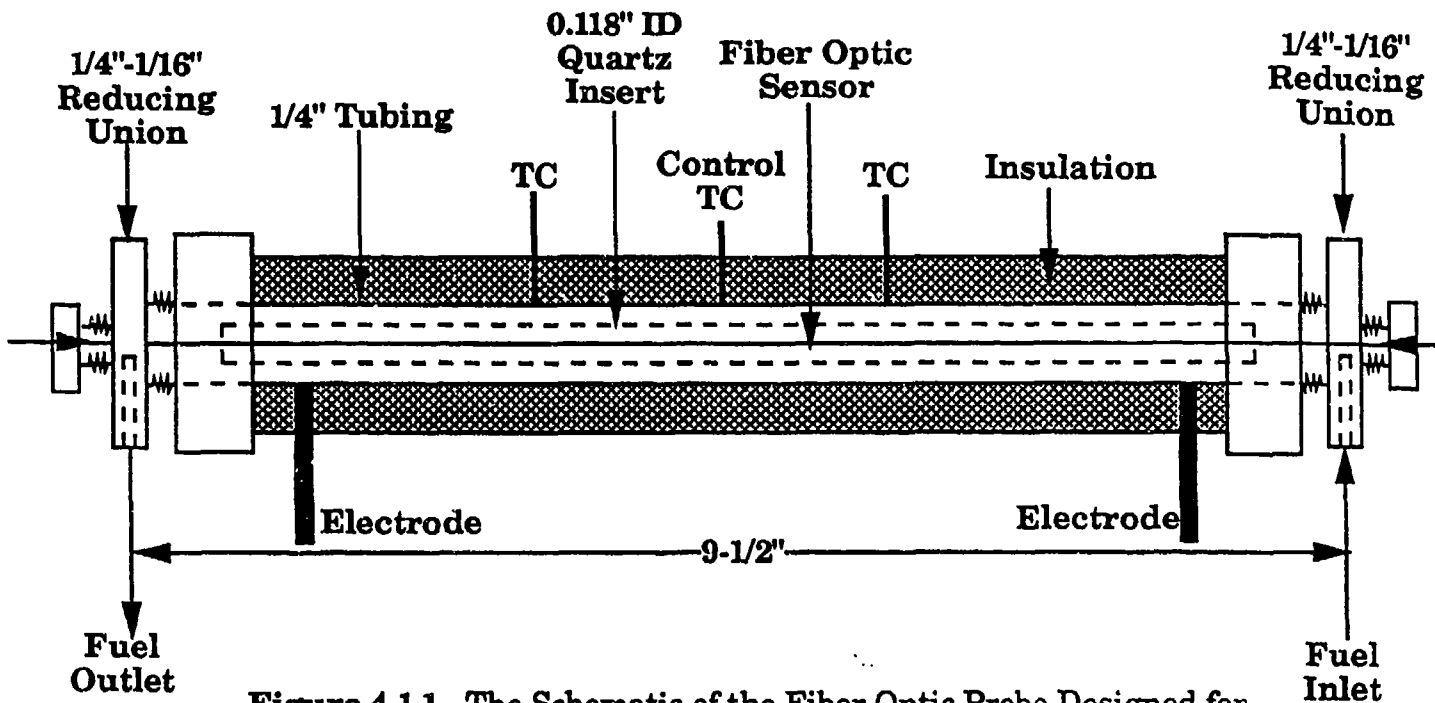


Figure 4.1-1. The Schematic of the Fiber Optic Probe Designed for the Jet Fuel Thermal Stability Studies (not to scale).

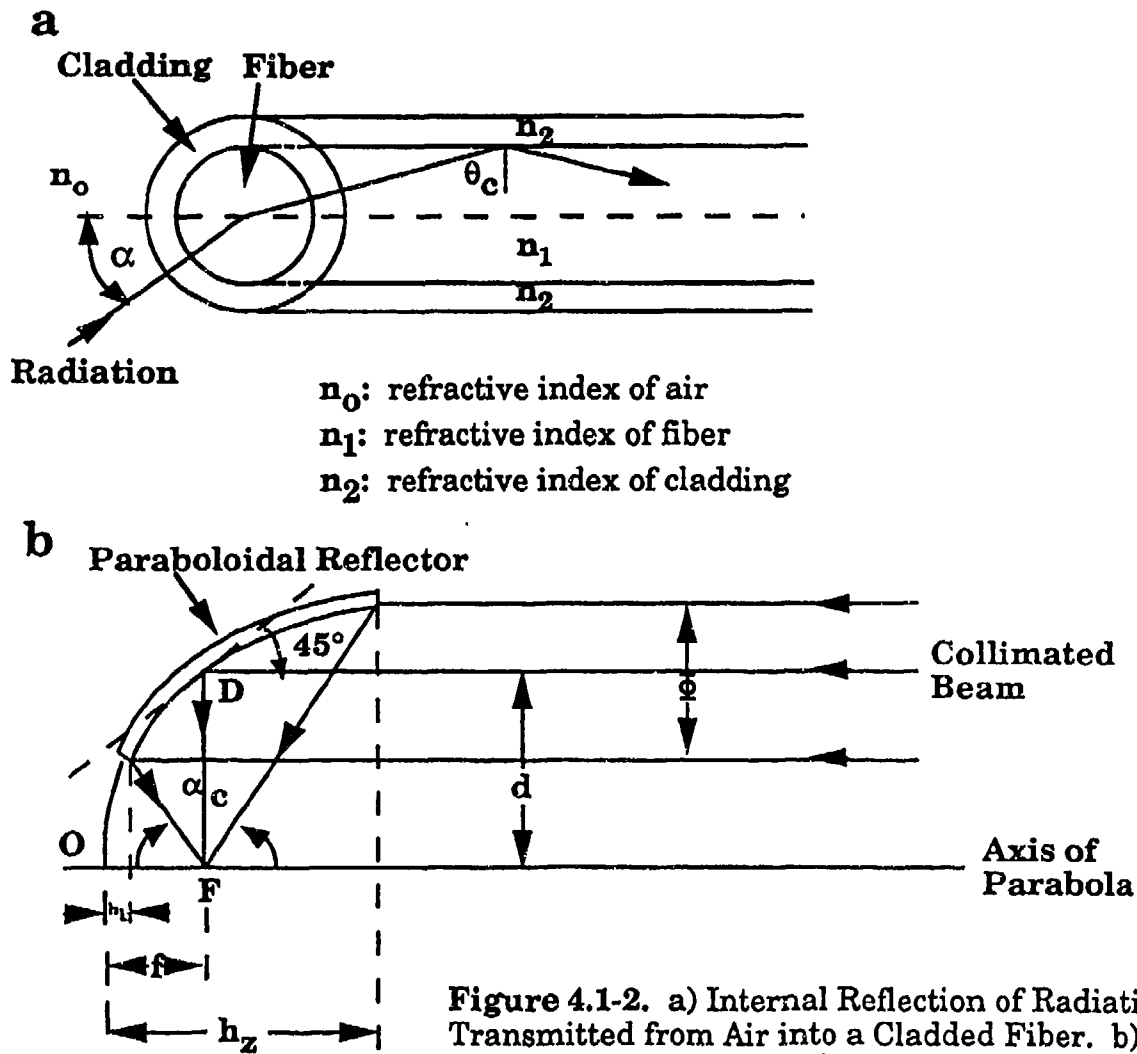


Figure 4.1-2. a) Internal Reflection of Radiation Transmitted from Air into a Cladded Fiber. b) Ray-Focussing of a Paraboloidal Reflector.

Selection of Optical Fibers - Three different IR fibers have been suggested in previous studies as suitable probes for monitoring the reactions of condensed phases (62,63). These fibers are heavy metal fluoride glass (HMFG), chalcogenide glass, and sapphire. The characteristics of these fibers are shown in Table 4.1-1. The HMFG fiber has the lowest loss in IR transmission. However, as shown in Table 4.1-1, it has a refractive index of 1.51, which is close to that of the species in a typical jet fuel. The refractive index of jet fuels is in the range of 1.4-1.6. For a sensor fiber, the conditions for total internal reflection require the refractive index of the sensor to be greater than that of the sample. Therefore, in this study, the fluoride glass was only used as a transmission link between the sensor fiber and the FT-IR spectrometer and detector and not as the sensor element.

According to Table 4.1-1, the chalcogenide glass fibers have a refractive index higher than that of the jet fuel, and transmit through most of the IR range. However, they cannot withstand the high temperature conditions required for thermal stability testing. Sapphire fiber appears to be the most suitable sensor material for in-situ monitoring of jet fuel, since it can withstand high temperatures, and has a refractive index above that of jet fuel. The only disadvantage of using sapphire is that it does not transmit below 2500 cm^{-1} , so some of the mid-IR information is lost.

Based on the above considerations, it was decided to use a sapphire fiber as the sensor in the jet fuel thermal stability probe in the Phase I program, and zirconium fluoride (ZrF) fiber cables, which have lowest transmission loss, to link between the sensor fiber to the FT-IR spectrometer and detector. It would be possible to use chalcogenide fibers to monitor the thermal stability at temperatures less than $250\text{ }^{\circ}\text{C}$. These fibers will be evaluated under the Phase II program.

FTIR Spectrometer and Detector - The Phase I work was performed on the Michelson 100 (M100) Spectrometer. This spectrometer was determined to have good performance in IR throughput, resolution and frequency range for the chemistry to be followed when coupled with the fiber optical system of the jet fuel thermal stability probe and an Indium Antimonide (InSb) IR Detector. The spectrometer's range is from 500 to 6500 cm^{-1} with 4 cm^{-1} resolution. The relatively low signal of this type of fiber optic system requires a strong IR source and time averaging of data to improve signal to noise. The M100 spectrometer source and clock speed were increased to improve S/N and reduce multi-scan time. The reduction of scan time allows following of the chemistry of the jet fuel over time more accurately. The optical system employed focusing optics for IR coupling into the ZrF cables leading to the sensor element and for collection of the exiting IR beam from the ZrF transmission cable leading from the sensor. An InSb detector was chosen for its frequency range (to observe any overtones) and sensitivity. Typical MCT detectors are an order of magnitude less sensitive and have lower cutoff frequencies than InSb detectors. A vacuum fiber optic interface was designed at AFR to directly link the ZrF cable to the liquid nitrogen cooled InSb detector element. The direct connection of the cable to the detector greatly improves signal reception. This fiber optic interface can be adapted to any standard type 905 SMA fiber optic connector and sits in place of the IR transmitting crystal window normally used in the detector dewar.

Setup of the Test System - The test system included the optical interfaces between the spectrometer IR beam source and ZrF transmission fiber, and the ZrF transmission fiber and sapphire sensor fiber.

The schematic of a fiber optic element is shown in Fig. 4.1-2. A schematic of the coupling of the jet fuel thermal stability reactor to the FT-IR spectrometer is shown in Fig. 4.1-3. A multiple path optical bench was designed and constructed which could sequentially monitor the fiber optic probe, an ATR circle cell and a transmission cell using a single FT-IR spectrometer. This optical bench is discussed further under Section 4.3.

TABLE 4.1-1 CHARACTERISTICS OF IR FIBER MATERIALS
(Data Supplied by Foster-Miller, Inc.)

Property	Chalcogenide	Fluoride	EFG ¹ Sapphire	LAPG ² Sapphire	AgBr/Cl
Core Diameter	250 μ	250 μ	250 μ	250 μ	250 μ
Coating Thickness	45 μ	45 μ	none	none	none
Cladding Thickness	30 μ	40 μ	core only	core only	core only
Wavelength Range	3 to 10 μ 3300-100 cm ⁻¹	0.5 to 4.3 μ 20,000-2325 cm ⁻¹	0.2 to 4 μ 50,000-2500 cm ⁻¹	0.2 to 0.4 μ	3 to 20 μ 3300-500 cm ⁻¹
Attenuation	0.5 dB/m at 6 μ m	0.02 dB/m at 2.6 μ	20 dB/m at 3 μ	2 dB at 3 μ	0.7dBm at 10.6 μ
Refractive Index	2.9	1.51	1.7	1.7	2.0
Use Temperature	300°C	250°C	> 900°C	> 1400°C	400°C

¹ EFG - Edge Fed Growth Method

² LAPG - Laser Assisted Pedestal Growth Method

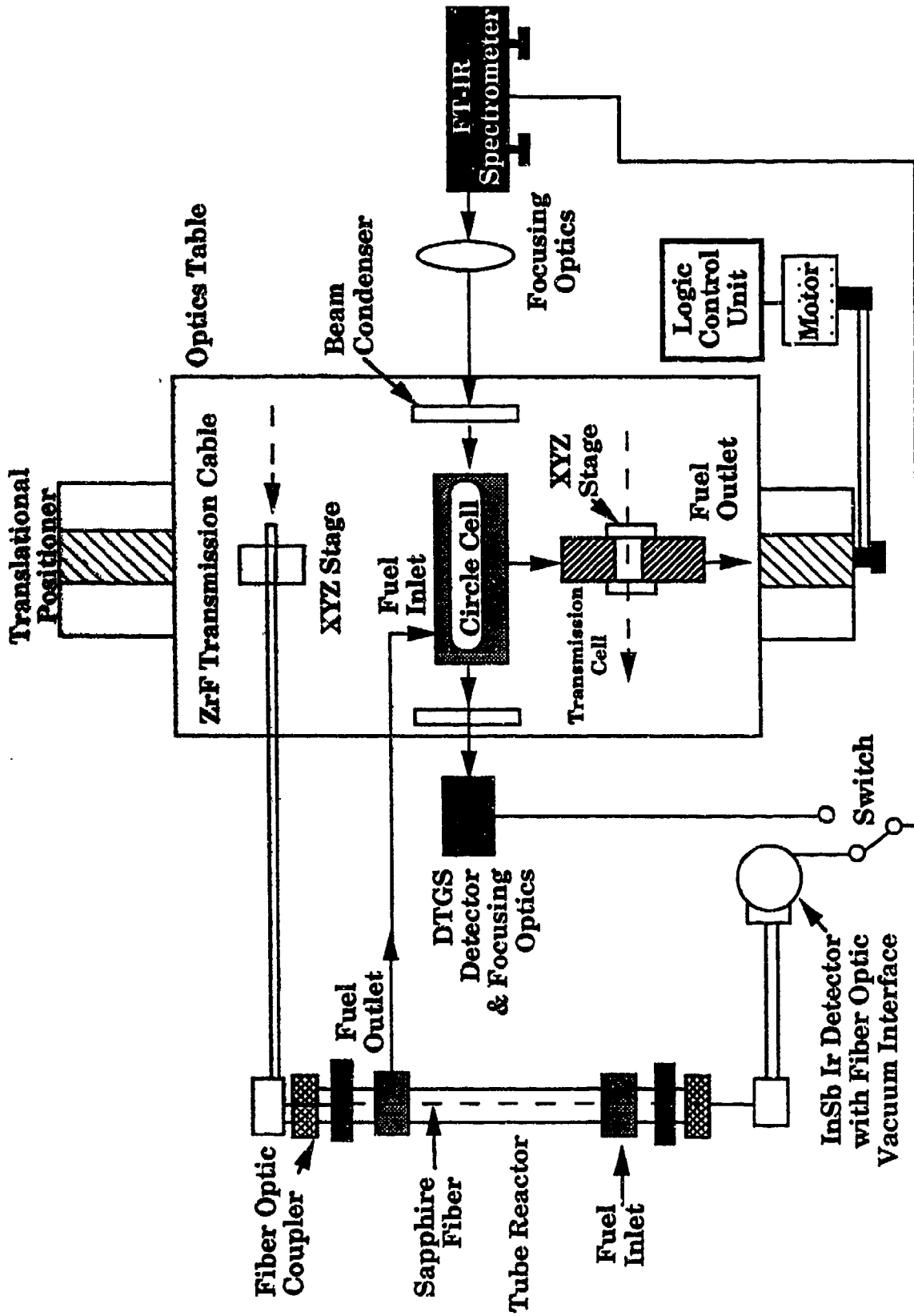


Figure 4.1-3. Schematic of FT-IR Deposit Monitor System with Multiple Path Optical Bench.

(a) Interface between IR Beam Source and Transmission Fiber - In order to successfully conduct IR radiation through the transmitting fiber (ZrF fiber in this case), one must consider the fiber numerical aperture, which is a measure of the light gathering power and is one of the principal properties of a fiber. Figure 4.1-2a shows radiation transmitted from air into a cladded cylindrical fiber and reflecting from the interface at the critical angle θ_c , which represents the smallest angle at which total internal reflection occurs. The fiber acceptance angle, α , is determined as the maximum angle at which radiation can be accepted for total transmission along the fiber.

From Snell's law one can obtain:

$$n_o \sin \alpha = (n_1^2 - n_2^2)^{1/2} \quad (4.1-1)$$

where n_o , n_1 and n_2 are the refractive indices of air, the zirconium fluoride fiber and the cladding material. The term $(n_1^2 - n_2^2)^{1/2}$ is called the numerical aperture (NA) of the fiber cable. The zirconium fluoride fiber cable used in this system has an NA of 0.21. According to Eq. 4.1-1, the fiber acceptance angle α can be determined:

$$\alpha = \sin^{-1} (NA/n_o) = \sin^{-1} (0.21/1.0) = 12.1^\circ \quad (4.1-2)$$

Since the IR rays emitted from the spectrometer are collimated, a paraboloidal reflector is required to focus the IR radiation into the ZrF fiber. Figure 4.1-2b shows the ray-focusing ability of a paraboloidal reflector. We can see in Fig. 4.1-2b that all rays entering the reflector, which are parallel to the axis of the parabola, will be reflected to a focal point where the ZrF fiber end will be located.

From a geometrical calculation, the ray-collecting angle, α_c , shown in Fig. 4.1-2b, can be determined:

$$\alpha_c = 2 \tan^{-1} (h_z/f)^{1/2} - 2 \tan^{-1} (h_o/f)^{1/2} \quad (4.1-3)$$

where f is the distance from the focal point to the center of the parabola, and h_z and h_o are the distances along the axis of parabola to the top and bottom of the off-axis paraboloidal reflector, respectively. There are criteria for the selection of a paraboloidal reflector. They are:

- α_c should be less than 2α , i.e., 24.2° in this case, so that all the collected light from the spectrometer can be accepted for total transmission along the fiber.
- The ray collection width of the reflector, Φ , should be as wide or wider than the beam to be focused. The beam exit KBr window of our Bomem spectrometer is about 5 cm in diameter, and, therefore, Φ should be no less than 5 cm.
- The focal distance, d , which is the distance between the focal point and the reflector, and perpendicular to the axis of the parabola, should be minimal to reduce dispersion effects.

The above requirements led to selection of a Melles Groit Type 02POA015 off-axis paraboloidal reflector, as the interface between the IR source and the zirconium fluoride transmitting fiber.

(b) Interface between ZrF Transmission Fiber and Sapphire Sensor Fiber - The ZrF transmission fiber cable is not able to connect directly with the sapphire sensor fiber, since they have different

sizes. A pigtail type coupler provided by Foster-Miller, Inc. was used to connect the ZrF and sapphire fibers. A detail of this coupler is shown in Fig. 4.1-4. The pigtail is made of ZrF, and is about 25 cm in length and 0.5 mm in diameter. It has a connector on one end to attach the ZrF fiber cable. The other bare end can be coupled with the sapphire fiber by using a metal sleeve. The tip of the sapphire fiber was cleaned with acetone before coupling, in order to obtain good transmission results.

The system was set up according to the design discussed above. It was demonstrated that this test system can successfully conduct the infrared rays emitted from the spectrometer, along the optical fibers, and obtain a distinct signal in the detector.

Summary

In this task, a jet fuel thermal stability probe which incorporates a FT-IR/fiber optic system was designed and constructed. The probe is made of 1/4 inch stainless tubing and Swagelok tube fittings. A sapphire fiber, which was between 12 and 15 inches in length and 0.25 mm in diameter, is used as an ATR sensor in the probe. A zirconium fluoride fiber cable is used as a transmitting fiber to link between the sensor fiber and the FT-IR spectrometer and detector. The FT-IR spectrometer used was a Bomem Michelson 100 with an Infrared Associates InSb detector. Using a paraboloidal reflector, the infrared rays emitted from the spectrometer can be focused to and totally transmitted along the zirconium fluoride fiber. A pigtail type of connector is used to conduct the infrared rays between the zirconium fluoride fiber and the sapphire fiber. It was shown that this test system can successfully transmit the infrared rays from the spectrometer through the optical fibers to obtain distinct signals in the detector.

4.2 Task 2 - Design and Construction of a QCM Deposit Probe

Objective

Design and construction of a quartz crystal microbalance (QCM) for on-line monitoring of deposit formation and growth.

Methodology

Introduction - A QCM was constructed for in situ measurements of the deposits that form in jet fuels as a result of thermal stress. This measurement technique uses a piezoelectric device, first designed and built by Robinson and Smedley (61) and known as the Smedley viscometer. While it was designed as a viscometer, its use as a mass detector has been illustrated in several publications and it uses the same principle as the mass detectors used in silicon chip technology (61). The advantage of the QCM constructed for this program is that the sensitive quartz piezoelectric crystals are remote from the fluid, and only the rugged probe is in contact with the fluid. The device can therefore be used over a wider range of conditions and can be used to examine the effect of probe surface composition.

Principle of the Quartz Crystal Microbalance (QCM) - The Smedley viscometer is based on the principle that the frequency of a pair of coupled torsionally-vibrating quartz crystals will be affected by the viscosity of the medium into which they are immersed (Figure 4.2-1). The advantage of having a pair of coupled crystals is that the system can be driven to always oscillate at its resonant frequency, which can be measured to high accuracy with a frequency counter. When only a single crystal is used, one must either scan over a frequency range to determine the frequency with minimum impedance or use sophisticated network analyzers to locate the resonant frequency.

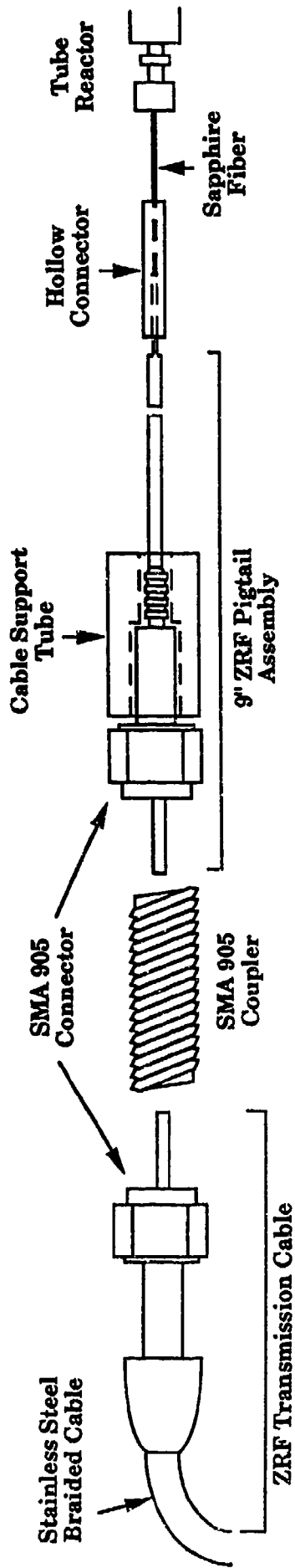


Figure 4.1-4. Detail of Fiber Optic Coupler.

The resonant frequency will also be affected if, instead of the crystals, a probe rod that is directly attached to them is immersed in the medium. The torsional oscillations set a series of nodes and antinodes along the entire length of the system (i.e., crystals and the probe rod). Changes in the mass of the probe due to deposit formation as well as formation of a viscous film on the probe will also affect the resonant frequency of the crystal-probe assembly. The change in resonant frequency Δf caused by a mass increase Δm is given by the relationship:

$$\Delta f = -2f^2 \Delta m / A (\mu\rho)^{1/2} \quad (4.2-1)$$

where A is the area, μ is the shear modulus and ρ is the density of quartz

Because there is no displacement at the nodes, it is possible to weld the probe rod at the nodes, and thereby provide a means of sensing changes in a fluid at high pressures and/or temperatures.

Results

Initial tests were conducted using the existing viscometer and frequency counting electronics. The cup that held the fluid was modified with a Conflat flange cover to operate at pressures up to 700 psi. The cup was placed inside a heater and the frequency as well as the drive voltage required were monitored as the system was heated. A schematic of the system is shown in Fig. 4.2-2. The results of the first few shake-down tests are given in Table 4.2-1.

The system worked without leaks and the crystals remained glued together.

The resonant frequency decreased about 1% when the system was heated to 300 °C in air, due primarily to the temperature coefficient of the crystal. This change was reproduced upon subsequent cooling and reheating the following day. An old sample of JP-5 was used for the next series of tests. Upon heating to 300 °C, the frequency again drops relative to the room temperature value, this time to a significantly lower value than obtained without the fuel (i.e., in air alone). The sample was cooled and reheated again the following day. Essentially identical frequencies were obtained for the room-temperature readings, although at 300 °C the second day's reading was noticeably higher. These data are consistent with the formation of a viscoelastic film. After emptying the cup, the probe rod was examined and it showed signs of a thin film.

These first tests illustrated the need for several improvements. In these experiments, the oil and the probe are heated but the quartz crystals remain close to ambient temperature. However, because temperature has a strong influence on the resonant frequency, the crystals were insulated and their temperature was monitored. Additionally, the drive crystals were insulated and their temperature was monitored with a separate thermocouple. Finally, the drive crystal was incorporated into a crystal-controlled oscillator to ensure constant operation at resonance, and an interface was built for computerized data acquisition.

Table 4.2-1.

VARIATION OF DRIVE VOLTAGE AND RESONANT FREQUENCY
WITH MEDIUM, TEMPERATURE, AND TIME

	Medium	Temperature (° C)	Drive Voltage (V)	Resonant Frequency (kHz)
Air	Test 1	24	10.75	40.455
		300	9.69	40.066
	Test 2	300	9.90	40.069
JP-5	Test 1	24	9.62	40.463
		300	11.66	40.013
	Test 2	23	9.756	40.467
		300	11.3	40.030
Air	Test 3	24	9.78	40.460

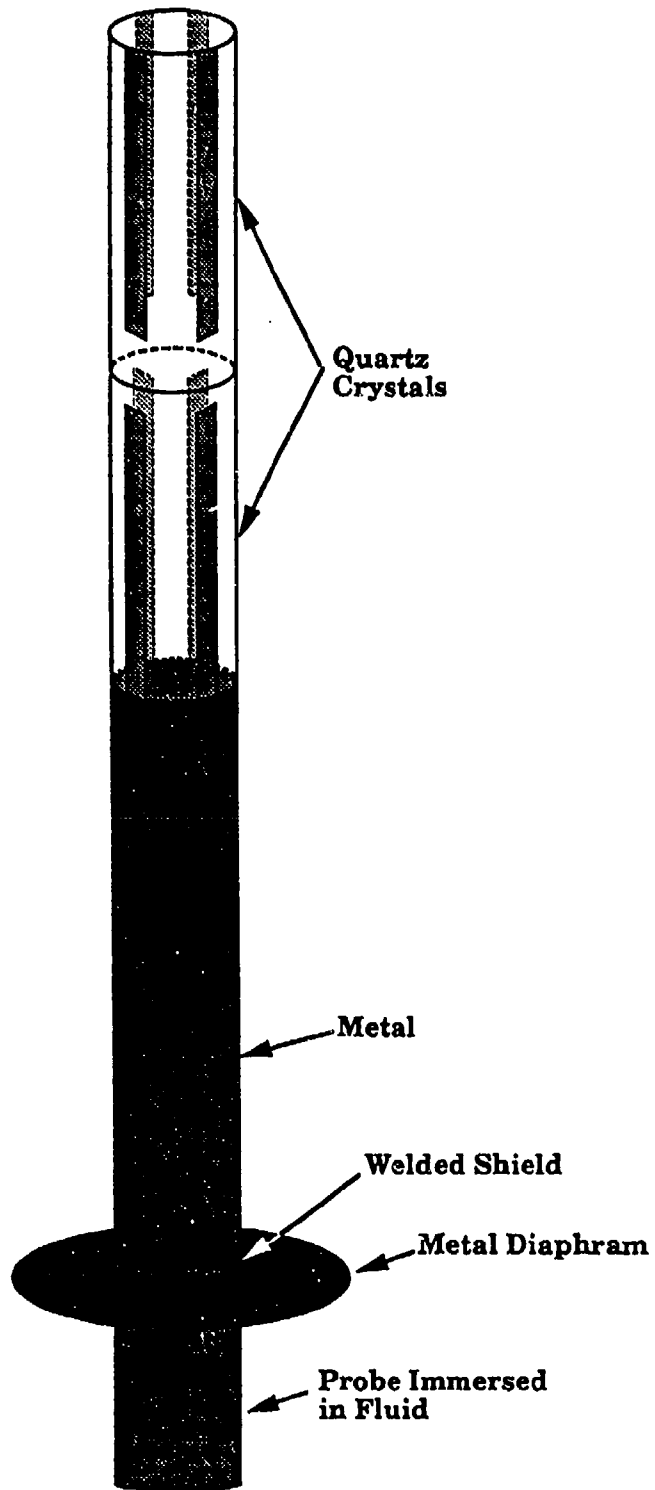


Figure 4.2-1. Quartz Crystal Oscillator with Probe Attached.

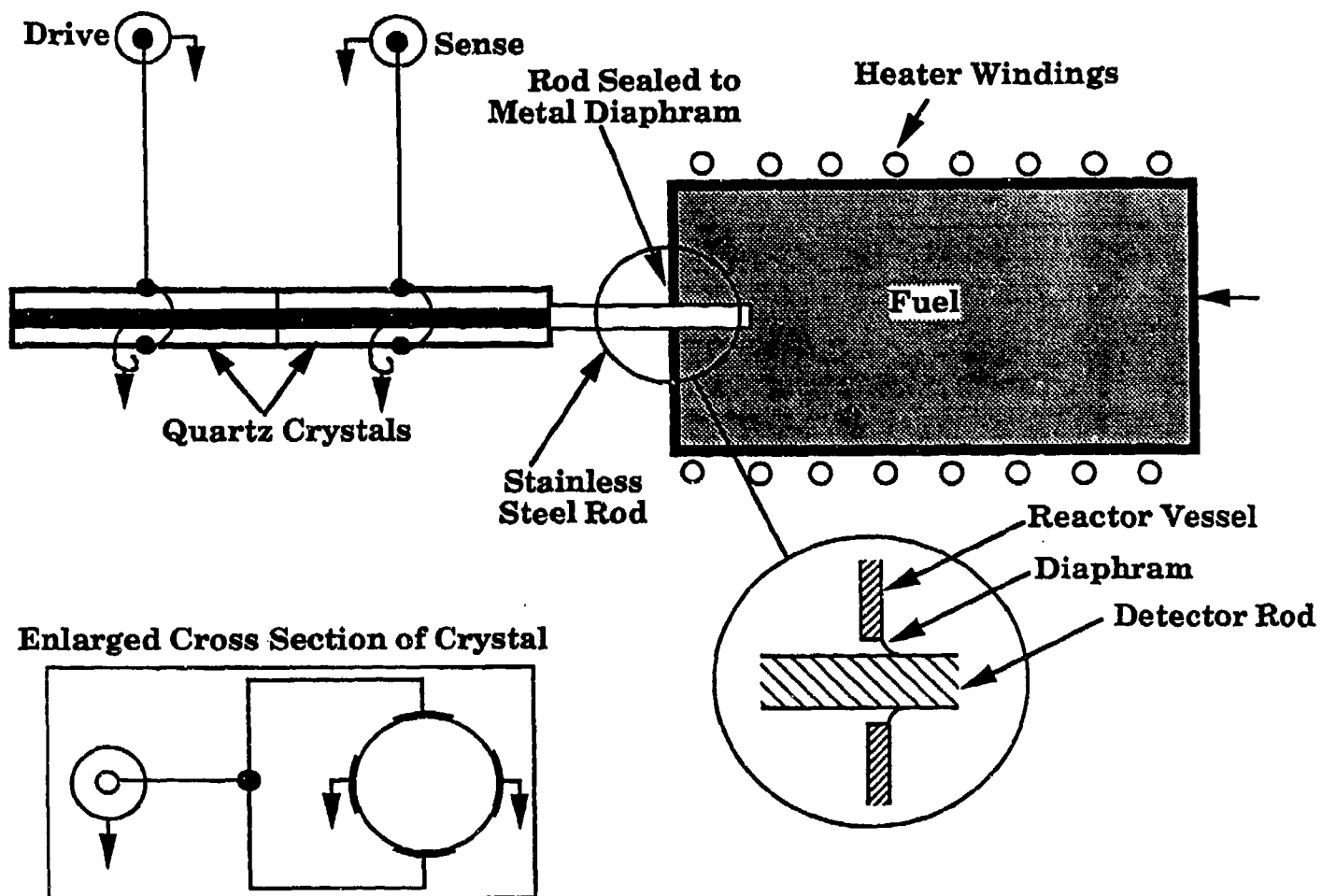


Figure 4.2-2. Quartz Crystal Mass Detector and Reactor Vessel.

Further tests were conducted using the Shell Jet A fuel and heating it to 400 °C. The fuel was obtained from Wright Laboratory. Figure 4.2-3 shows a typical time-temperature plot. It shows that the system heats up in about 30 min and stays at the set temperature. Figure 4.2-4 shows the changes in frequency with time for a blank run and a run with the Shell Jet A fuel. The ratios of the frequencies are shown in Fig. 4.2-5. After an initial excursion, which is largely due to temperature mismatch between blank and fuel runs, the ratio of frequencies settles at about 1.008. In other words, in the presence of the fuel, the frequency was about 0.8% lower. Results from a second experiment are shown in Fig. 4.2-6. In this case, the final ratio is about 0.6% lower with the fuel.

The next experiment was conducted using the Sun Jet A-1 fuel. However, during this run, the joint between the rod and the vessel failed and the experiment had to be aborted. Upon closer examination, the brazed joint at the probe rod node appears to have been leaking fuel, and under pressure and repeated heating/cooling cycles, failed due to shear stress. As a consequence of the failure, the entire crystal assembly was shattered, and a new assembly had to be fabricated for the flow cell, as discussed in Section 4.3.

Summary

Initial static cell tests were conducted using the existing viscometer. Based on these tests, several improvements were made to the QCM probe. Further tests were then conducted under static conditions using the Shell Jet A fuel. Finally, the static QCM probe was adapted so it could be incorporated into the advanced FSTS.

4.3 Task 3 - Integration and Testing of On-Line Diagnostics

Objective

Installation and testing of the on-line diagnostics developed in Tasks 1 and 2 on a previously developed Fuel Stability Test System (FSTS).

Methodology

The fiber optic probe and the QCM were incorporated into the Fuel Stability Test System developed under a previous contract (17) and shown in Fig. 4.3-1. The 44 inch long heated reactor tube with a wire deposit probe was replaced with the sensors developed in Tasks 1 and 2. These sensors were installed in parallel so that the system could be operated using either the QCM probe or the fiber optic probe.

It has been found that the optical properties of sapphire fiber vary with temperature (63,64). Since the jet fuel thermal stability tests were performed under nonisothermal conditions using a sapphire fiber as the ATR sensor, the temperature effect on the optical property of the sapphire fiber was studied by obtaining spectra in air at different temperatures.

In previous work (63), the spectra of benzene, toluene, o-cresol, tetralin, and benzylmethylamine were obtained using a sapphire fiber optic probe. By comparing these spectra to ones in standard reference libraries, the diagnostic capabilities of the sapphire fiber optic/ATR probe were established. In addition, the higher temperature spectra of o-cresol and tetralin were obtained and analyzed, in order to demonstrate that the thermal decomposition behavior of a pure compound could be followed. Some of these results were included in this section in order to demonstrate the capabilities of the system.

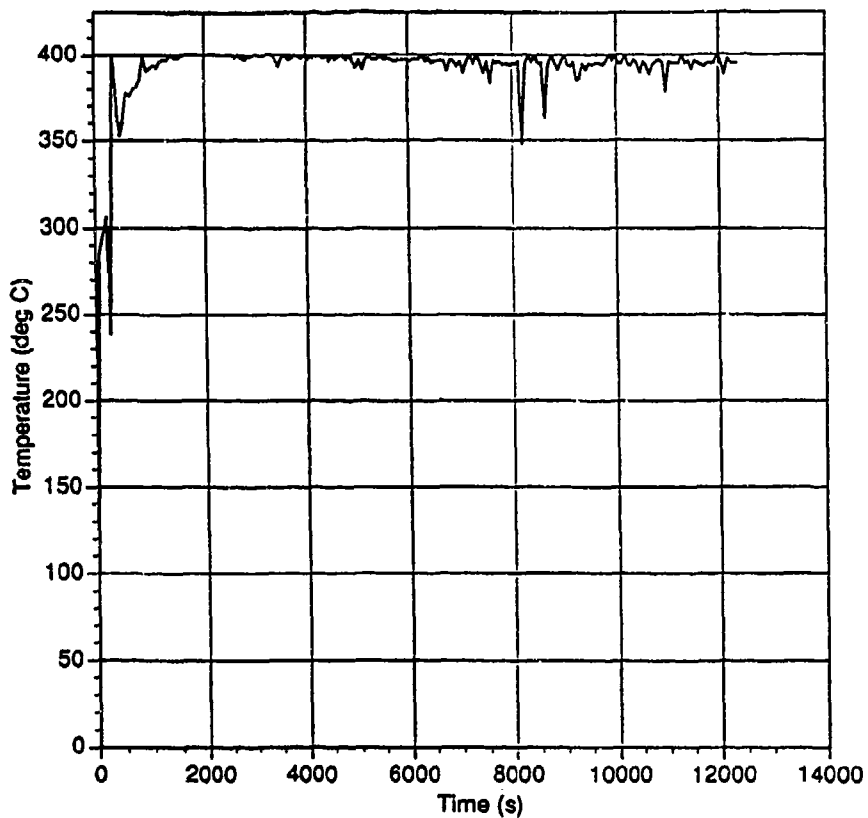


Figure 4.2-3. Typical Time-Temperature Plot for SRI QCM Test Cell.

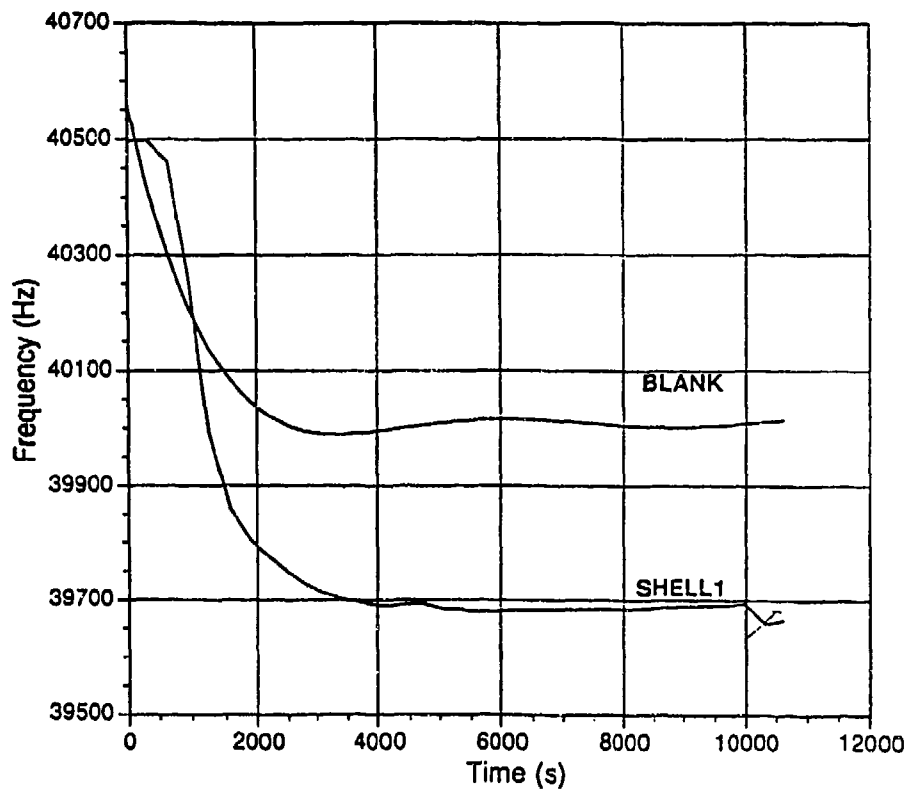


Figure 4.2-4. Change in Frequency with Time for a Blank (air) Run and a Run with Shell Fuel Heated to 400°C.

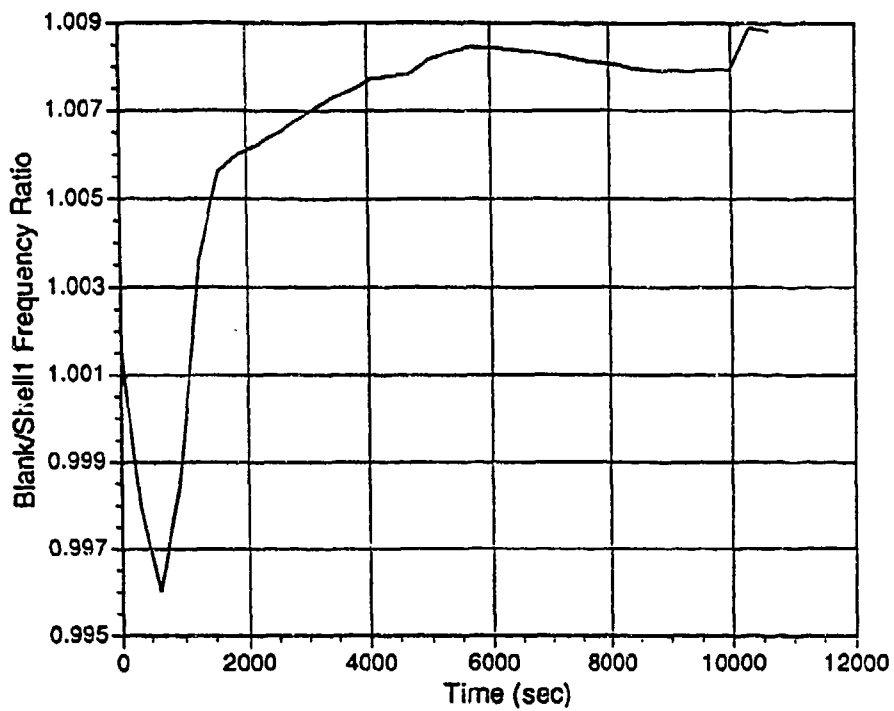


Figure 4.2-5. Ratio of Frequency Changes for Blank (air) and Shell Fuel Runs using Data from Fig. 4.2-4.

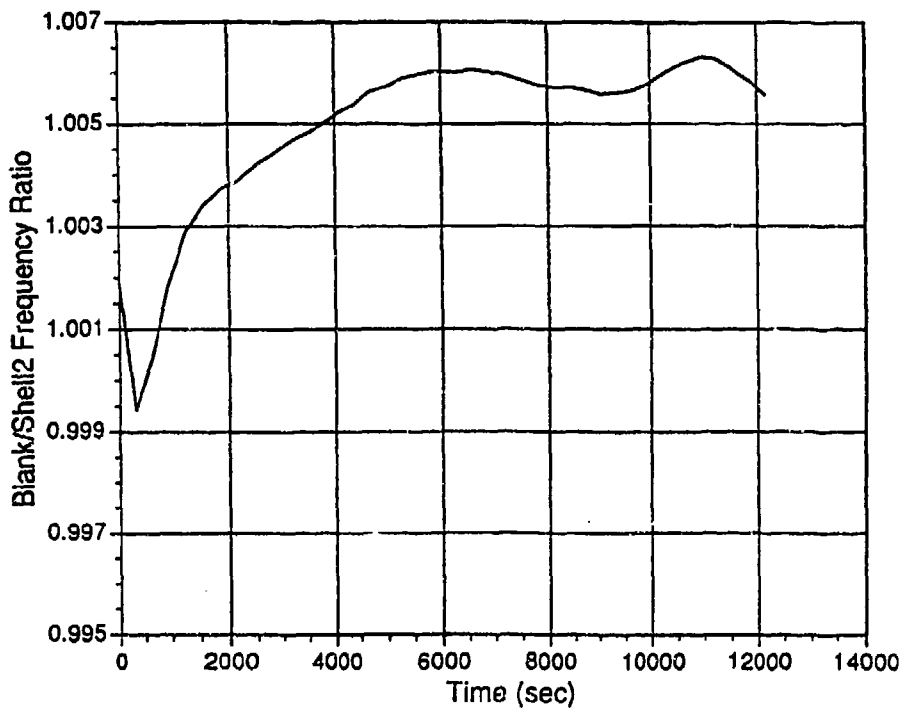


Figure 4.2-6. Ratio of Frequency Changes with Time for Repeat Blank (air) and Shell Fuel Runs.

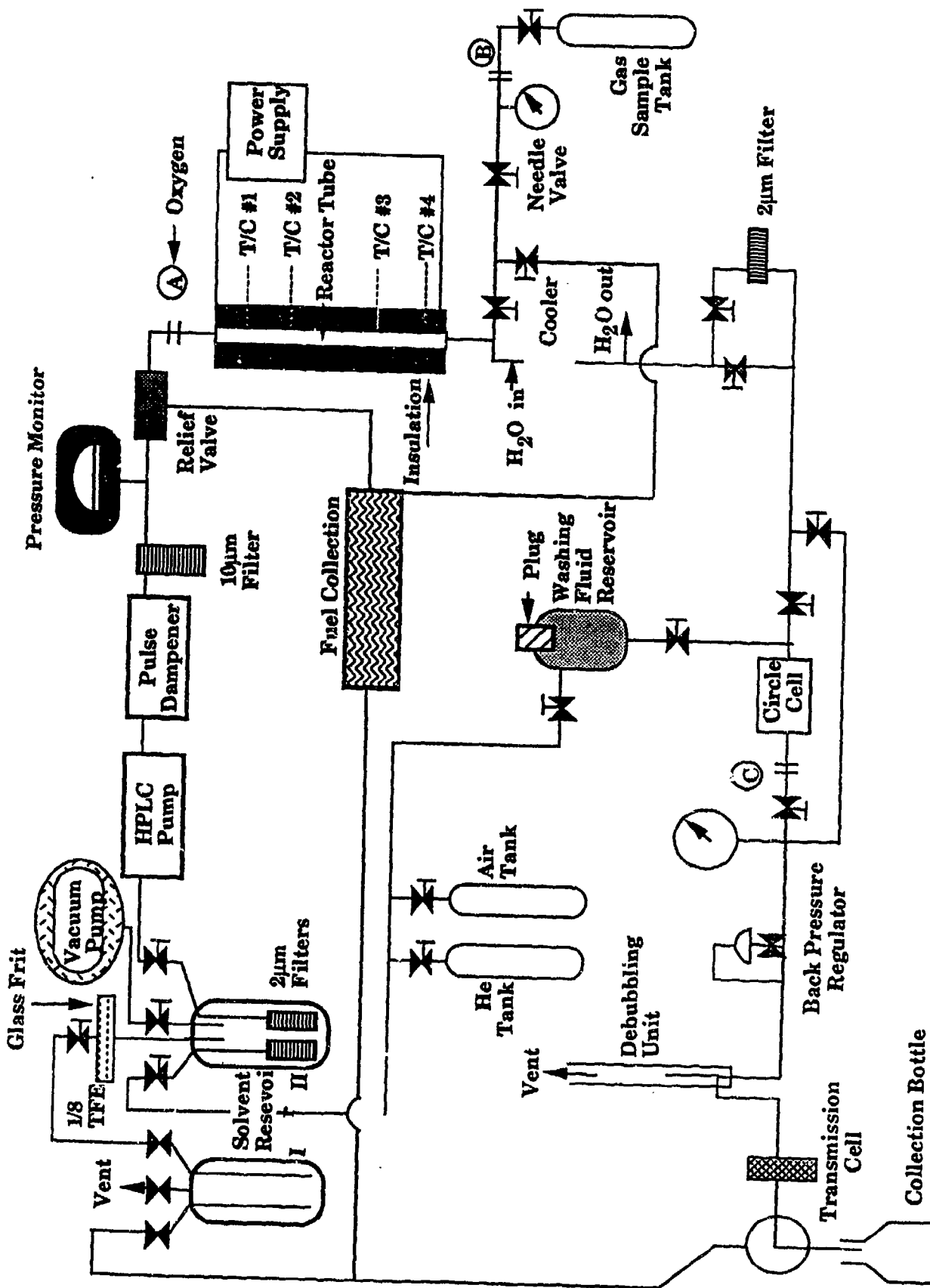


Figure 4.3-1. Schematic of First Generation Fuel Stability Test System (FGSTS).

Results

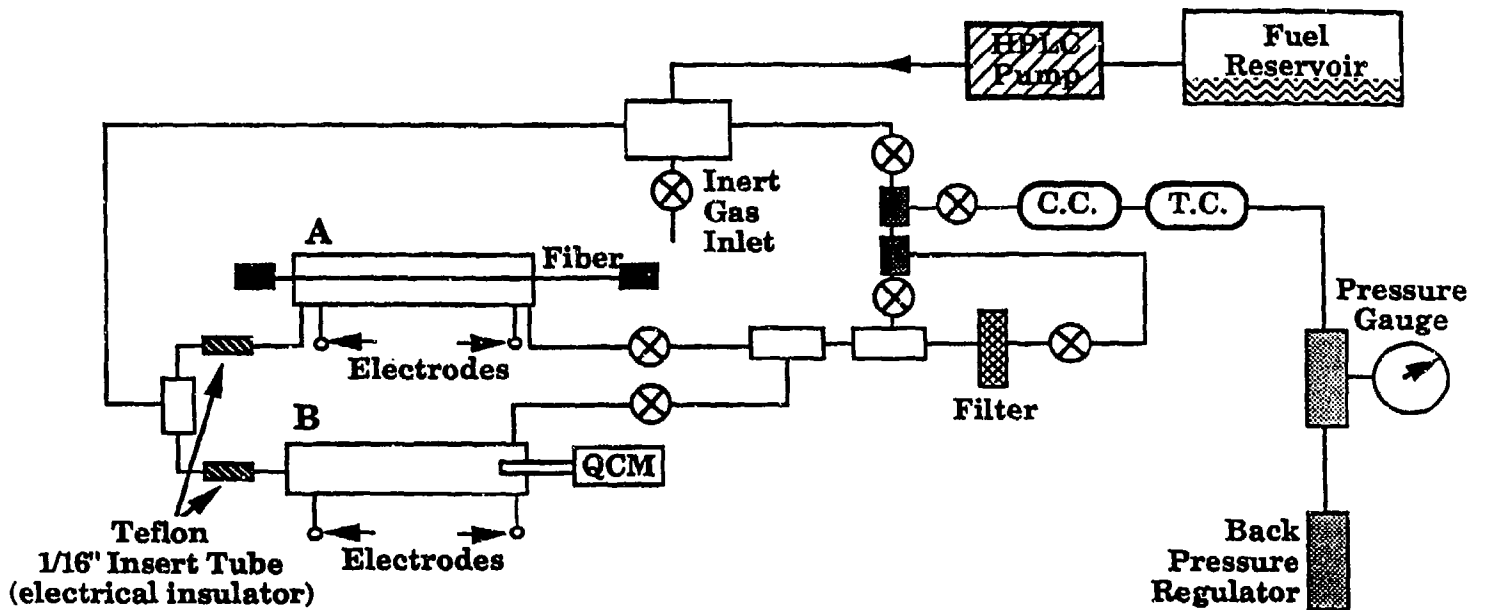
Fuel Stability Test System (FSTS) - The QCM and fiber optic probe were incorporated into a previously developed Fuel Stability Test System (FSTS) (17). The system was assembled from relatively low cost, modular, high pressure liquid chromatography (HPLC) components. Figure 4.3-1 is a schematic of the previously developed FSTS and Fig. 4.3-2 is a simplified schematic of the advanced FSTS with parallel QCM and FT-IR fiber-optic probes.

The jet fuel was stored in an HPLC reservoir with a multi-valved cap. To remove any dissolved oxygen from the jet fuel, the fuel was sparged with nitrogen and then stored in a nitrogen environment. Prior to starting a test, the fiber optic reactor tube was purged with air and reference spectra were obtained for the sapphire at different temperatures.

A HPLC pump was used to meter the jet fuel at 0.75 ml/min from the reservoir through a 5-micron fritted glass filter. At the outlet of the pump, a pressure transducer measured the fuel pressure which ranged from 600 to 1100 psig. The jet fuel can then be directed either through the QCM or the fiber optic probe which were plumbed in a parallel flow configuration. This setup enabled the data from both probes to be directly compared when exposed to the same test conditions. The fuel residence time in the hot zone of each probe was approximately 1.7 minutes. Both reactor tubes were insulated and heated directly using an AC power supply. Three thermocouples located at 3 3/4 inches, 5 1/2 inches, and 7 inches from the fuel inlet measured the outside wall temperature. The control thermocouple was located 5 1/2 inches from the fuel inlet and the desired tube temperature was maintained by regulating the power supply voltage. Figure 4.3-3a presents the wall temperature profile at different control thermocouple temperatures. To determine the jet fuel temperature profile, the fiber optic probe was replaced with a thermocouple and the jet fuel temperature was measured at 4 locations. The jet fuel temperature profile at different control thermocouple temperatures is presented in Fig. 4.3-3b.

After the fuel was thermally stressed, it could either be passed through a 2-micron filter or pumped directly to the Spectra Tech circle cell. The circle cell was a high pressure (1500 psig) version which was also equipped with a high temperature jacket for operation at elevated temperature (250 °C). However, the current design could not operate at high temperature and high pressure simultaneously. The cell volume was about 3 ml and was installed with a ZnSe crystal which was the best general purpose crystal for our application. Due to the heat loss from the jet fuel, the spectra obtained from the circle cell was close to ambient temperature. It was proposed that a Buck Scientific 1.5 mm transmission cell would be located in series with the circle cell. The transmission cell is limited to low pressure operation, but was modified to withstand the high pressure operating conditions. However, during system check out, the transmission seal failed when exposed to the 600-1100 psig test conditions. In Phase II, it will be determined if the carbonyl information provided by the transmission cell is important for measuring or monitoring fuel stability. The jet fuel pressure was then reduced to ambient pressure after passing through a 600 psig back pressure regulator.

To collect sequential spectra from the fiber optic probe and the circle cell at the same test conditions, the end of the zirconium fluoride fiber and the circle cell were mounted on a translational table. A stepping motor along with a logic circuit moved the table so that the infrared beam was either focused through the circle cell or into the end of the zirconium fiber. The optical box was enclosed and purged with dry air to ensure that the moisture in the ambient air did not interfere with the single beam spectra. A schematic of the multiple path optical bench is shown in Fig. 4.1-3.



A - Reactor Tube (I.D. 1/4"; length between electrodes 7-1/2") with ATR Fiber
 B - Reactor (same as A) with QCM Detector

Both Reactors have Direct AC Heating

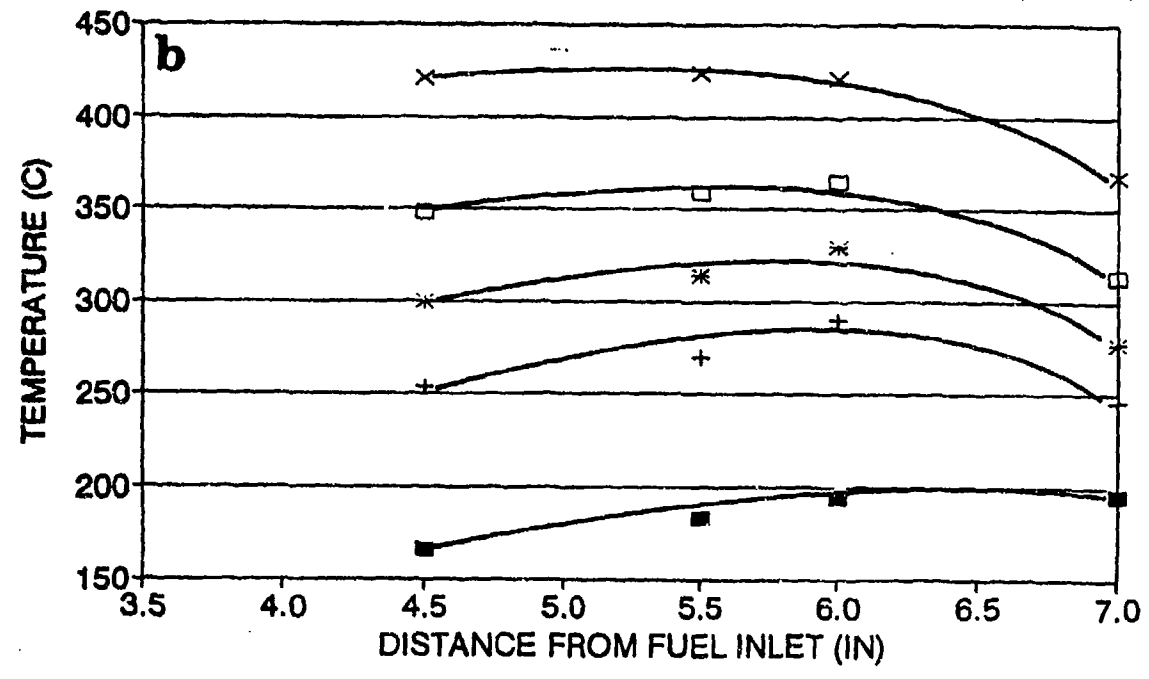
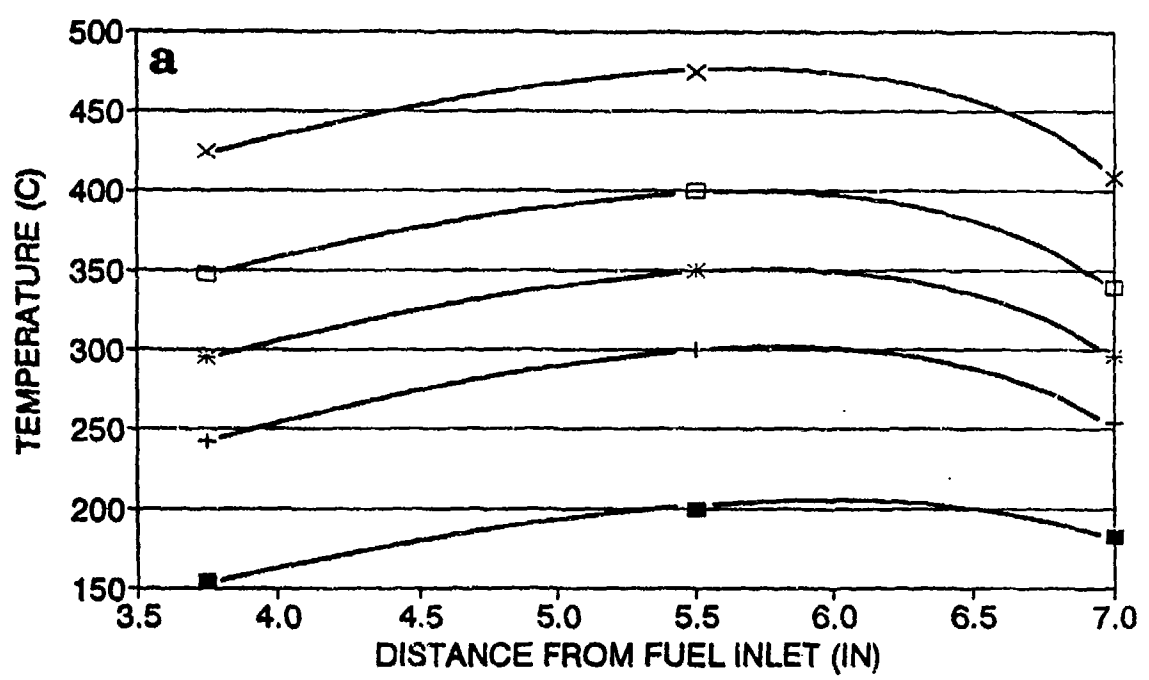
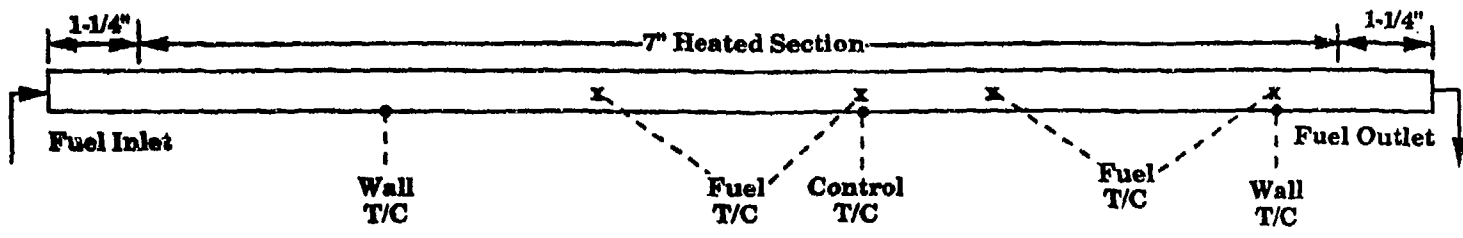
C.C. - Circle Cell

T.C. - Transmittance Cell

Inert Gas Inlet: for Cleaning Purposes

⊗ Valves

Figure 4.3-2. Modified Reactor for Jet-Fuel Thermal Stress Measurements.



■ 200 C CONTROL TC + 300 C CONTROL TC * 350 C CONTROL TC
 □ 400 C CONTROL TC × 475 C CONTROL TC

Figure 4.3-3. Temperature Profile for a) Wall and b) Jet Fuel for Experiments done at Different Control Temperatures.

At the conclusion of each test, the fiber optic probe or the QCM probe was purged with dry air. The probe was removed from the reactor tube and cleaned of any deposits using a cotton tipped applicator with acetone or isopropanol.

F-O/ATR of Sapphire Fiber - Certain samples absorb too strongly to allow infrared transmittance spectra to be obtained. For example, liquid hydrocarbon streams are highly absorbing and are difficult to analyze by an infrared transmittance technique. The use of a fiber optic as an ATR element has provided the possibility of transmitting the IR light through a jet fuel stream at high temperature and high pressure conditions.

Normally, infrared radiation exiting from a transparent element is partially reflected. However, if the angle of incidence of the infrared radiation is sufficiently large (say, larger than the critical angle), the radiation will be totally reflected. This element can then be called an internal reflection element (IRE). The critical angle for total reflection is determined by the refractive indices of the IRE and the sample in contact with the element. According to the law of refraction, the critical angle is given as: $\theta_c = \sin^{-1}n_s/n_p$, where n_p and n_s are the refractive indices of the IRE and the sample, respectively.

If a less dense and partially transmitting sample (i.e., with a smaller refractive index) is placed in contact with an IRE, the radiation can pass a short distance into the sample as a so-called evanescent wave. The totally reflected radiation will be partially absorbed by the sample. By analyzing the spectra of the partially absorbed infrared, one can determine the chemical structure of the sample. This technique is called Attenuated Total Reflectance (ATR) spectroscopy (65,66).

A fiber optic with the cladding removed can serve as the IRE. In Task 1, it was decided to use a sapphire fiber as the IRE, since it can withstand the high temperature and high pressure conditions in a jet fuel system. Some important chemical and physical properties of sapphire are shown in Table 4.3-1.

In ATR spectroscopy, the depth of penetration (d_p) of the evanescent wave into the sample is defined as the distance at which the intensity of evanescent wave reaches 1/e times its value at the sample-element interface. d_p is given by:

$$d_p = \frac{\lambda}{2\pi n_p (\sin^2\theta - n_{sp}^2)^{1/2}} \quad (4.3-1)$$

where λ = wavelength of the radiation

θ = angle of incidence

$n_{sp} = n_s/n_p$

Since n_p varies little with temperature and n_s is a decreasing function of temperature, d_p would decrease with temperature. This indicates that the absorbance of the radiation by the sample would decrease with temperature.

Table 4.3-1. TYPICAL PROPERTIES OF SAPPHIRE (64)

GENERAL

Chemical Formula: Al_2O_3

Crystallographic Structure: Rhombohedral Single Crystal

PHYSICAL/MECHANICAL

Density: 0.143 lb/in³ (3.97 gm/cm³)

Specific Gravity: 3.97

Tensile Strength: 60,000 PSI (approx.-design min.) (at 25 °C)
39,000 PSI (approx.-design min.) (at 500 °C)
51,000 PSI (approx.-design min.) (at 1,000 °C)

Compressive Strength: 350,000 PSI

Young's Modulus: 51×10^6 PSI (at 25 °C)

Modulus of Rupture: 67,000 to 95,000 PSI

Modulus of Rigidity: 25×10^6 PSI

Bulk Modulus: 33×10^6

Poisson's Ratio: 0.28 - 0.33

Hardness: 9 MOHS, 1800 Knoop parallel to C-axis
2200 Knoop perpendicular to C-axis

Coefficient of Friction: 0.15 against steel

Porosity: 0

THERMAL

Melting Point: 2053 °C

Maximum Operating Temperature: 2000 °C

Thermal Coefficient of Expansion:

$5.3 \times 10^{-6}/^\circ\text{C}$ parallel to C-Axis (at 25 °C)

$4.5 \times 10^{-6}/^\circ\text{C}$ perpendicular to C-Axis (at 25 °C)

Thermal Conductivity: 0.086 cal/sec - cm °C

Specific Heat: 0.12 cal/gm (at 25 °C)

Heat Capacity 77.8 joules/deg. mole

OPTICAL

Transmission: Up to 98.5% total transmission as measured by integrating sphere method.

Index of Refraction: (Birefringent) No: 1.768 (sodium D line)
Ne: 1.760 (sodium D line)

Emittance <0.02 at 880 °C where $\lambda = 2.6$ to 3.7 micron

Thermal Optic Coefficient (dn/dT): $13 \times 10^{-6}/^\circ\text{C}$ (visible)

CHEMICAL

Acid Resistance: Resistant to all acids at room temperature.
Some etching occurs with boiling phosphoric acid.

Weathering Resistance: Not affected by exposure to any atmospheric phenomenon, including industrial pollution.

Salt water Resistance: Not affected by salt water.
Resists the growth of salt water algae.

Medical: Non-thrombogenic. Not affected by body fluids.

According to Eq. (4.3-1), the ratio of d_p at two different temperatures can be written as:

$$\frac{d_{p2}}{d_{p1}} = \left\{ \frac{\sin^2\theta - [(n_{sp})_1]^2}{\sin^2\theta - [(n_{sp})_2]^2} \right\}^{1/2} \quad (4.3-2)$$

assuming n_c is constant with temperature.

It should also be noted that transmittance of infrared radiation would be attenuated in the fiber by an amount (62):

$$I = I_0 e^{-\gamma z} \quad (4.3-3)$$

where, γ , is the absorption coefficient per unit length of fiber, z .

Data in Fig. 4.3-4a, which was provided by Saphikon, Inc., show that the absorption coefficient of a sapphire fiber varies with temperature. This, of course, would result in the variation of transmission in a sapphire fiber with temperature. Figure 4.3-4b, which is also provided by Saphikon, Inc., shows that infrared transmission in sapphire decreases with temperature for wavelengths higher than $3.5 \mu\text{m}$ in the temperature range of our concern ($<500^\circ\text{C}$). Since the data shown in Fig. 4.3-4a are measured for sapphire fibers of a different size from those used in this study, it is necessary to construct a calibration curve at different temperatures, similar to Fig. 4.3-4b, for our system.

Transmittance spectra in air at different reactor temperatures were taken, and the results are shown in Fig. 4.3-5. It shows that the transmittance through the sapphire fiber decreases with temperature for wavenumbers lower than approximately 3000 cm^{-1} , but increases with temperature at higher temperatures. These spectra were used as a reference set for jet fuel experiments at corresponding temperatures. It is also of interest to see the transmittance spectra for various optical configurations. Figure 4.3-6 shows that the transmittance is significantly attenuated by the zirconium fluoride pigtail and the sapphire fiber sensor in the test cell. However, the signal is still strong enough with both the pigtail and sensor coupled, to allow useful information to be obtained. This will be demonstrated in the following section.

Sapphire Fiber-Optic (F-O)/ATR Spectra of Reference Compounds - Since it was decided to use a sapphire fiber as the sensor in the reactor, the information below 2500 cm^{-1} in the infrared spectrum was cut out. However, significant amounts of chemical structural information can still be determined in the wavenumber range of 2500 cm^{-1} to 4000 cm^{-1} .

Important bands that can be obtained in the infrared spectrum using sapphire fiber optics are summarized in Table 4.3-2.

In a previous study (63), reference compounds were used to validate the fiber optic system. The F-O/ATR spectra of benzene, toluene, o-cresol, benylmethylamine, and tetralin were obtained and compared with the Aldrich Library spectra.

Table 4.3-2. Important IR Bands in Sapphire Fiber Optics

<u>Wavenumber</u> <u>(cm⁻¹)</u>	<u>Assignment</u>
2500 - 3000	carboxyl O-H stretching
2565	S-H stretching of sulfide band
2720	C-H stretching of CHO (aldehyde)
2780	C-H stretching of N-CH ₃
2835	C-H stretching of anisole (Ar-O-CH ₃)
2850 - 2960	aliphatic C-H stretching: -CH ₂ - 2930, 2850; -CH ₃ 2960, 2870
3000 - 3100	aromatic C-H stretching, with 3 bands
3100	alkene C-H stretching
3200 - 3500	hydroxyl O-H stretching
3335 - 3400	N-H stretching of amines
3450	C=O overtones
3600 - 3700	Minerals

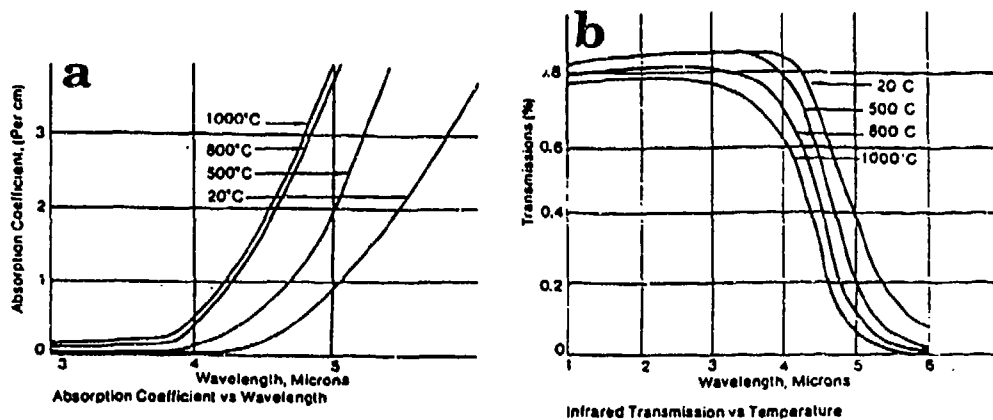


Figure 4.3-4. a) Absorption Coefficient of Sapphire at Different Temperatures. b) Infrared Transmission of Sapphire at Different Temperatures. Data are from Saphikon, Inc.

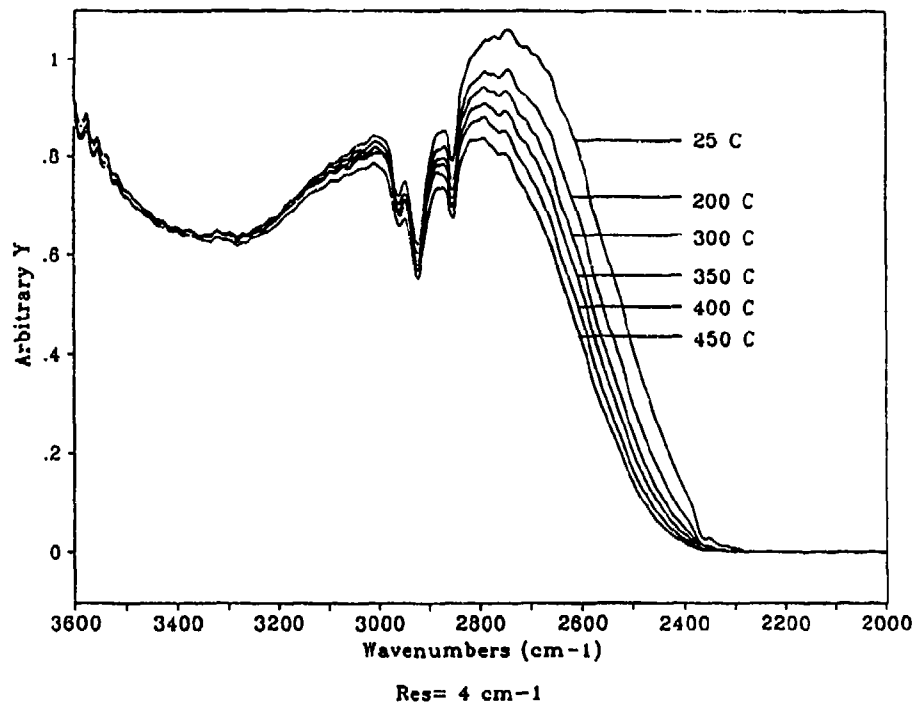


Figure 4.3-5. Infrared F-O/ATR Spectra in Air at Different Temperatures, using 15" Sapphire Sensor.

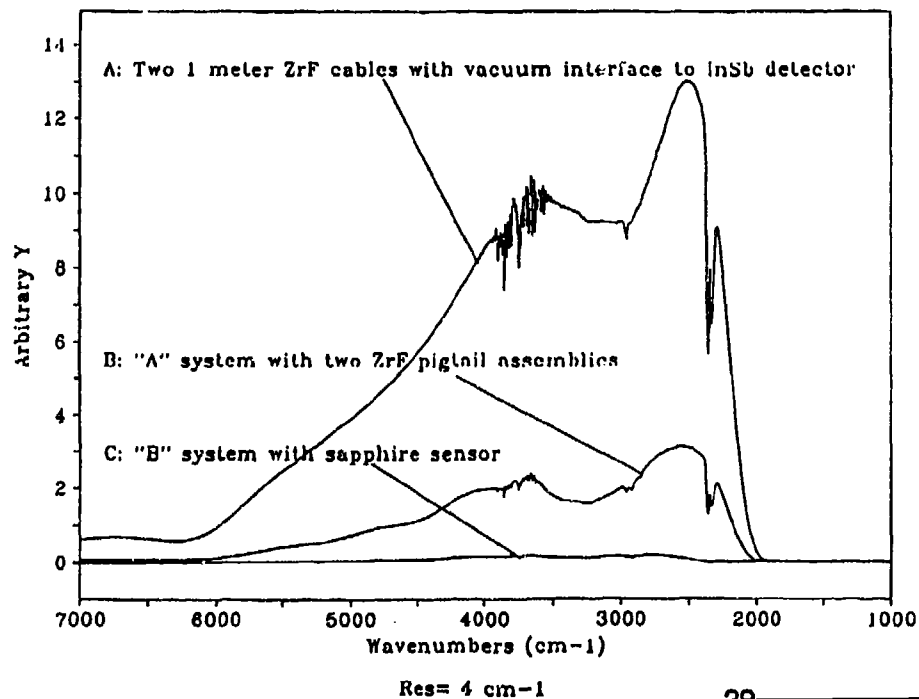


Figure 4.3-6. Spectra for Various Optical Configurations (in air).

Figure 4.3-7 shows the infrared transmission spectra from F-O/ATR spectroscopy for benzene and toluene at room temperature. Three aromatic C-H stretching peaks in the region of 3000-3100 cm^{-1} are clearly shown in both the benzene and toluene spectra. The toluene spectrum also shows aliphatic C-H stretching in the region of 2800-3000 cm^{-1} . The Aldrich Library spectra are also shown for comparison. It can be seen that the infrared spectra, in the C-H stretching region (3100-2800 cm^{-1}), obtained from F-O/ATR spectroscopy in this study are in excellent agreement with the standard spectra from the Aldrich Library.

Since the chemical species in the jet fuel are mainly hydrocarbon compounds, information from the C-H stretching region is very valuable in understanding the thermal stability of the jet fuel. The results shown in Fig. 4.3-7 indicate that this F-O/ATR spectroscopy system has the ability to obtain information on C-H bonds for jet fuel.

Figure 4.3-8 shows the infrared transmission spectra from F-O/ATR spectroscopy for o-cresol and benzylmethylamine at room temperature, while Fig. 4.3-9a shows the spectrum for tetralin (1,2,3,4-Tetrahydronaphthalene). The structures of these three compounds are also shown in Figs. 4.3-8, and 4.3-9a. The spectra of all three compounds show aromatic and aliphatic C-H stretching in the region of 3100-2800 cm^{-1} . However, there is an additional peak at 2780 cm^{-1} shown in the benzylmethylamine spectrum. This peak represents the methyl C-H stretching in a methylamine compound. In addition to the C-H stretching, the spectra of o-cresol and benzylmethylamine show absorbances at higher wavenumbers. The strong absorbance at 3200-3600 cm^{-1} in the cresol spectrum represents hydroxyl O-H. The absorbance at 3300-3400 cm^{-1} in the benzylmethylamine spectrum represents amine N-H stretching. As compared with the Aldrich Library spectra, the F-O/ATR spectroscopy system again demonstrates the ability to obtain reliable chemical structure information, including C-H, O-H and N-H groups.

Figures 4.3-7 and 4.3-8 show that the F-O/ATR spectroscopy system is able to obtain reliable chemical information in the mid-infrared region for wavenumbers higher than 2500 cm^{-1} . For wavenumbers higher than 3600 cm^{-1} and extended to about 12,500 cm^{-1} , there are many absorption bands resulting from harmonic overtones of fundamental bands and combination bands often associated with hydrogen atoms. Since the information below 2500 cm^{-1} would be cut out by using sapphire as the sensor fiber, the absorption information from harmonic overtones at high wavenumbers may be valuable for this system. The overtone infrared spectra have not been well studied in the literature. However, we observe some interesting overtone absorption in the spectra of some model compounds. Figure 4.3-9b shows the harmonic overtone absorptions for benzene and toluene. The harmonic overtones for jet fuels will be further studied in Phase II.

The above results have demonstrated that the test cell with a F-O/ATR element can obtain reliable spectra for several reference compounds. However, these spectra were all taken isothermally at room temperature. Non-isothermal experiments were carried out for o-cresol, and the chemical structure changes in the reaction system were monitored by the F-O/ATR sensor. The infrared spectra of o-cresol from F-O/ATR spectroscopy at different temperatures are shown in Fig. 4.3-10. It can be seen from the spectra that the infrared absorbance decreases with temperature. This result is expected, since the depth of penetration of the infrared evanescent wave into the sample decreases with temperature, as discussed above (see equation 4.3-2). From Fig. 4.3-10, one can observe the chemical structure changes of o-cresol with temperature, especially in the O-H stretching region. The results show the shift of O-H stretching toward higher wavenumbers with increasing temperature. This is consistent with the reported results (67) that hydrogen-bonded O-H groups have infrared absorptions at lower wavenumbers around 3400 cm^{-1} and monomeric O-H groups have absorptions at higher wavenumbers around 3600 cm^{-1} . Figure 4.3-10 supports the conclusion that thermal treatment of o-cresol weakens H-bonding on the hydroxyl groups to generate more monomeric hydroxyl groups at higher temperature. However, as discussed above,

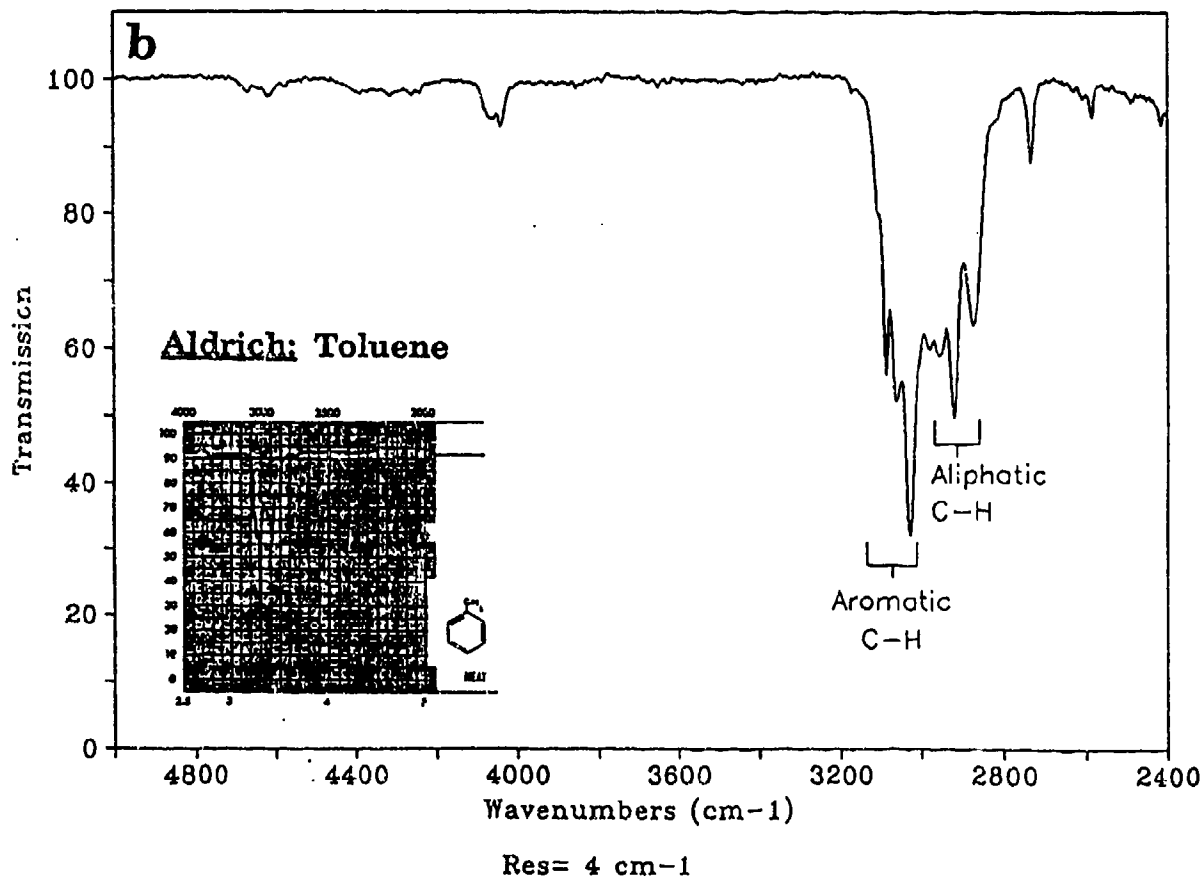
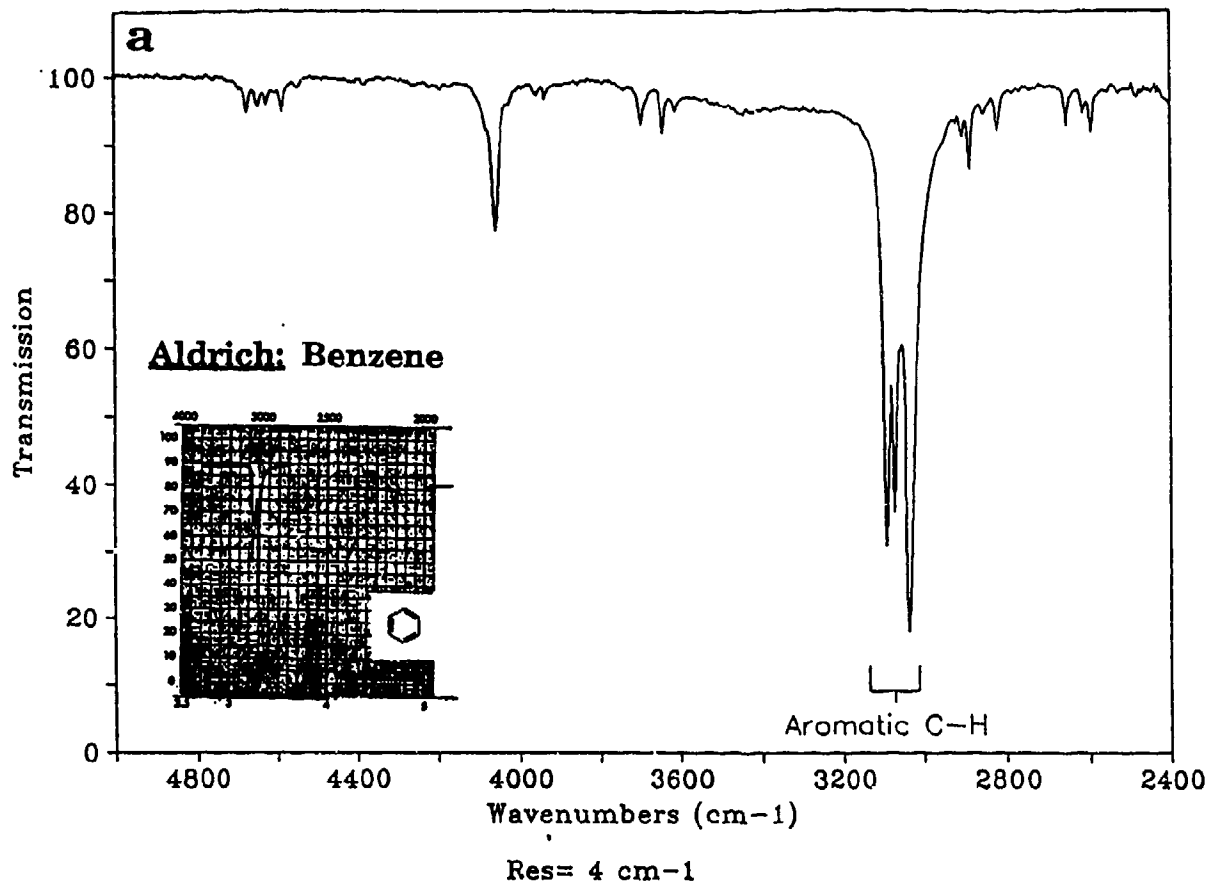


Figure 4.3-7. Infrared Spectra from F-O/ATR Spectroscopy Compared with Aldrich Library Spectra. a) Benzene; b) Toluene (63).

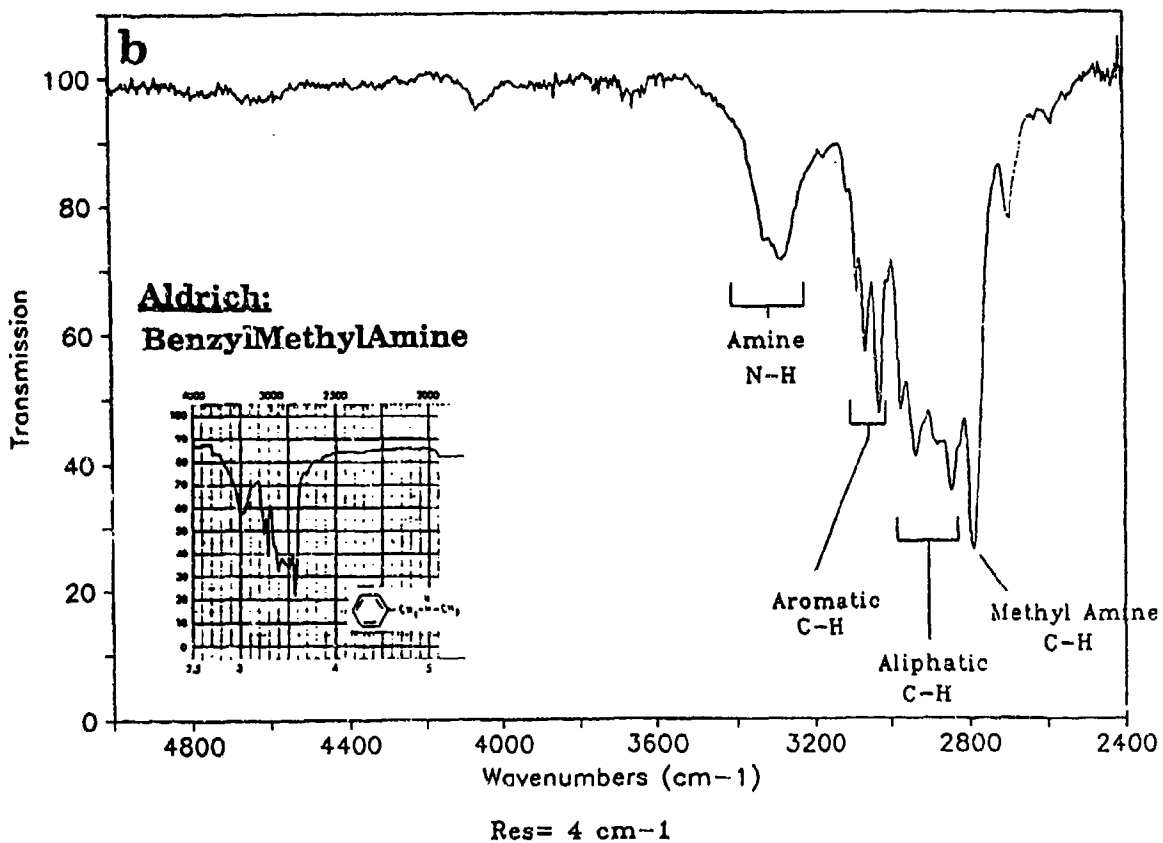
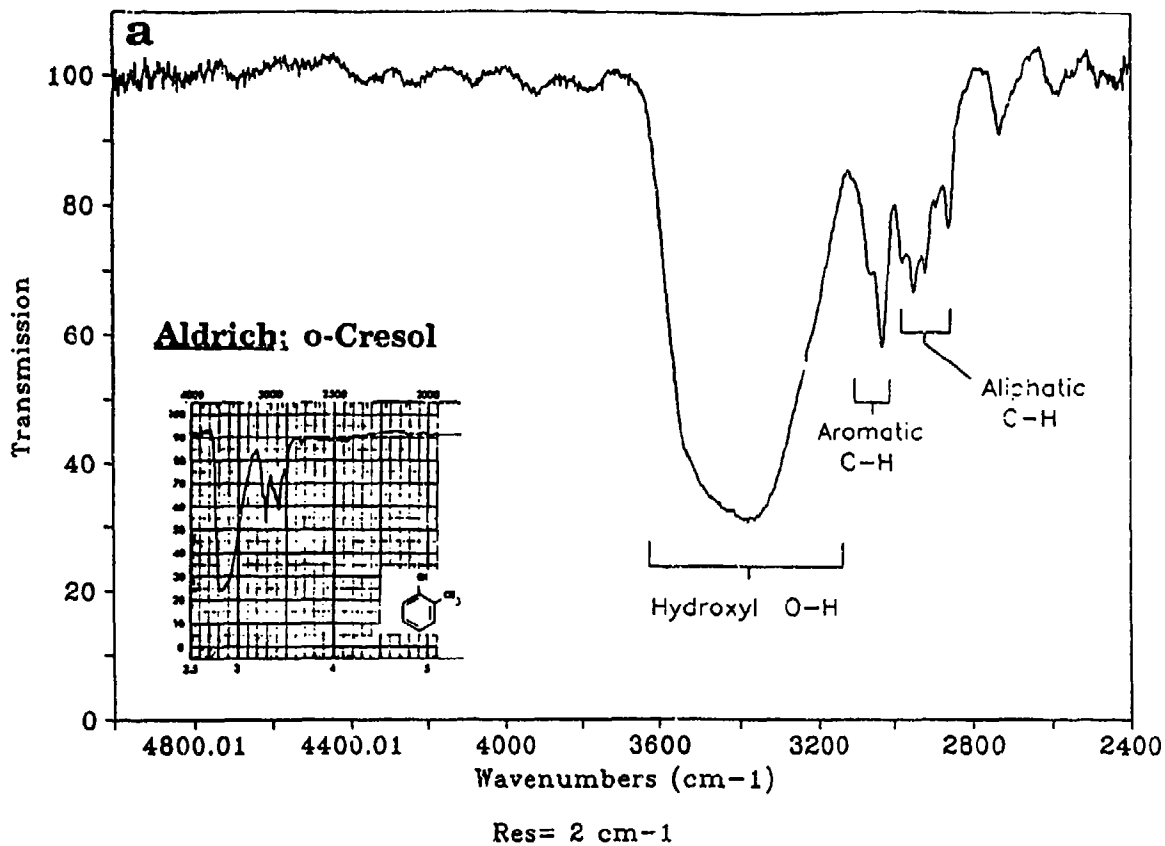


Figure 4.3-8. Infrared Spectra from F-O/ATR Spectroscopy Compared with Aldrich Library Spectra. a) o-Cresol; b) Benzylmethylamine (63).

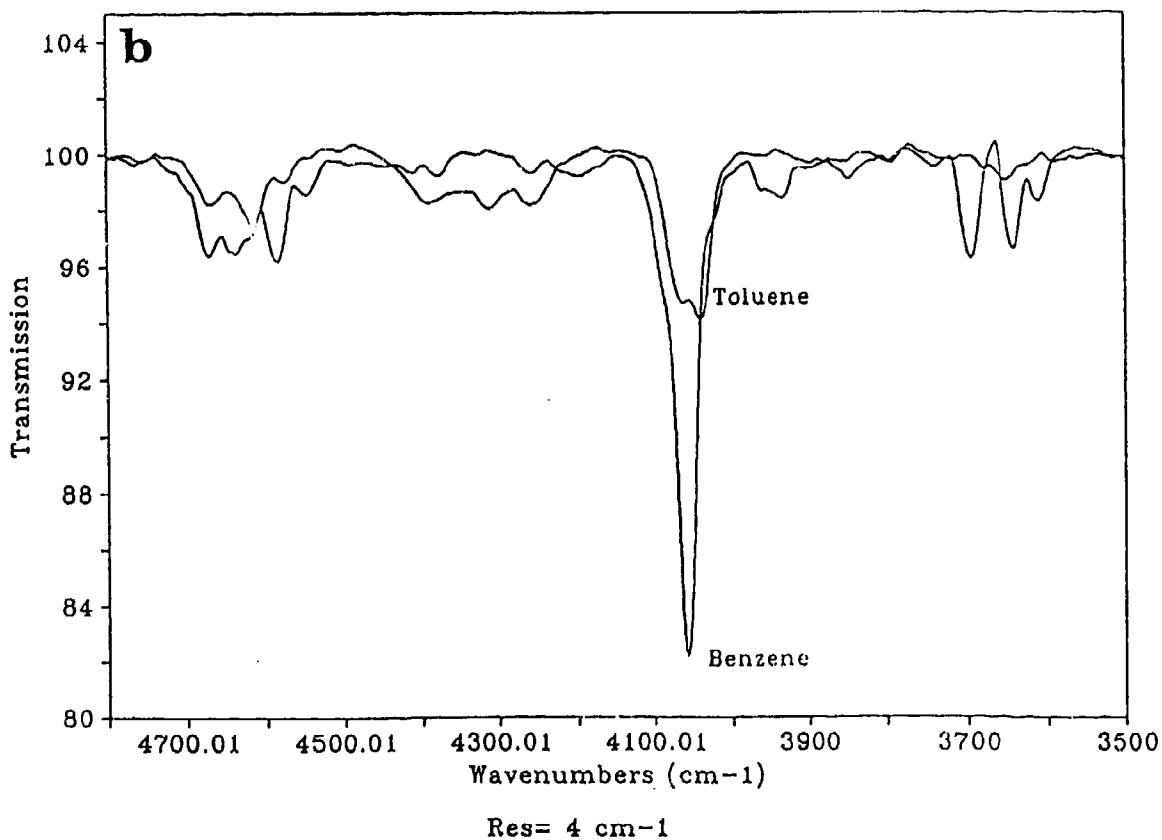
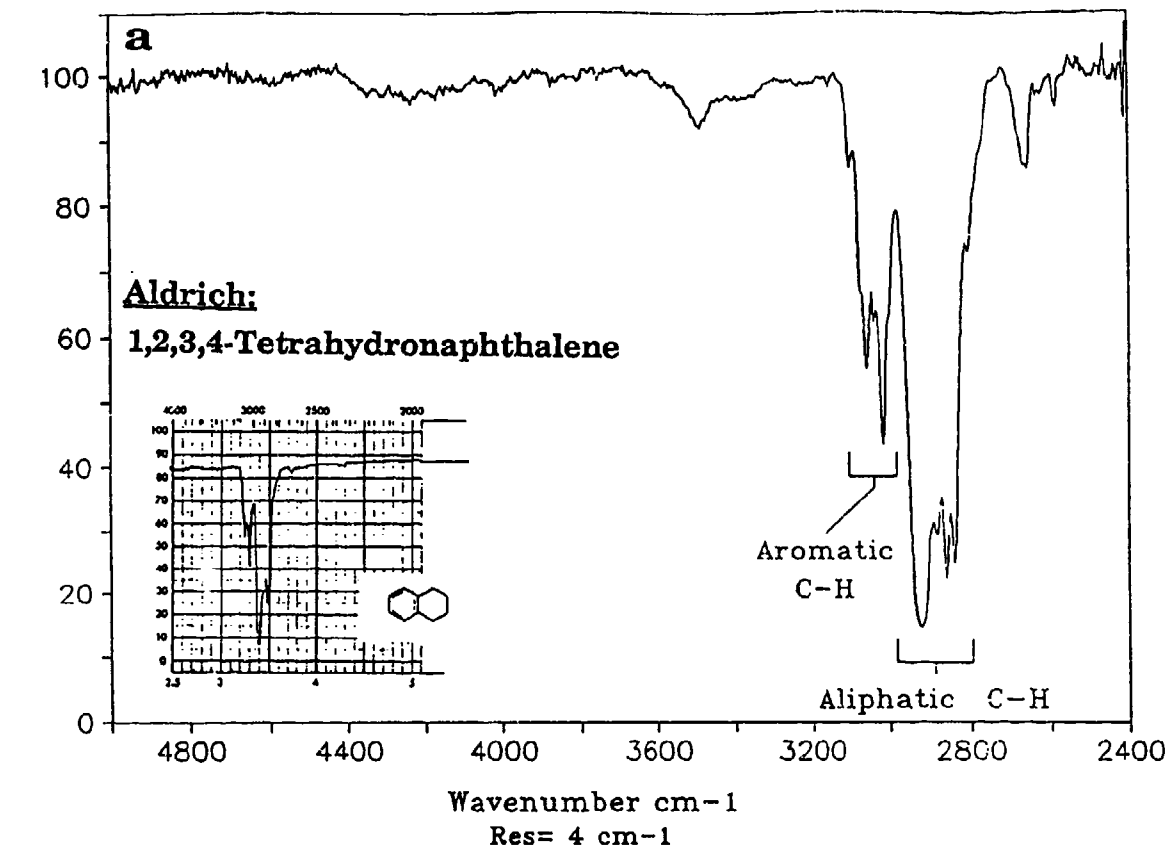


Figure 4.3-9. a) Tetralin Infrared Spectra from F-O/ATR Spectroscopy Compared with Aldrich Library Spectra; b) Absorption Bands from Harmonic Overtones of Benzene and Toluene (63).

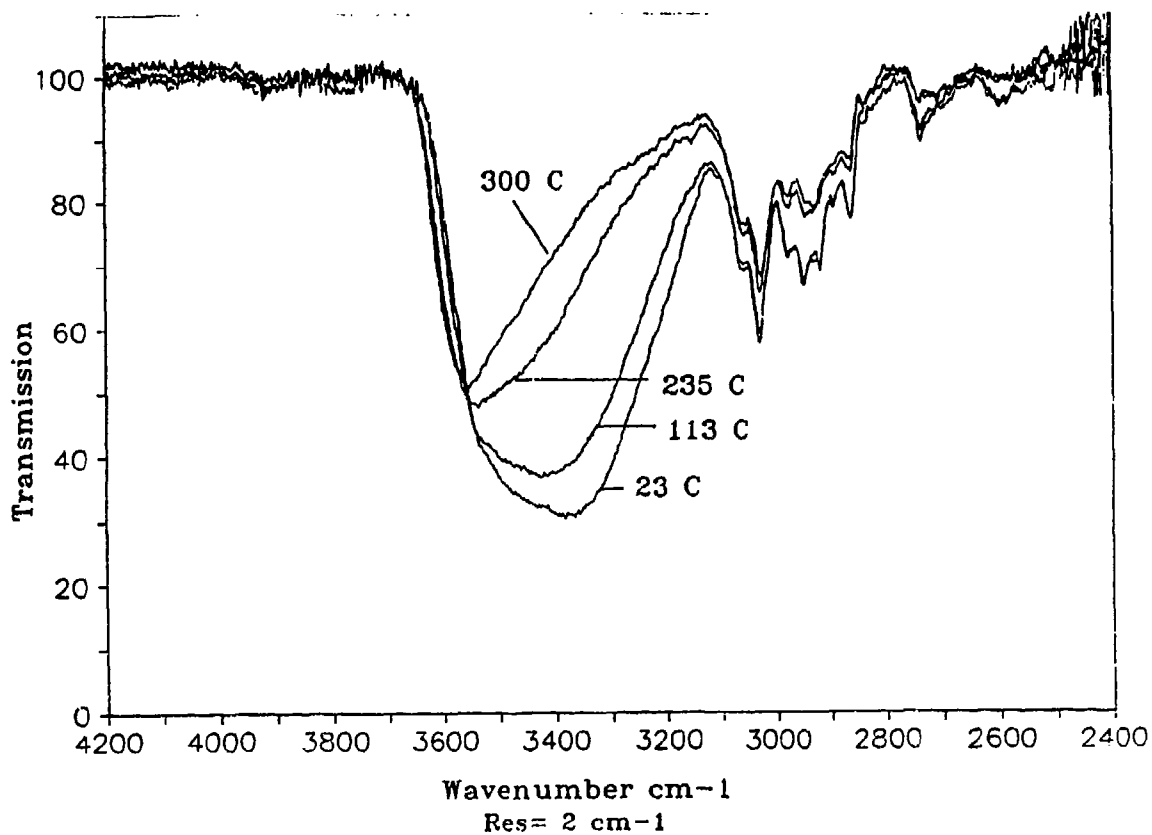


Figure 4.3-10. The Transmission Spectra of o-Cresol from F-O/ATR Spectroscopy a Non-Isothermal Experiment (63).

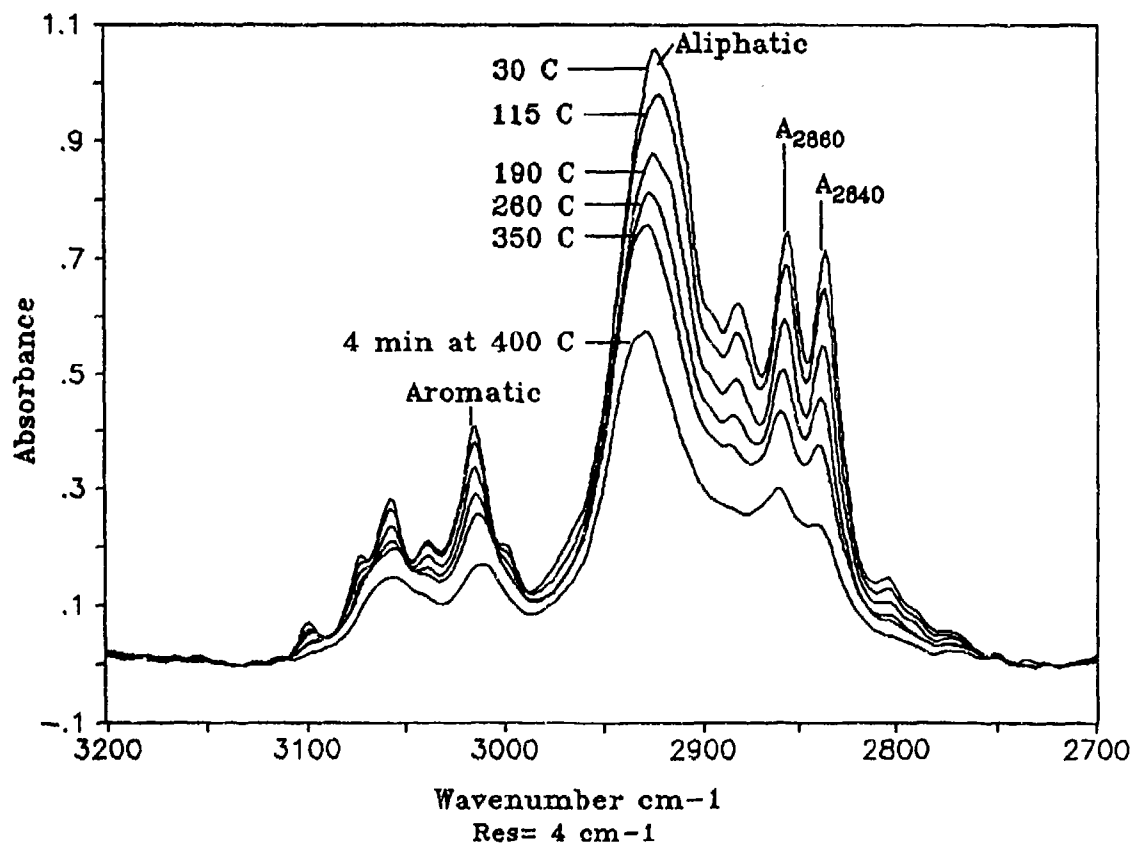


Figure 4.3-11. The Absorbance Spectra of Tetralin from F-O/ATR Spectroscopy in a Non-Isothermal Experiment (63).

the contributions of changes in the optical system with temperature must also be considered when interpreting spectral changes.

Nonisothermal experiments were also performed using tetralin in a previous study (63). Figure 4.3-11 shows the tetralin absorbance spectra in the C-H stretching region at different temperatures. Since tetralin does not contain oxygen functional groups, the focus of the analysis was on the C-H stretching region. Since tetralin is nearly inert under these conditions, the reduction in absorbance is primarily due to the reduction in the penetration depth of the IR light with temperature. Consequently, it should be noted that the formation of a deposit layer from jet fuel on the sapphire will be superimposed on a general decline in absorbance in the case of a nonisothermal experiment.

Designing a Flow Cell for the QCM - The final design for the flow cell configuration is shown in Fig. 4.3-12. The primary constraint of the design is the need to use a 1/4 inch diameter tube fitting to connect the QCM to the advanced FSTS. In addition, since the flowing fuel must be exposed to the full length of the probe rod, and must then be allowed to exit the system, the final design had to incorporate the large central fitting shown in Fig. 4.3-12. This fitting is designed to provide the fuel with a flow path of nearly constant cross sectional area so that a constant flow rate and pressure can be maintained. Both the fuel entrance and exit ports are part of the male half of the fitting, while the probe rod is rigidly welded onto the mating section. The two sections are sealed with a soft copper gasket and knife edges on both mating halves. The removable probe rod section also provides a mount for the crystals. Because the entire length of the QCM (probe rod and crystals) is supported at only the single node within the fitting, the preferred mounting orientation for this instrument is vertical. Operation in a horizontal position should be possible provided that the undue strain on the welded node joint can be avoided. In future designs, a second support point could be located along the probe rod at one of its other nodal positions. The new method of attaching the probe rod nodal point to the support structure should eliminate the shear stresses that resulted in failure of the earlier prototype device.

The stability of the QCM detector was tested by reviewing it overnight and monitoring the frequency. Figure 4.3-13 shows the data from this run. As can be seen, the frequency was remarkably constant over this period. For a short while (after about 5 hours runtime) the data acquisition system quit for an unknown reason. There was also one data point corresponding to a very high frequency. Except for these glitches, the system worked remarkably well under isothermal conditions at room temperature. Data from a run in which the QCM was tested with heated air is shown in Fig. 4.3-14. The frequency of the QCM decreased upon heating and the system operated quite smoothly during this run. Unfortunately, with the current system, the probe could not be heated much above 100 °C with only air flowing. As shown below, in the presence of flowing fuel, the probe could be heated to above 350 °C.

Summary

The fiber optic probe and the QCM were integrated into the FSTS. The F-O/ATR spectroscopy system using a sapphire fiber as a sensor was discussed. From theory, it was concluded that the depth of penetration of an evanescent wave into the sample decreases with temperature, which would cause a corresponding decrease in the infrared absorbance. It was previously found that the infrared transmittance attenuation in a sapphire fiber varies with temperature and wavenumber.

Spectra in air at different temperatures were taken and served as backgrounds for other experiments. The ability of F-O/ATR spectroscopy to obtain reliable chemical information was demonstrated by the excellent agreement between spectra obtained from a similar test cell for

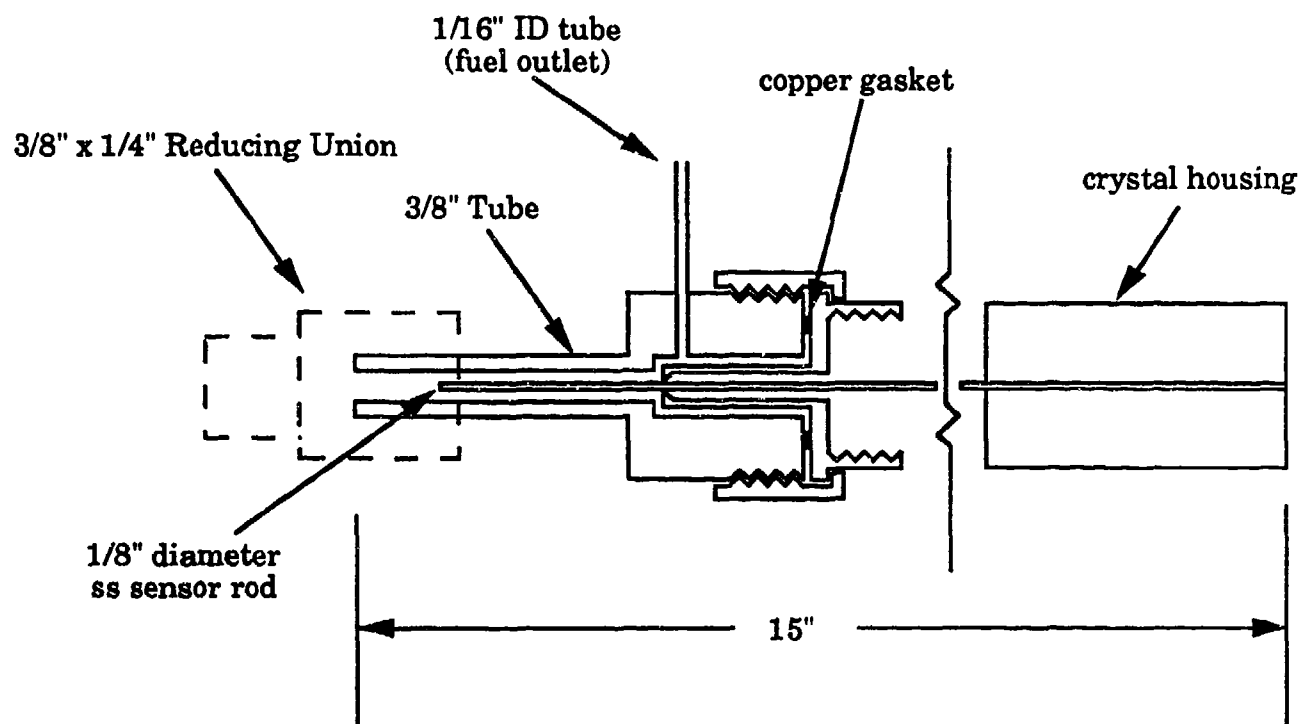


Figure 4.3-12. Outline drawing of the QCM flow cell mounting configuration.

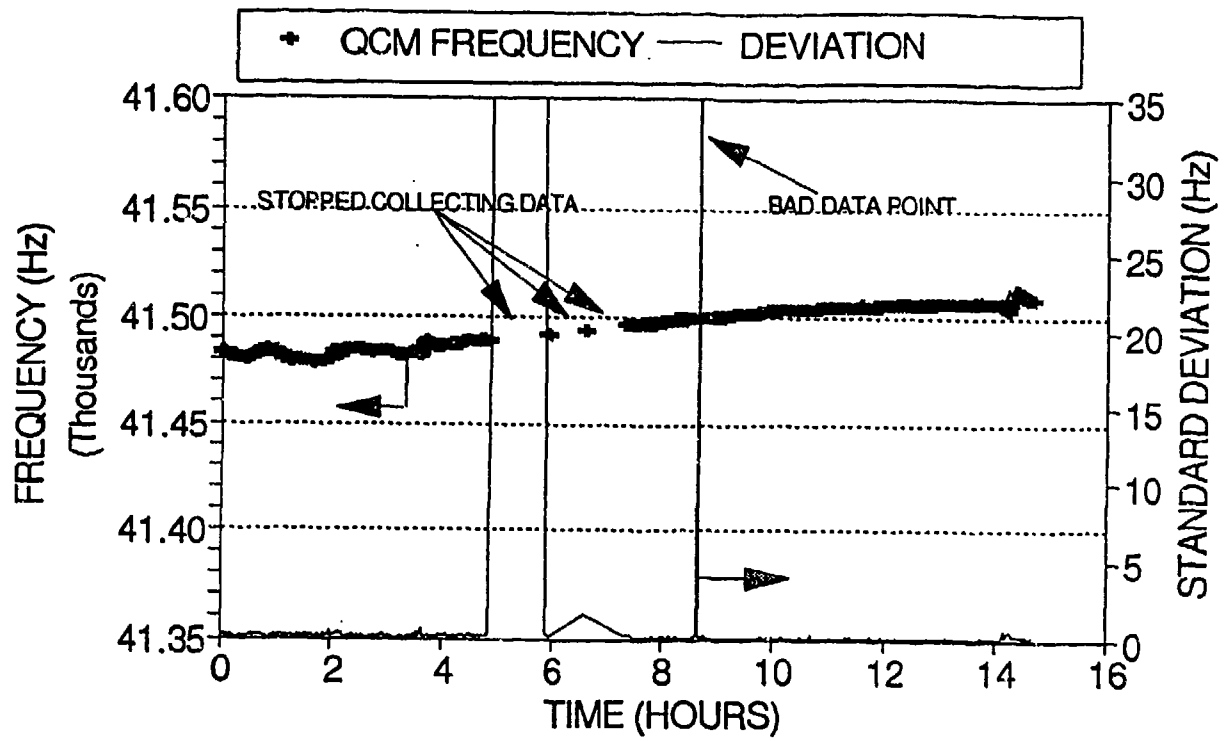


Figure 4.3-13. QCM Frequency Data from an Overnight Test Run at Ambient Temperatures.

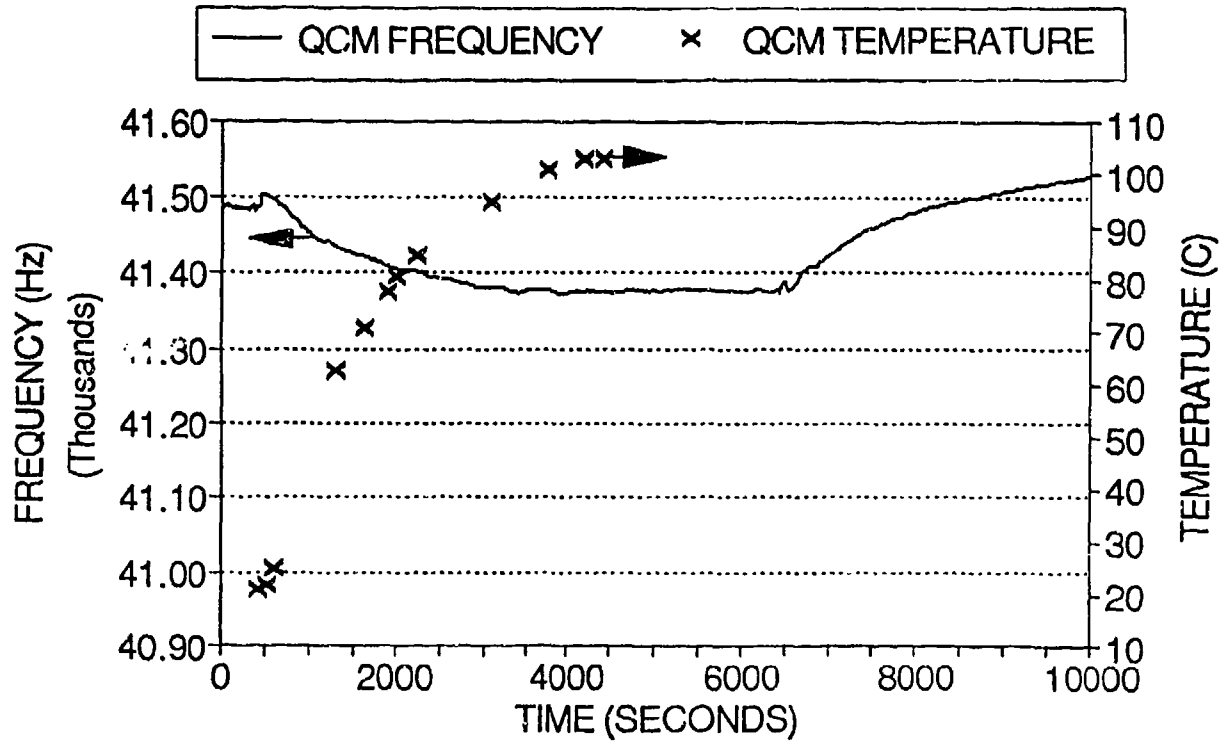


Figure 4.3-14. Data from a Test Run with Heated Air Flowing Over the QCM Probe.

benzene, toluene, o-cresol, benzylmethylamine, and tetralin and standard reference spectra. The results for non-isothermal experiments for o-cresol and tetralin show that sapphire F-O/ATR spectroscopy can monitor chemical reactions in-situ over a wide range of temperatures and at relatively high pressures (500-700 psig).

The flow version of the QCM was tested in air and was found to be fairly stable in flowing air at room temperature and at temperatures of about 100 °C.

4.4 Task 4 - Demonstration of the Advanced FSTS Over a Range of Fuel Stressing Conditions

Objective

Demonstration of the ability of the improved FSTS to monitor surface deposits formed from jet fuel by doing experiments over a range of fuel stressing conditions.

Methodology

FT-IR Based Deposit Monitors - Two different jet fuels were thermally stressed over a range of conditions. The fuel's thermal stability was monitored at different temperatures by obtaining fiber optic and circle cell spectra.

Sun Jet A-1 and Shell Jet A were the fuels tested. Both fuels were obtained from the Air Force. Based on JFTOT test data, the break point of the Sun fuel was 332 °C while the break point of the Shell fuel was 266 °C. Since the jet fuels have significantly different thermal stabilities, the advanced FSTS can be evaluated based on its ability to differentiate between a "stable" and an "unstable" fuel.

The jet fuel thermal stability experiments were performed by initially obtaining fiber optic and circle cell spectra of the unstressed fuel. The fuel was then thermally stressed by heating the fiber optic probe to 100 °C. After the fiber optic probe was at 100 °C for 15 to 30 minutes, fiber optic spectra were obtained of the hot fuel. The translational table was then energized in order to move the circle cell into the focus of the infrared beam. Circle cell spectra were obtained at ambient temperature of the unfiltered fuel, and also of the fuel filtered of insoluble gums greater than two microns in size. A minimum of two times the circle cell volume (6 ml) was pumped through the circle cell in between obtaining the filtered and unfiltered fuel spectra. The reactor tube temperature was increased in 50 °C intervals and data obtained using the above procedure. Due to the pressure limitations of the current system, the test sequence was concluded at 500 °C.

In addition, a series of fiber optic tests were conducted in which the fuel was thermally stressed to different temperatures and then cooled to room temperature. Fiber optic spectra were obtained before and after thermally stressing the fuel. By using this test procedure, the fiber optic data did not have to be corrected for the temperature dependence of the penetration depth.

The fiber optic spectral data was analyzed by examining the absorbance of the aliphatic C-H stretching region from 2850 cm^{-1} to 2960 cm^{-1} . The composition of the fuel and/or deposit was calculated by curve resolving the CH_3 peaks at 2873 cm^{-1} and 2955 cm^{-1} , the CH_2 peaks at 2854 cm^{-1} and 2921 cm^{-1} , and the CH peak at 2895 cm^{-1} . To determine if the initial deposits were unbranched aliphatic hydrocarbons (wax), the CH_2/CH_3 ratio was calculated at different temperatures. Also, the aromatic C-H stretching peak at 3030 cm^{-1} was compared to the aliphatic peaks to determine if the deposits were becoming more aromatic at the higher temperatures. The

circle cell measured the bulk fuel composition. Changes in the OH, aliphatic, olefin, and aromatic constituents were calculated by subtracting the raw fuel from the stressed fuel spectra.

QCM - QCM measurements were made using a flow cell connected to a heated tube. The dimensions of the tube were the same as those of the one used with the fiber optic probe detector. Tests were conducted with N₂ sparged and aerated jet fuels (Shell Jet A and Sun Jet A-1) under similar conditions of fuel flow and temperature as were used for the tests with the FT-IR probe. The frequency of the QCM was monitored as the flowing fuel was gradually heated. Temperatures of the reactor wall near the center of the tube and near the QCM probe were also monitored.

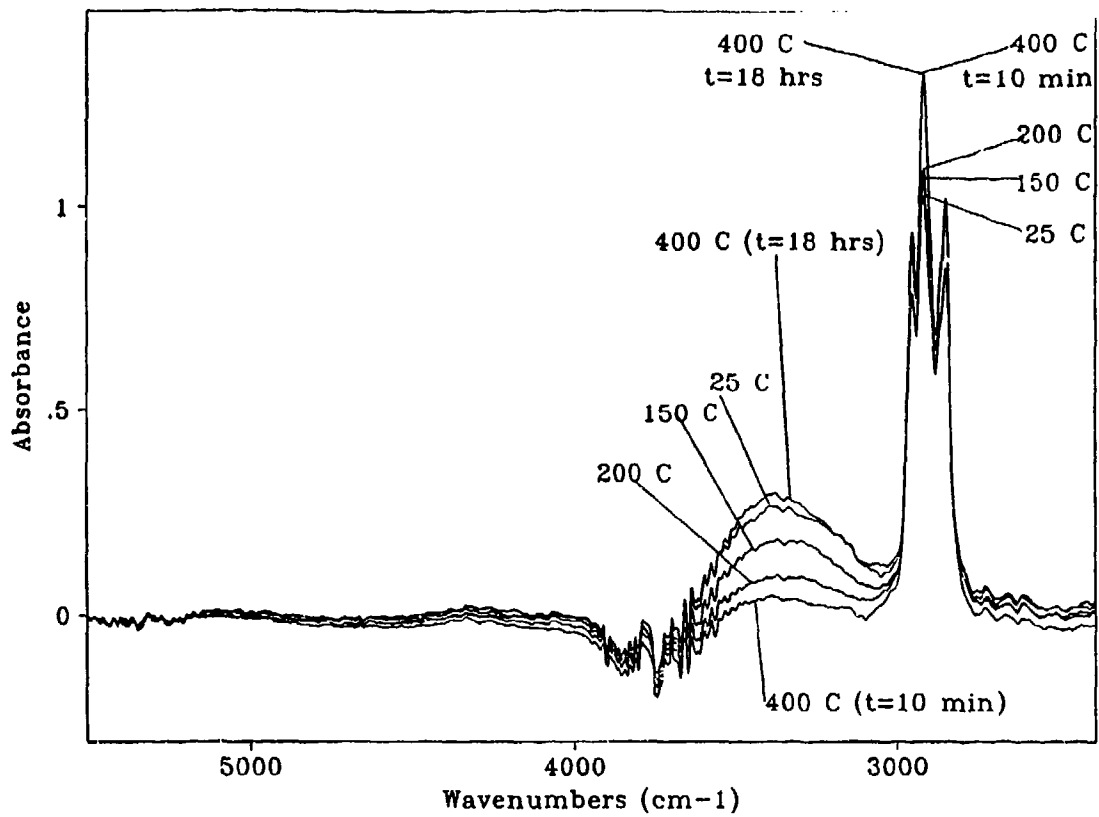
Results

The fiber optic and the QCM probe were designed to measure the mass and composition of the surface deposits at high temperature and pressure while the circle cell monitors the changes in the bulk fuel composition. Together these diagnostic instruments monitor the thermal degradation of the jet fuel and can determine fuel stability as well as provide a better understanding of the chemistry that results in the surface deposits.

The results of the fiber optic probe, circle cell, and QCM probe will be discussed in this section. The temperatures reported are of the control thermocouple which was located 5 1/2 inches from the fuel inlet on the outside wall of the reactor tube. In the previous section, the wall temperature profile and jet fuel temperature profile at different control thermocouple temperatures were discussed and presented in Fig. 4.3-3.

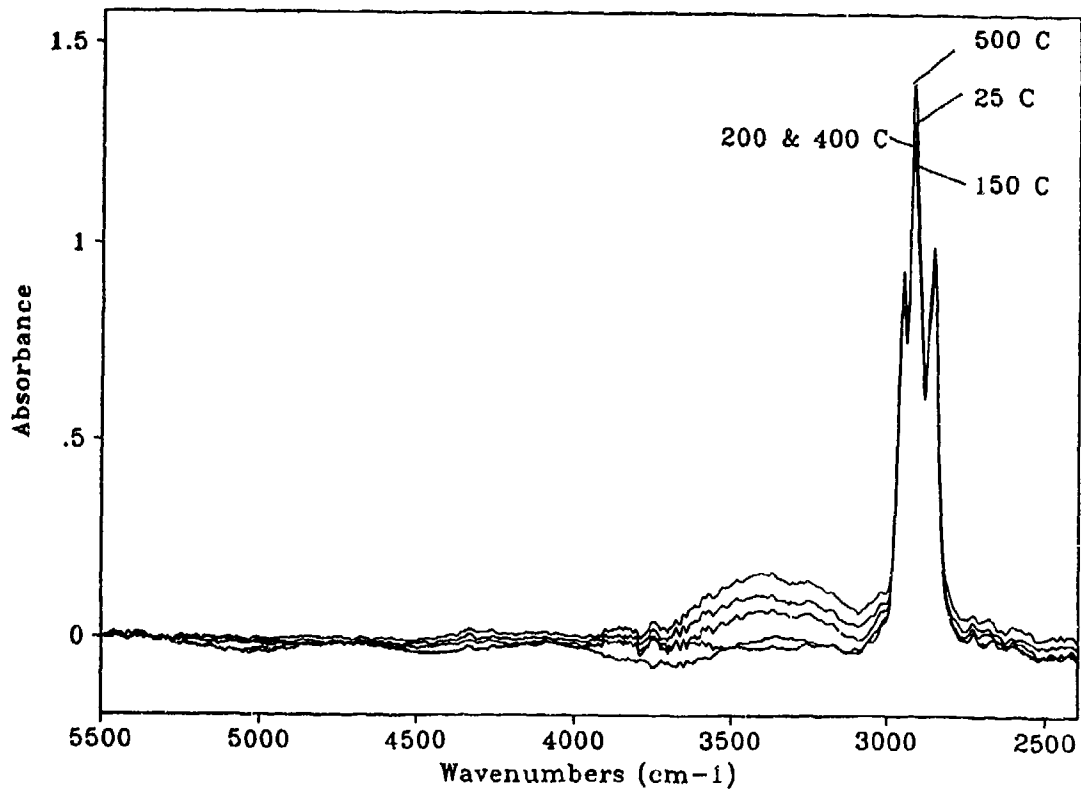
Fiber Optic Probe - It was discussed in the previous section that the degree of infrared attenuation in an internal reflection element varies with temperature. The observed absorbance is a product of the extinction coefficient (ϵ), the penetration depth (d_p), and the concentration, all of which vary with temperature. Initially, to remove the temperature dependence, a series of experiments was conducted in which the fuel was thermally stressed and then cooled to room temperature. The composition of any surface deposits was determined by comparing the room temperature spectra of the fuel before and after the thermal stressing. Figures 4.4-1 and 4.4-2 present the room temperature absorption spectra of the Shell and Sun fuels after various degrees of thermal stressing. In Figs. 4.4-3 and 4.4-4, the aliphatic C-H stretching region has been enlarged. For the Shell fuel, an aliphatic deposit began to form on the surface of the fiber at 150 °C and continued to grow as the fuel was heated to higher temperatures. Conversely, absorbance in the hydroxyl region decreases with increasing thermal stress temperature. To verify that the increase in the aliphatic C-H stretching was not due to displacement of the hydroxyl species (e.g., H₂O), the room temperature absorption spectra of the Shell fuel was obtained both 10 minutes and 18 hours after being thermally stressed at 400 °C. Since the aliphatic C-H absorption remained constant while the OH absorption returned to its unstressed value, it was concluded that the increase in the C-H absorption was due to a deposit. In contrast, the Sun fuel absorption remained almost constant. The aliphatic absorption only started to increase after being thermally stressed at 500 °C for 30 minutes.

In order to determine the composition of the aliphatic region, the CH, CH₂, and CH₃ peaks were curve resolved. From reference libraries (68), the CH peak is located at 2895 cm⁻¹, the CH₂ peaks are located at 2854 cm⁻¹ and 2921 cm⁻¹, and the CH₃ peaks are located at 2873 cm⁻¹ and 2955 cm⁻¹. The curve resolving is accomplished by adding absorption peaks with Gaussian shapes and variable positions, widths, and heights. As an example, the curve resolving of the unstressed Shell fuel is presented in Fig. 4.4-5. Since the absorption spectra were obtained at the same temperature, the absolute absorbances of these peaks can be compared and are shown in Fig. 4.4-6. The total CH₂ absorbance was calculated by summing the CH₂ absorbances at 2854 cm⁻¹



Res= 4 cm⁻¹

Figure 4.4-1. Shell Fuel Sapphire FT-IR/ATR Absorption Spectra After Thermal Stressing to Various Temperatures.



Res= 4 cm⁻¹

Figure 4.4-2. Sun Fuel Sapphire FT-IR/ATR Absorption Spectra After Thermal Stressing to Various Temperatures.

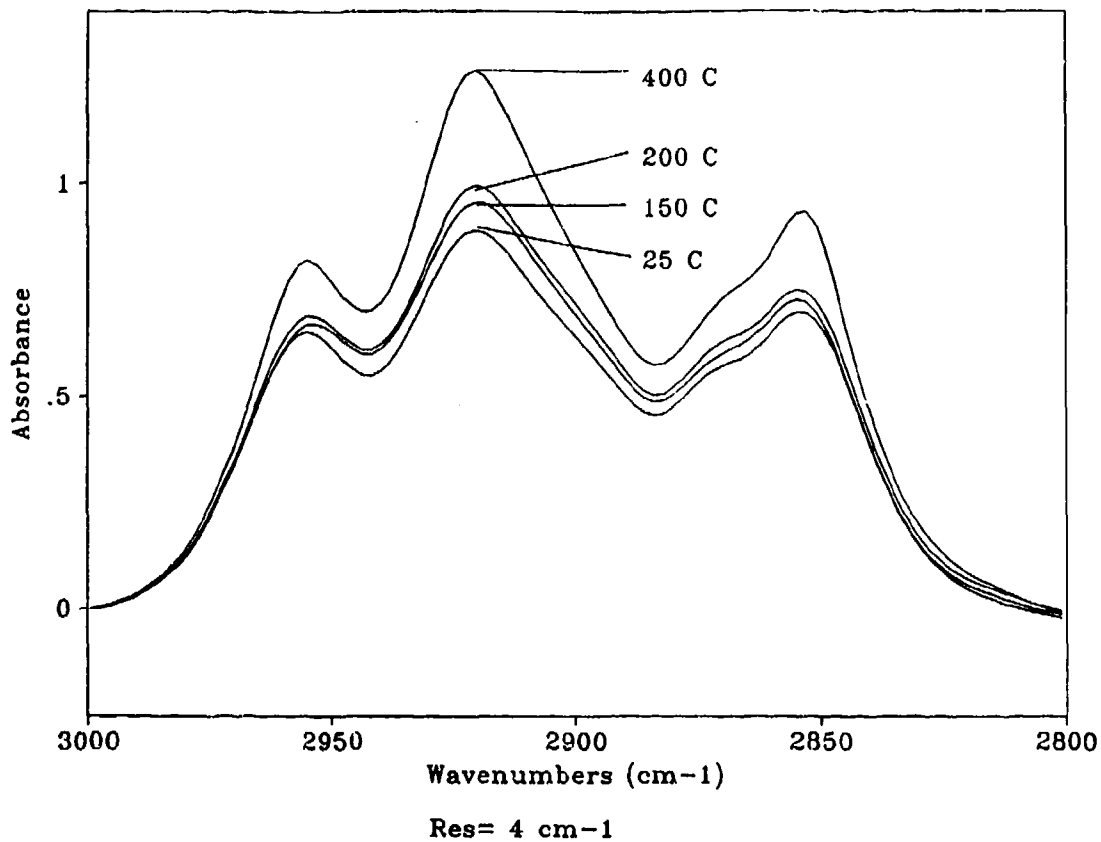


Figure 4.4-3. Shell Fuel Sapphire FT-IR/ATR Absorption Spectra for Aliphatic Region After Thermal Stressing to Various Temperatures.

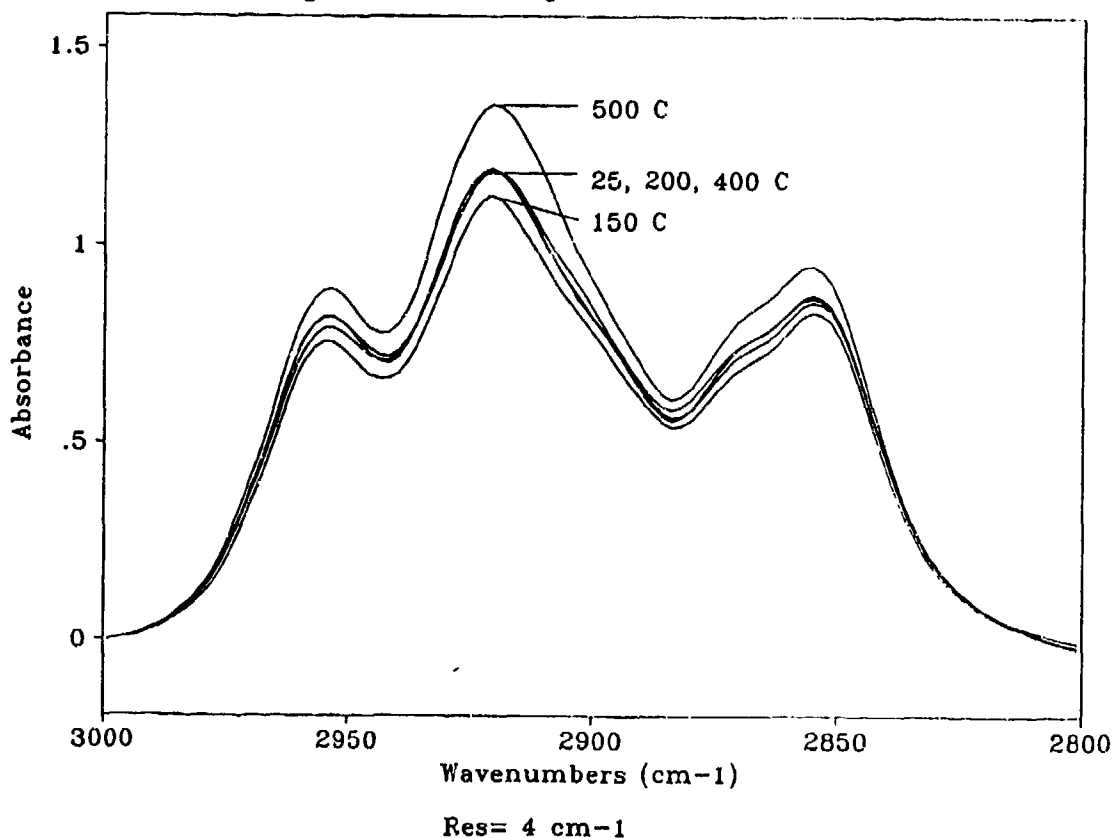


Figure 4.4-4. Sun Fuel Sapphire FT-IR/ATR Absorption Spectra for Aliphatic Region After Thermal Stressing to Various Temperatures.

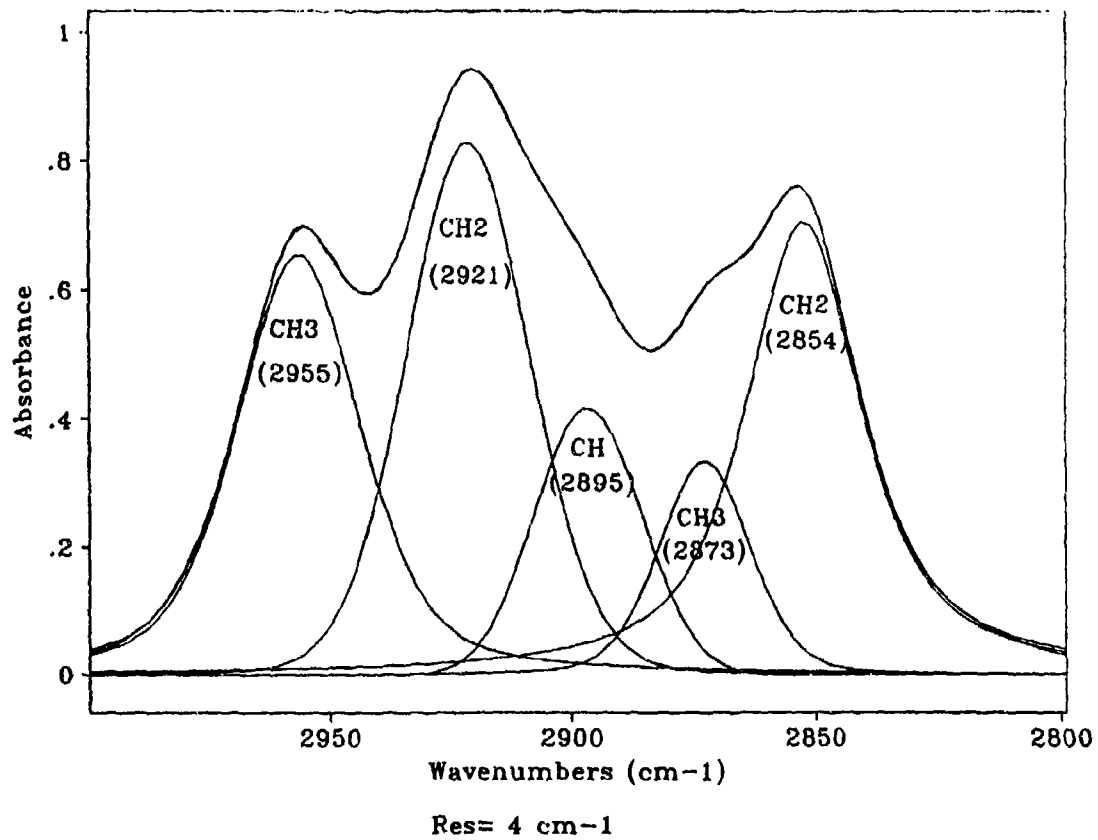


Figure 4.4-5. Curve Resolving of the Shell Fuels CH, CH₂ and CH₃ Peaks.

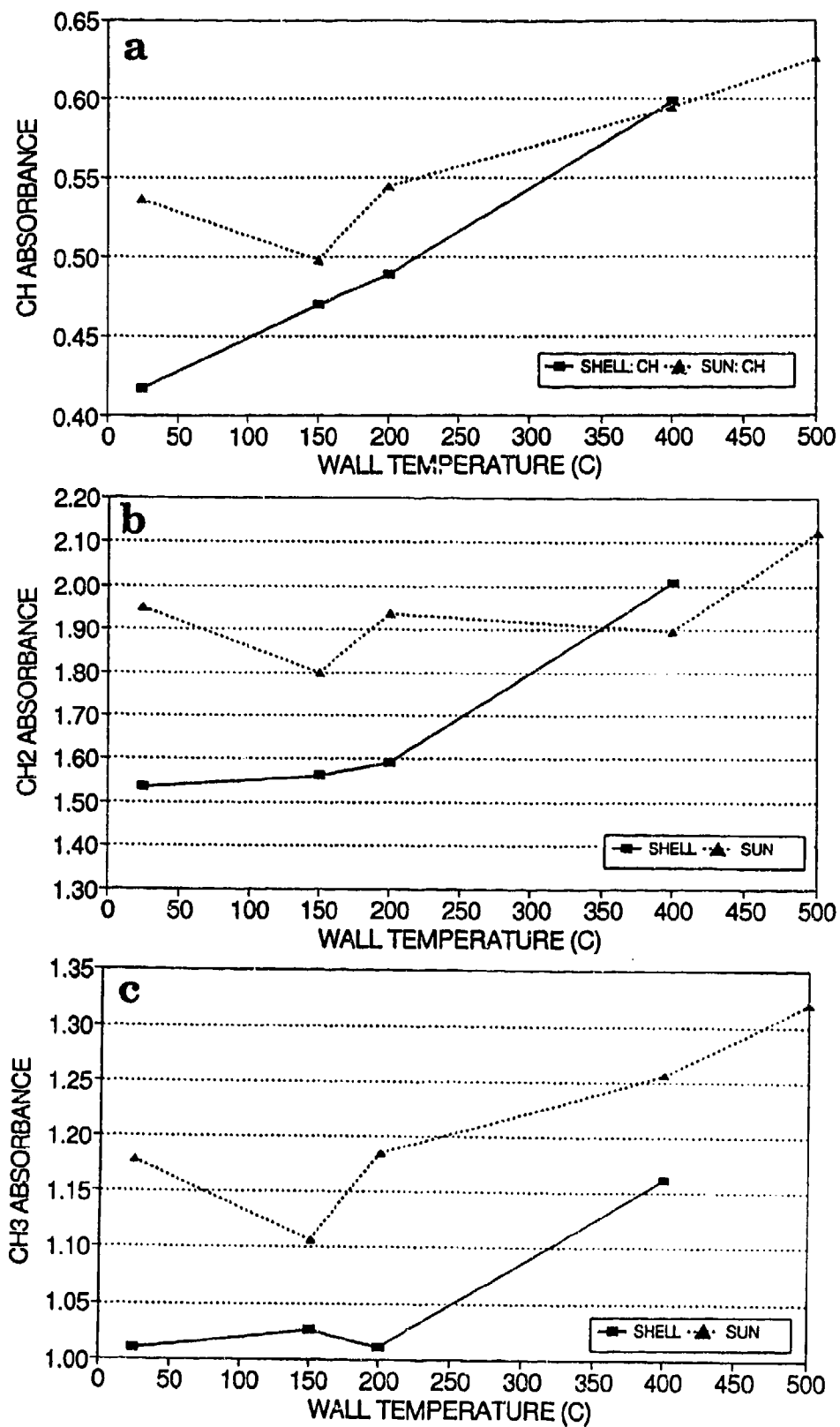


Figure 4.4-6. Sapphire FT-IR/ATR Absorbance Data for Two Fuels Stressed to Various Temperatures. a) CH; b) CH₂; c) CH₃. Results Based on Analysis of Room Temperature Spectra after Stressing to Indicated Temperature.

and 2921 cm^{-1} . This additive technique was assumed to be valid since the $2921\text{ cm}^{-1}/2854\text{ cm}^{-1}$ ratio remained within 4% of the value for the unstressed fuel. Likewise, the total CH_3 absorbance was calculated using the same procedure since the $2955\text{ cm}^{-1}/2873\text{ cm}^{-1}$ ratio remained within 10% of the value for the unstressed fuel. The major difference between the two fuels was that the Shell fuel CH_2 absorbance increased significantly from $200\text{ }^\circ\text{C}$ to $400\text{ }^\circ\text{C}$ while the Sun fuel CH_2 absorbance was constant (Fig. 4.4-6b).

To determine the change in the relative composition of the Shell fuel deposit versus the unstressed fuel, the percent change in the CH_2/CH_3 ratio was calculated for both fuels and is presented in Fig. 4.4-7. The increase in the CH_2/CH_3 ratio at $200\text{ }^\circ\text{C}$ for the Shell fuel indicates that the initial deposits were long, unbranched, aliphatic alkane hydrocarbons, i.e., waxes. The results are consistent with previous FSTS experiments using a wire deposit probe (17,18). The high molecular weight waxes which form deposits are a result of the fuel degradation reactions.

Due to the relatively small amounts which were produced on the previous wire probe tests, they are probably not produced from the main decomposition path of the fuel. One possibility is that the waxes arise from the radical termination reactions resulting from either the oxidative or pyrolytic free radical decomposition of the fuel. Schulz (38) has recently reported that hexadecane was the largest component of deposits produced from a surrogate JP-8 fuel, which supports the results of the current and previous study (17).

The same test sequence was repeated for the Shell fuel and the percent change in CH_2/CH_3 ratio is also plotted in Fig. 4.4-7. While the increase in the CH_2/CH_3 ratio was somewhat different at $400\text{ }^\circ\text{C}$, the overall trend was identical. Both tests indicated that a deposit was starting to form on the fiber between $150\text{ }^\circ\text{C}$ and $200\text{ }^\circ\text{C}$.

To verify that the changes in the aliphatic region were a result of surface deposits on the fiber optic, the reactor tube was purged with dry air after the fuels were thermally stressed at $500\text{ }^\circ\text{C}$. By purging the reactor tube, it was assumed that the volatile jet fuel would evaporate while the nonvolatile deposit would remain on the fiber. After drying the fiber, the Shell fuel had a large absorption in the aliphatic region. This peak corresponded to the same increase observed in the room temperature absorption spectra after the fuel was thermally stressed. The Shell fuel deposit was curve resolved and the CH_2/CH_3 ratio was 2.3 compared to 1.5 for the unstressed liquid fuel. Again, this indicated that the increase in CH_2/CH_3 was due to the deposit consisting of longer chain aliphatics than the unstressed fuel. For the Sun fuel, the fiber was nearly identical optically to the air reference obtained prior to the thermal stress experiment. Therefore, the Sun fuel did not produce a permanent surface deposit when exposed to the $500\text{ }^\circ\text{C}$ test conditions of the Advanced FSTS. Figures 4.4-8 and 4.4-9 are the initial and dried absorption spectra of the stressed Shell and Sun fuels, respectively.

Since a deposit was not formed on the fiber when stressing the Sun fuel under the Advanced FSTS test conditions, the changes observed in its spectral features were due to the decomposition of the bulk fuel. In the case of the Shell fuel, a wax deposit began to cover part of the sapphire surface at $150\text{ }^\circ\text{C}$. Since the fiber is not exposed to a uniform temperature, the fiber optic was measuring both changes in the composition of the fuel and the deposit. For phase II, the fiber optic probe will be redesigned so that the fuel exposed to the fiber is at a constant temperature. This can be done by creating an optical "window" in the middle of the probe.

This experimental procedure demonstrated that the fiber optic probe was sensitive to determining the composition of surface deposits and also being able to distinguish between a "stable" and an "unstable" fuel. The next set of experiments involved heating the fuel in $50\text{ }^\circ\text{C}$ intervals and

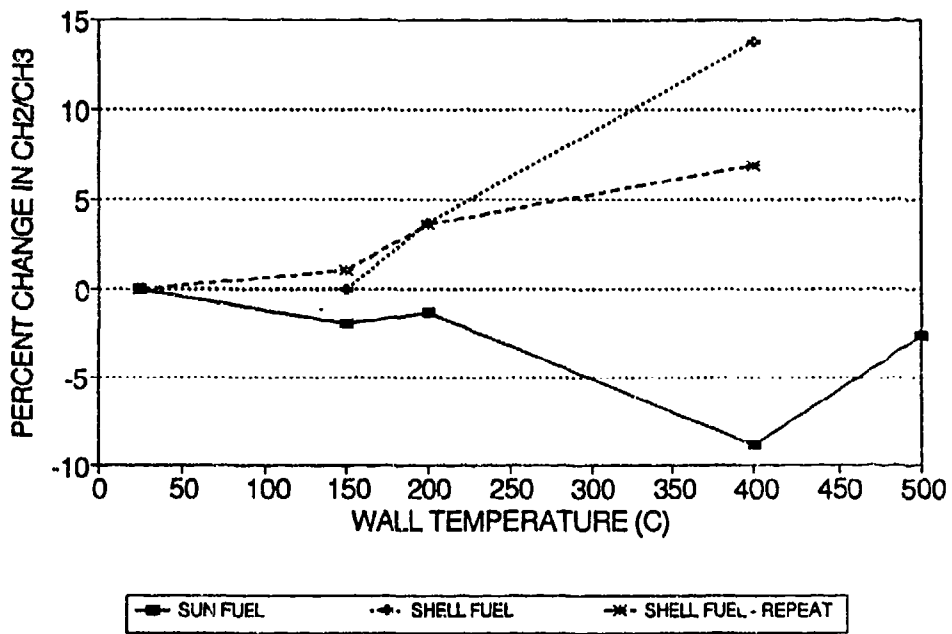


Figure 4.4-7. Percent Change in CH₂/CH₃ Absorbance Ratios for Shell and Sun Fuels Stressed to Various Temperature. Results Based on Analysis of Room Temperature Spectra after Stressing to Indicated Temperature.

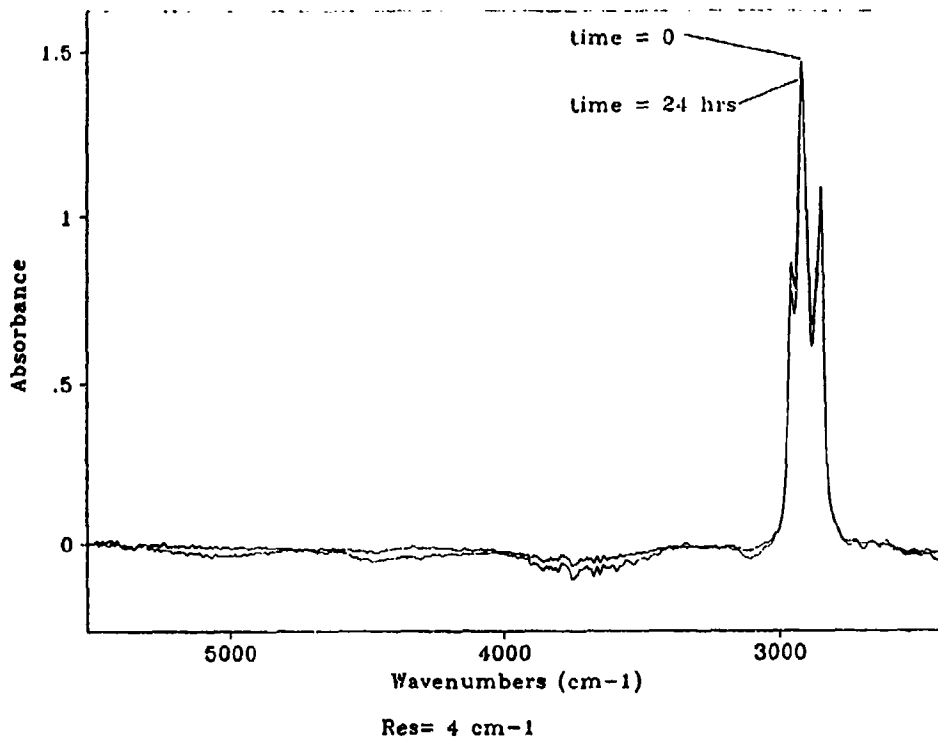


Figure 4.4-8. Comparison of Sapphire FT-IR/ATR Absorbance Spectra in Air after Exposing Fiber to Shell Fuel Stressed at Temperatures up to 500°C.

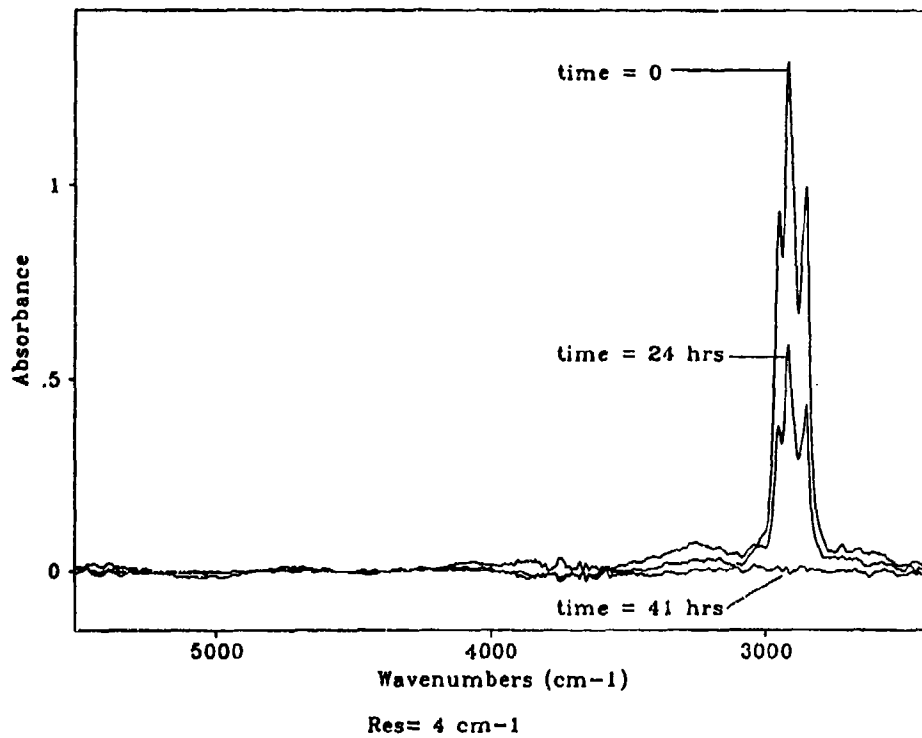


Figure 4.4-9. Comparison of Sapphire FT-IR/ATR Absorbance Spectra in Air after Exposing Fiber to Sun Fuel Stressed at Temperatures up to 500°C.

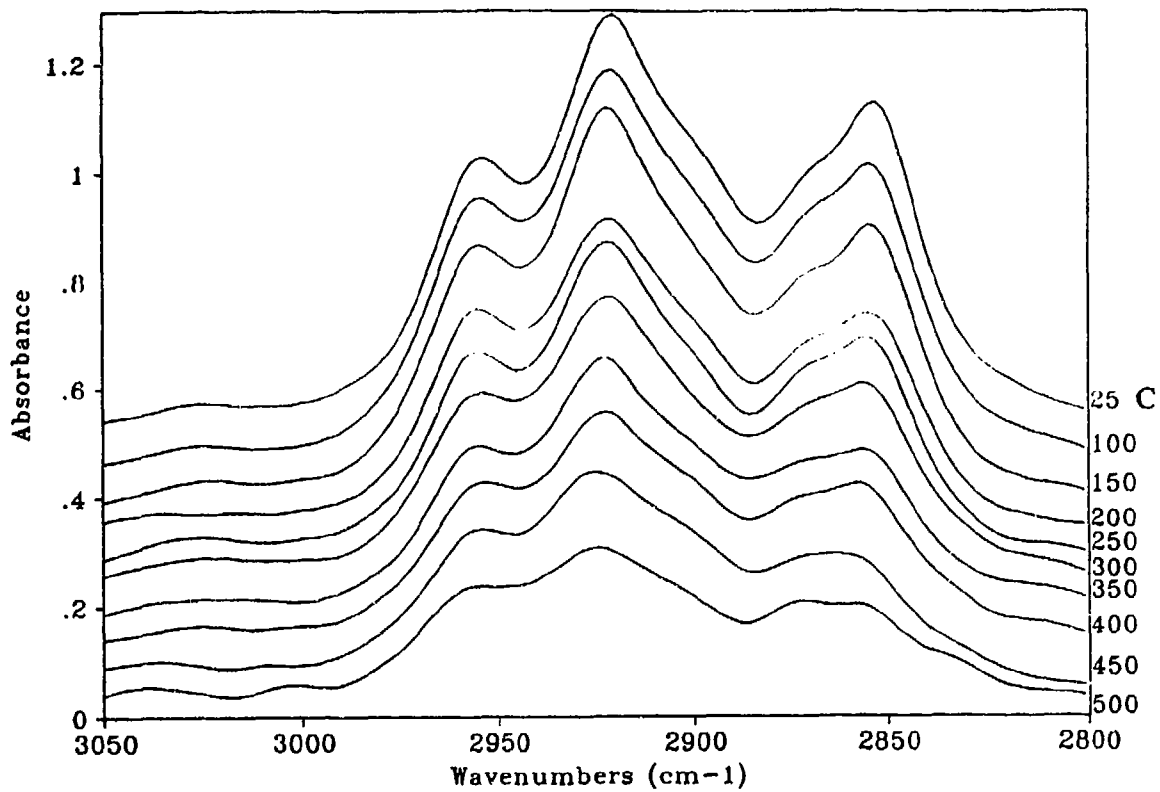
obtaining the spectra while the fuel was at temperature. This is the desired approach for a jet fuel thermal stability test instrument since it allows a more rapid and realistic assessment of the fuel stability.

Figures 4.4-10 and 4.4-11 are the absorption spectra at wall temperatures ranging from 25 °C to 500 °C for the Shell and Sun fuels, respectively. To remove the attenuation temperature dependence, the absorption spectra were calculated using air background spectra at the corresponding temperature. Due to the shorter penetration depth at higher temperatures, the absolute absorption spectra can not be directly compared. In phase II, the temperature dependence of the C-H stretching bands will be determined through calibration experiments in order to make a direct comparison. For phase I, the absorption spectra were analyzed by curve resolving the aliphatic C-H stretching peaks and comparing the CH₂/CH₃ ratio. The CH₂/CH₃ ratio at different wall temperatures is presented in Fig. 4.4-12. For the Shell fuel, the CH₂/CH₃ ratio increases from room temperature until 300 °C with a large increase observed between 150 °C and 200 °C. These data were consistent with the previous room temperature data. The reduction in the CH₂/CH₃ ratio from 300 °C to 450 °C was possibly a result of competing chemical reactions or could be a result of the approximations in the curve resolving procedure. Since the jet fuel was not at a constant temperature along the length of the fiber, the fiber optic was measuring both the wax formation on the cooler part of the fiber and the possible transformation or dissolution of the wax on the hotter part of the fiber. For the Phase II probe, the fiber optic will be redesigned so that the measurements are made in a small region of uniform temperature fuel. In the case of the Sun fuel, the CH₂/CH₃ ratio remained within 10% of the unstressed fuel during this test sequence, as shown in Fig. 4.4-12.

While the aromatic C-H stretching peak at 3030 cm⁻¹ was very small compared to the aliphatic C-H stretching peaks, the spectral data were analyzed to determine if the fuel was becoming more aromatic as it was thermally stressed. As with the aliphatic C-H stretching peaks, the absolute absorption of the aromatic C-H stretching peaks cannot be directly compared because of the reduction in penetration depth with temperature. Therefore, the region from 2800 cm⁻¹ to 3050 cm⁻¹ was curve resolved and the aromatic C-H stretching peak was ratioed to the aliphatic C-H stretching peaks. Figure 4.4-13 presents the aromatic to aliphatic ratio for both fuels. The ratio increased gradually from 25 °C to 400 °C with a definite increase in the aromatic composition of the fuel observed at the 450 °C wall temperature. For the Shell fuel, the wax deposit started to form on the fiber at 150 °C to 200 °C while an increase in the aromatic composition was observed at the 200 °C wall temperature. This ratio remains constant until 450 °C and then increases significantly. Consequently, it appears that changes in the aromatic absorbance at temperature are not as well correlated with the deposit formation processes since it is certainly affected by changes in the bulk fuel composition, as described below.

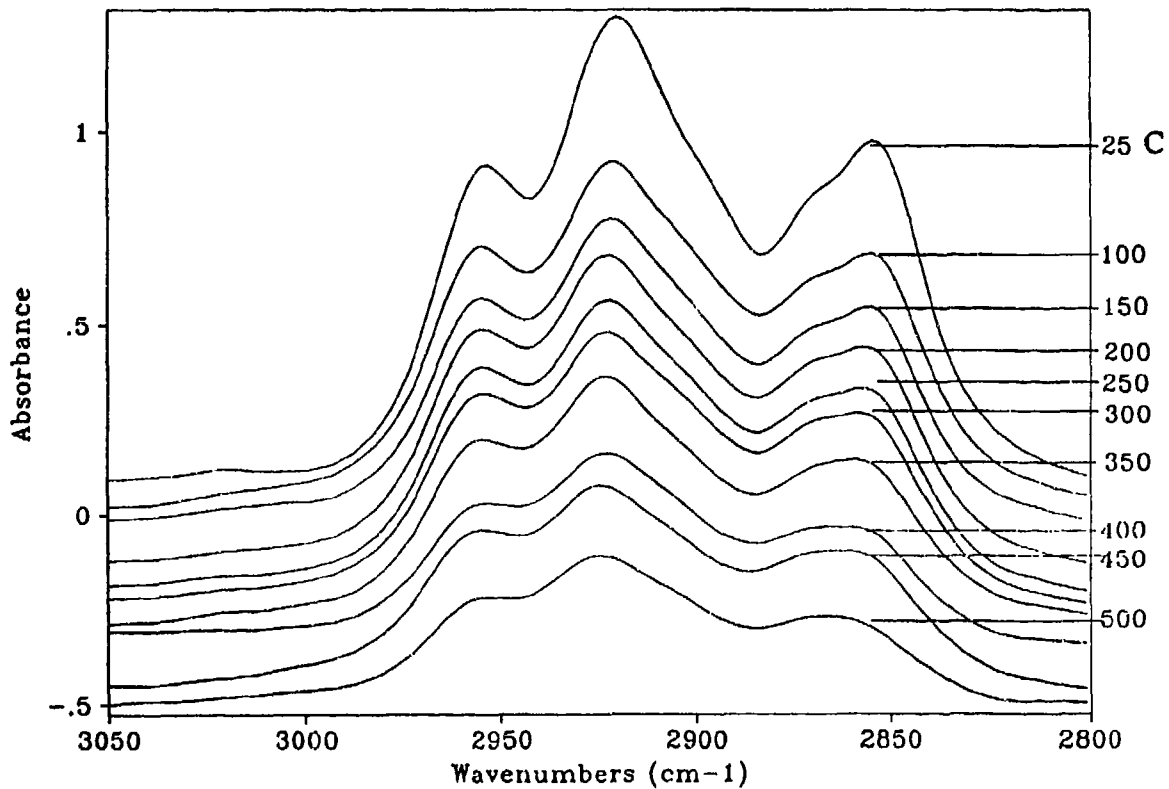
Circle Cell - The circle cell absorption spectra for the unstressed Shell and Sun fuels are shown in Fig. 4.4-14. Both fuels were primarily aliphatic, but also contained hydroxyl, alcohol, and aromatic groups. The filtered and unfiltered spectra of the Shell and Sun fuels after being thermally stressed at 500 °C are presented in Fig. 4.4-15. In addition to the spectral features observed in the unstressed fuel, the degraded jet fuel also contained olefins. Since the fuel was at reduced temperature and well mixed in the circle cell, these spectra represent the bulk fuel composition. The raw absorption spectra for all the experiments are in Appendix B.

The aliphatic peaks were curve resolved using the same procedure as described for the fiber optic probe. To determine if the deposit from the Shell fuel is a result of the primary fuel degradation reactions, the CH₂/CH₃ ratio was calculated and compared to the fiber optic data. Since the ratio



Res= 4 cm⁻¹

Figure 4.4-10. Absorption Spectra (at temperature) from Sapphire FT-IR/ATR Spectroscopy of Shell Fuel Stressed to Various Temperatures.



Res= 4 cm⁻¹

Figure 4.4-11. Absorption Spectra (at temperature) from Sapphire FT-IR/ATR Spectroscopy of Sun Fuel Stressed to Various Temperatures.

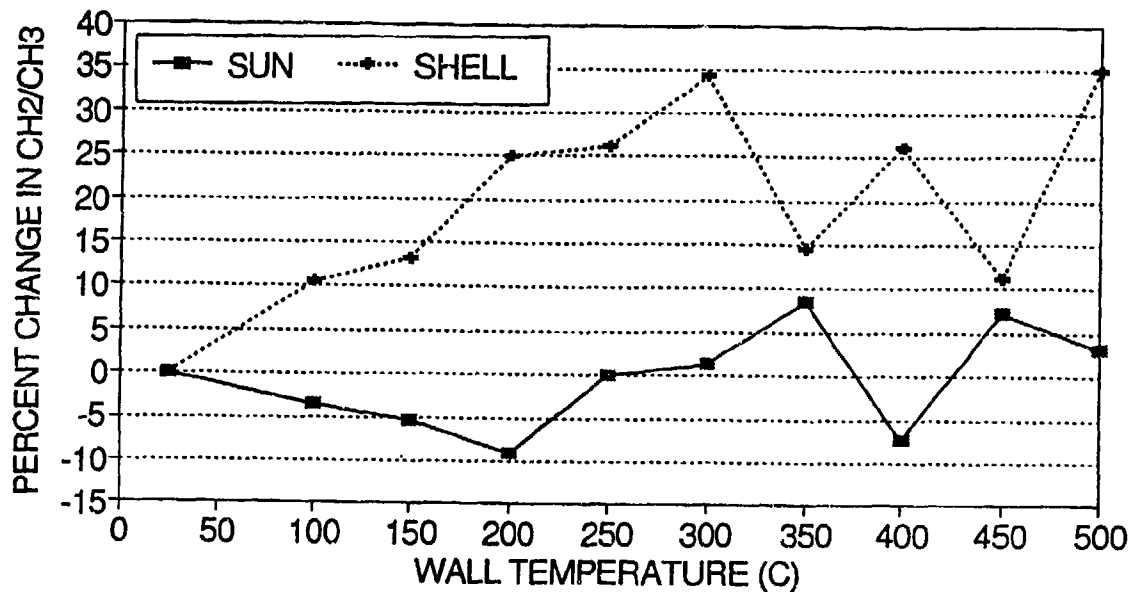


Figure 4.4-12. Comparison of Percent Change in CH₂/CH₃ Ratio from Absorbance Spectra (at temperature) from Sapphire FT-IR/ATR Spectroscopy of Shell and Sun Fuels.

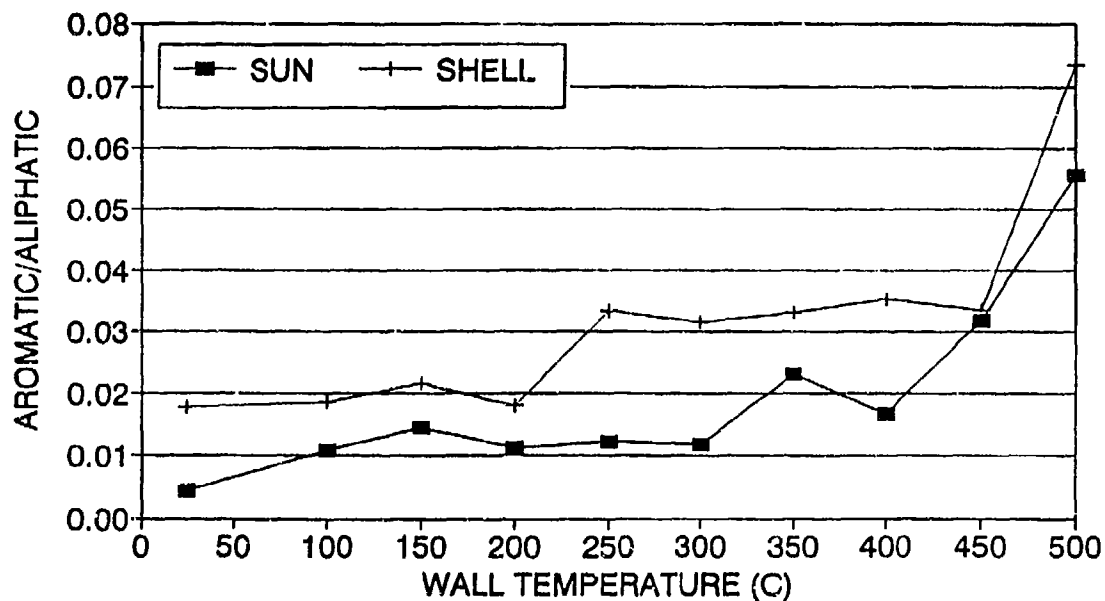
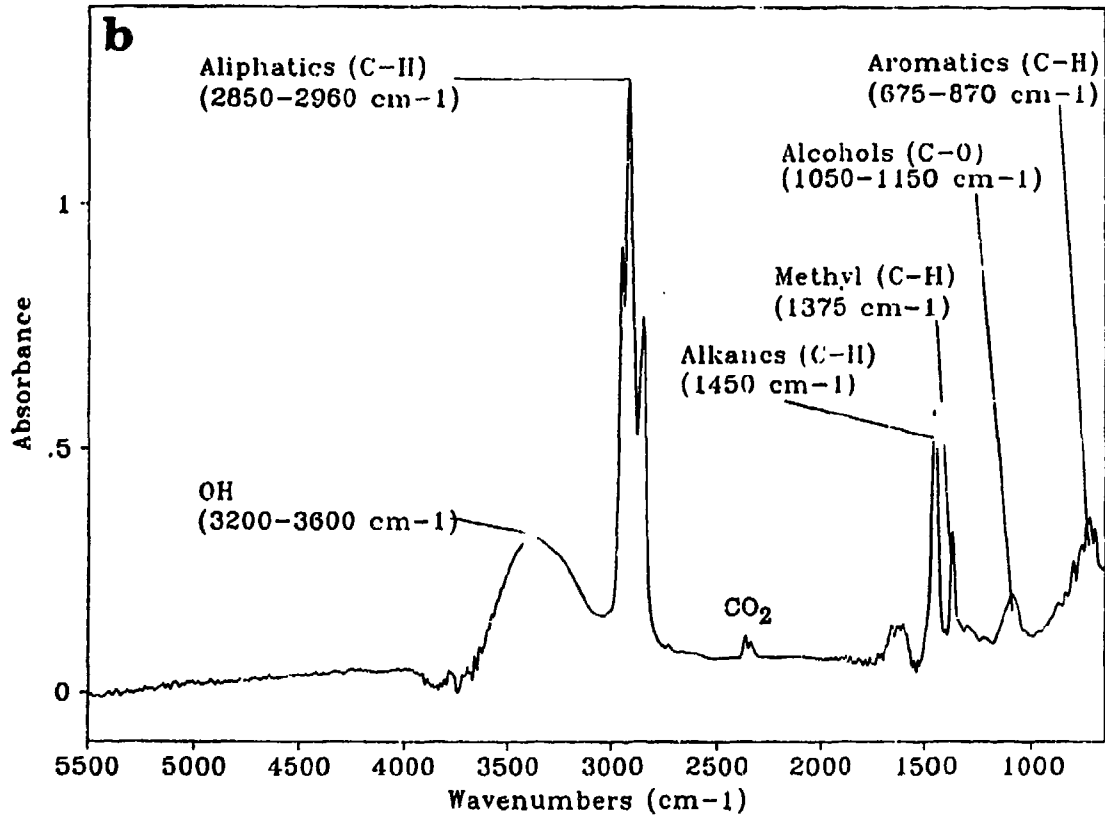
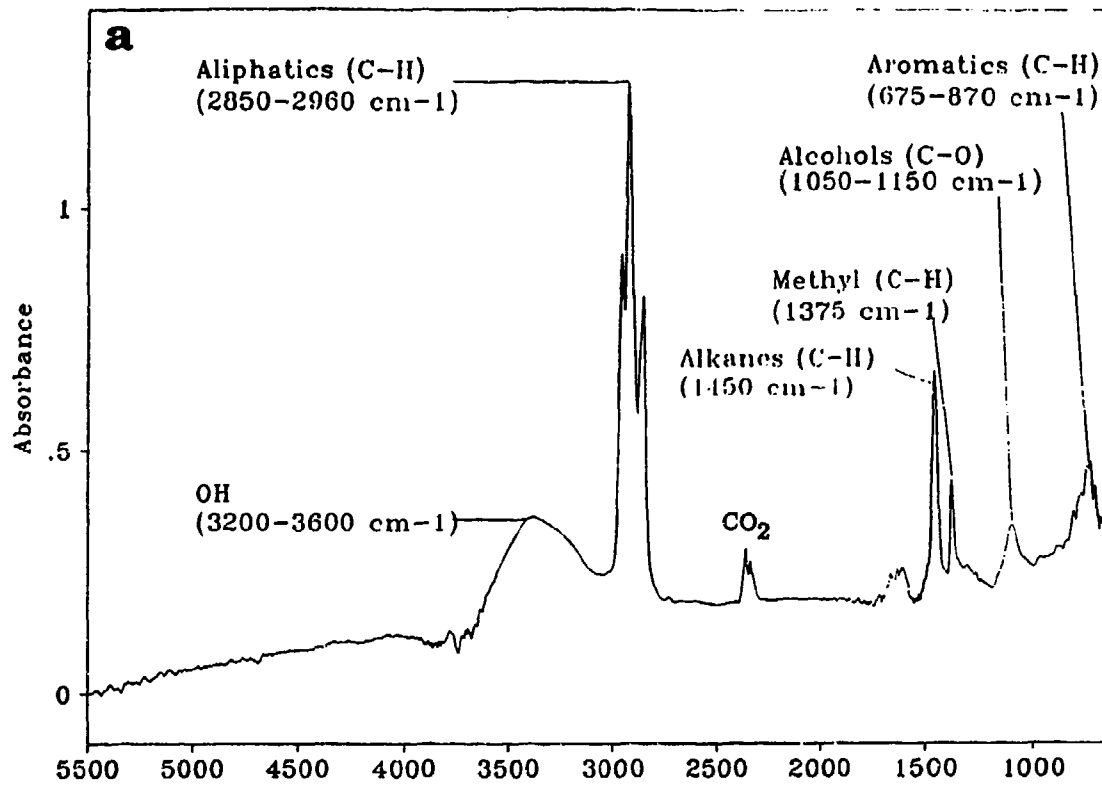


Figure 4.4-13. Comparison of Changes in Aromatic/Aliphatic Ratio from Absorbance Spectra (at temperature) from Sapphire FT-IR/ATR Spectroscopy of Shell and Sun Fuels.



Res = 4 cm^{-1}

Figure 4.4-14. FT-IR/ATR Absorption Spectra from Circle Cell for Unstressed Fuels. a) Shell Fuel; b) Sun Fuel.

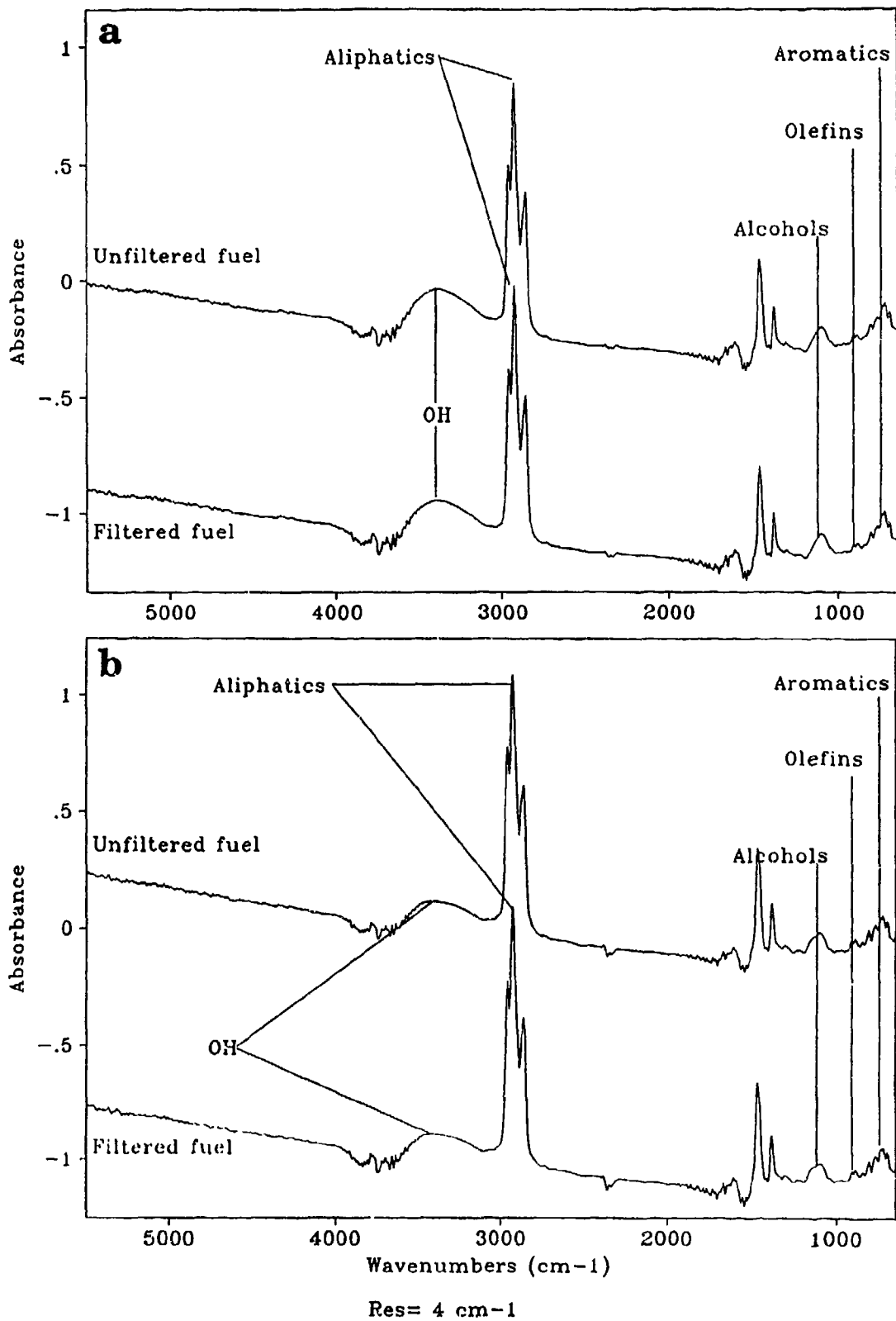


Figure 4.4-15. FT-IR/ATR Absorption Spectra from Circle Cell for Fuels Stressed at 500°C. a) Shell Fuel; b) Sun Fuel.

remained almost constant throughout the test sequence, the circle cell spectra of the bulk fuel composition indicated that the mechanism that resulted in a deposit was a side reaction. The CH_2/CH_3 ratio for both fuels is presented in Fig. 4.4-16.

The results of several prominent spectral features from the difference spectra (the raw fuel was subtracted out) are shown in Figs. 4.4-17 to 4.4-21. Results are presented with the filter on and filter off to indicate features which may be associated with the filtered insoluble gums. The difference spectra for all of the experiments are also given in Appendix B.

The olefin absorbances at 890 cm^{-1} and 910 cm^{-1} are shown in Figs. 4.4-17 and 4.4-18, respectively. The olefins started to appear in both fuels at $400\text{ }^\circ\text{C}$ and their concentration increased as the wall temperature was heated to $500\text{ }^\circ\text{C}$. Since both fuels behaved in the same manner when thermally stressed, the formation of olefins in a flow system was not an indication of whether a fuel will form a deposit.

There was little difference between the results for the filter on and filter off cases, which is consistent with the idea that the circle cell is reflecting changes in the bulk fuel composition. The small changes could be due to the removal of insoluble gums which may exist as suspensions in the fuel.

In Fig. 4.4-19, the height of the aromatic peak at 690 cm^{-1} is plotted versus temperature. An increased aromatic concentration was measured only for the Shell fuel at $500\text{ }^\circ\text{C}$ wall temperature. Again, the aromatic concentration of the unfiltered fuel was similar to the filtered fuel.

It should be noted that the circle cell results for both the olefin and aromatic absorbances (Figs. 4.4-17 to 4.4-19) indicate that the Sun fuel is also more stable with respect to bulk decomposition. The utility of the circle cell in an advanced FSTS will be in making the assessments for high temperature stability where bulk decomposition occurs. In addition, a comparison of spectral results between the two FT-IR ATR probes (fiber-optic and circle cell), after correcting for temperature differences and the differences in refractive indices can be used to determine if a deposit layer is being formed or whether both probes are measuring the bulk composition. This approach will be investigated in Phase II.

The results for changes in the OH absorption from circle cell spectra for the two fuels are shown in Fig. 4.4-20. These results may be influenced by the presence of water in the fuel and the affinity of the ZnSe crystal in the ATR cell for OH compounds. Consequently, additional work will be required before these trends can be interpreted.

Changes in the baseline slope of the FT-IR spectrum can occur from electronic effects due to increased aromatics content or from scattering of particulates. Figure 4.4.21 presents the change in the baseline slope at 5000 cm^{-1} for the Shell and Sun fuels. The change in the baseline slope was approximately the same for both fuels and was not affected by filtering out the particles larger than two microns. Parker et al. (47) have recently determined the particulates present in jet fuel from thermal stressing are much smaller than $2\text{ }\mu\text{m}$. While the baseline slope clearly provides information on the thermal degradation of the bulk fuel, additional data will be required to determine whether it provides any information on the deposit formation process.

Results for QCM Probe - Data from a run with deaerated N_2 sparged Shell Jet-A fuel is shown in Fig. 4.4-22. There are three sets of data in the figure: the QCM frequency, the reactor wall temperature, and the temperature near the QCM probe. While the reactor wall got as hot as $480\text{ }^\circ\text{C}$, the QCM probe temperature rose only to about $350\text{ }^\circ\text{C}$. The initial frequency of the QCM at

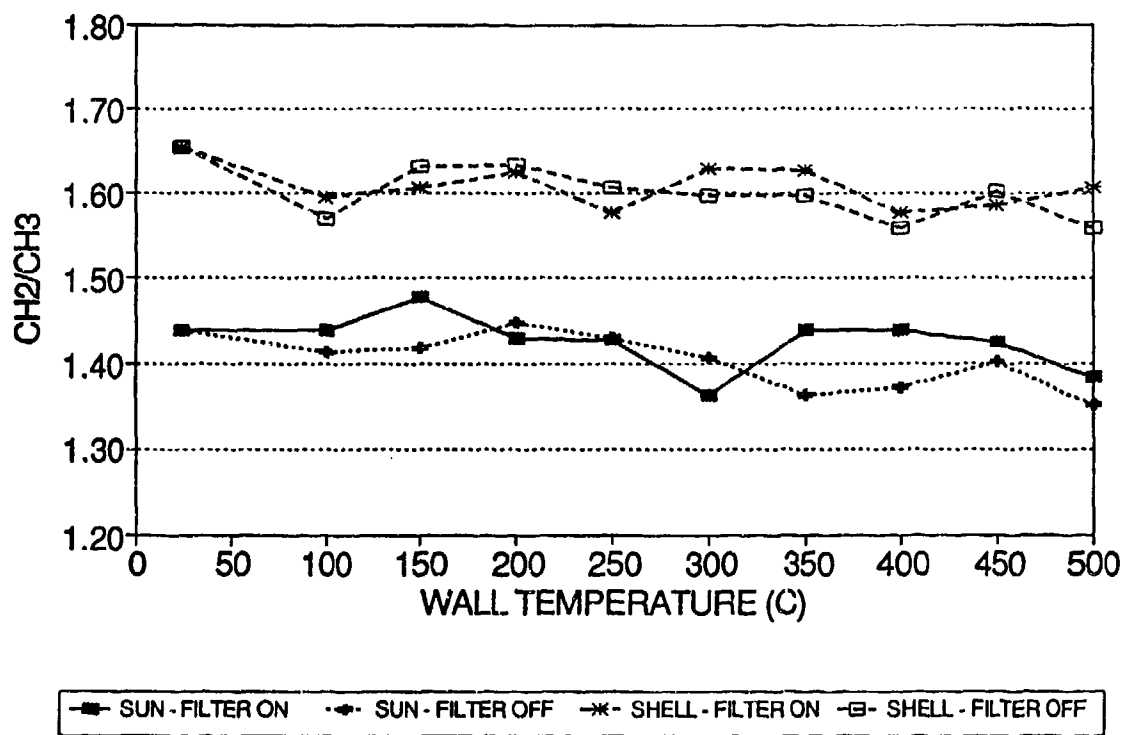
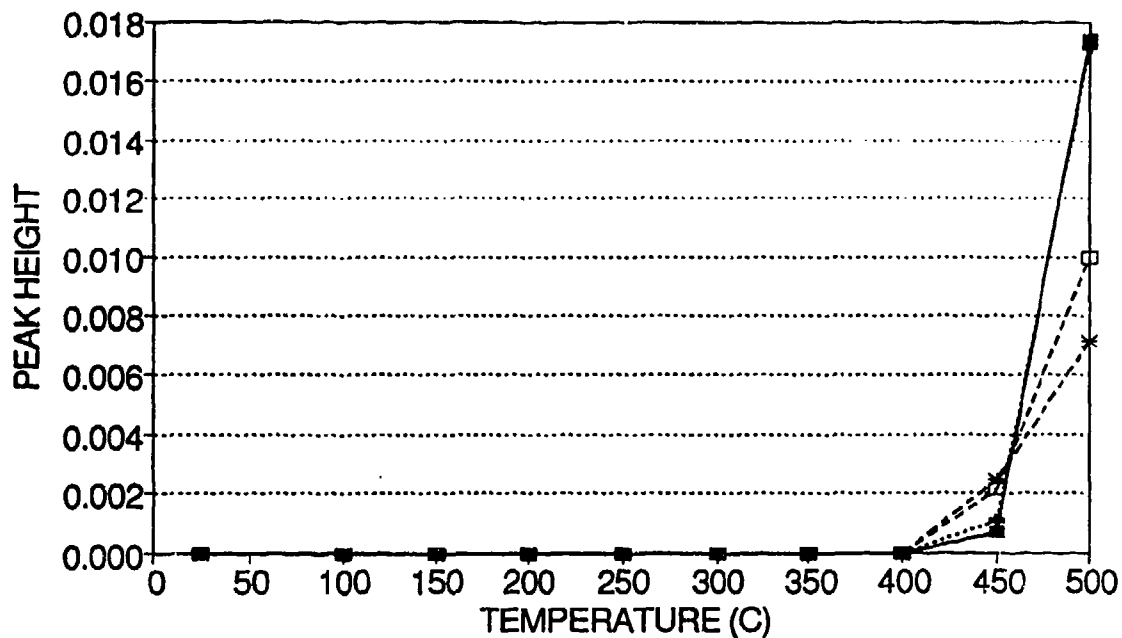
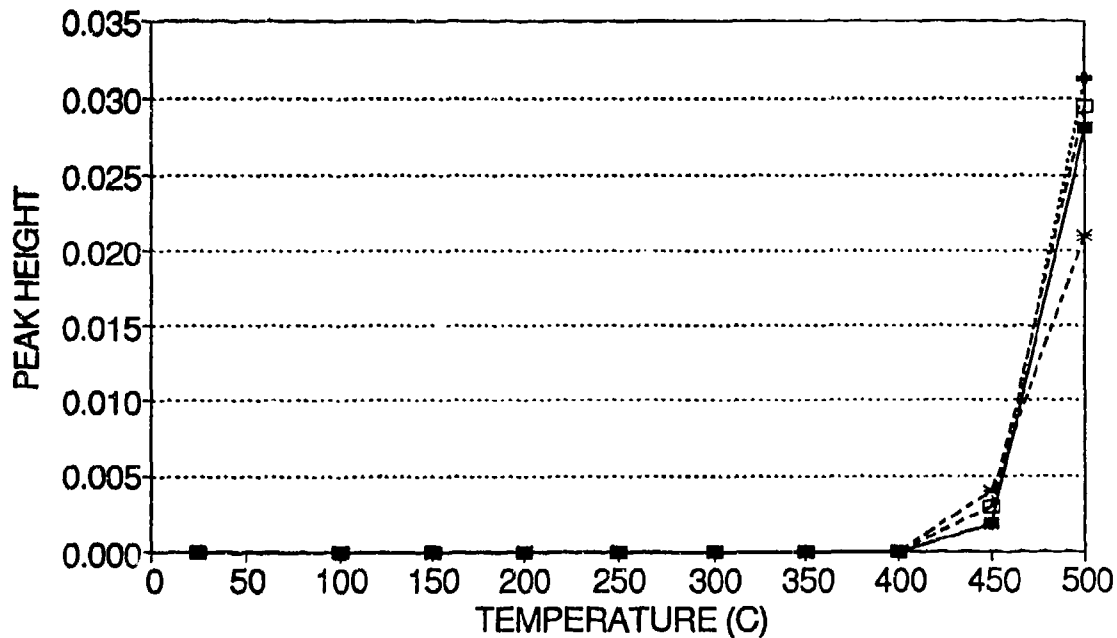


Figure 4.4-16. FT-IR/ATR Absorption Data for CH₂/CH₃ Ratio Data from Circle Cell for Shell and Sun Fuels Stressed to Various Temperatures.



STABLE: FILTER ON
 STABLE: FILTER OFF
 UNSTABLE: FILTER ON
 UNSTABLE: FILTER OFF

Figure 4.4-17. FT-IR/ATR Absorption Data from Circle Cell Subtraction Spectra for Height of $R_2C=CH_2$ Absorbance (890 cm^{-1}) for Stable (Sun) and Unstable (Shell) Fuels.



STABLE: FILTER ON
 STABLE: FILTER OFF
 UNSTABLE: FILTER ON
 UNSTABLE: FILTER OFF

Figure 4.4-18. FT-IR/ATR Absorption Data from Circle Cell Subtraction Spectra for Height of $RCH=CH_2$ Absorbance (910 cm^{-1}) for Stable (Sun) and Unstable (Shell) Fuels.

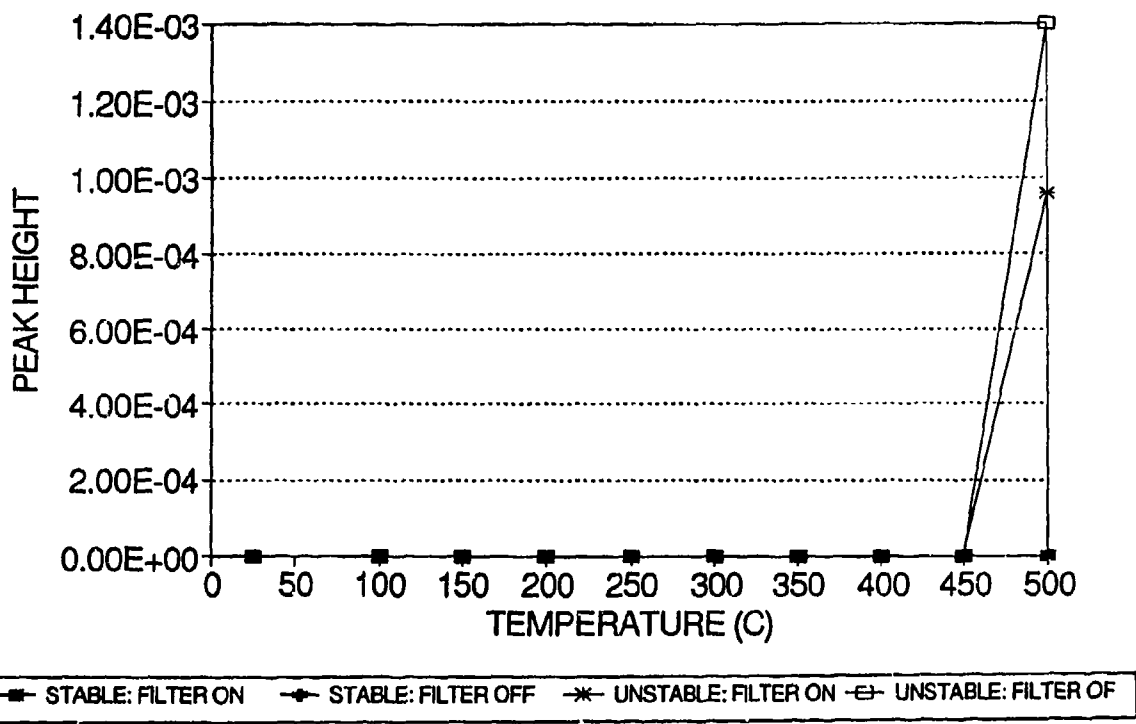


Figure 4.4-19. FT-IR/ATR Absorption Data for Height of Aromatic C-H (690 cm^{-1}) Absorbance from Circle Cell Subtraction Spectra for Stable (Sun) and Unstable (Shell) Fuels Stressed to Various Temperatures.

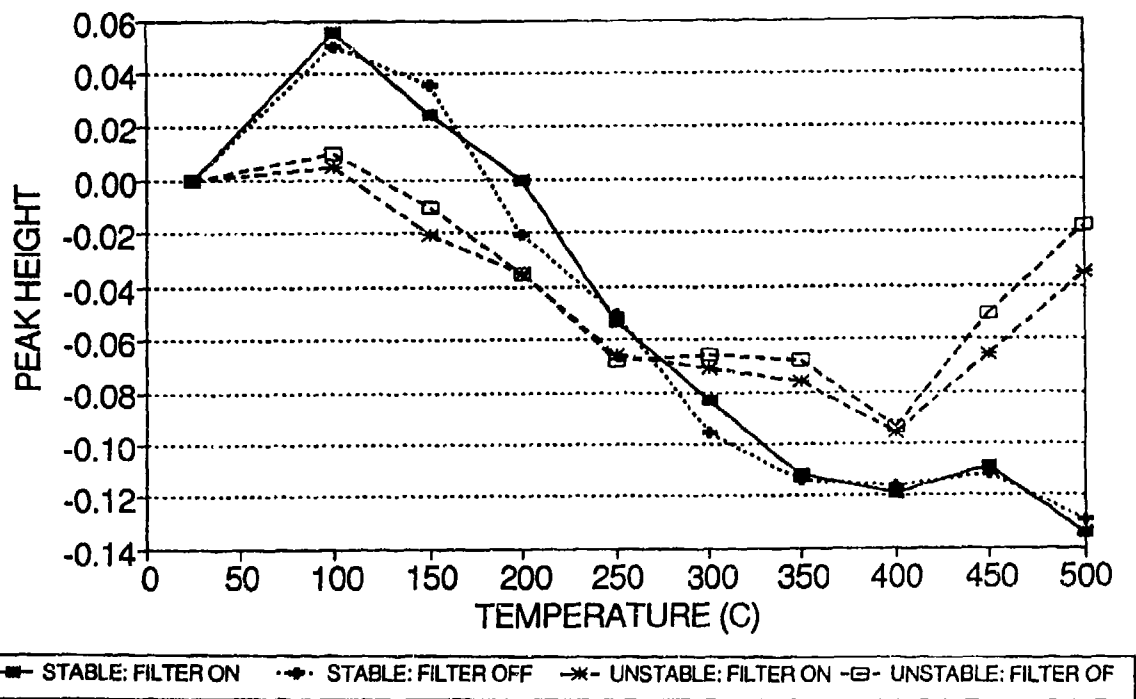


Figure 4.4-20. FT-IR/ATR Absorption Data for Height of OH (3300 cm^{-1}) Absorbance from Circle Cell Subtraction Spectra for Stable (Sun) and Unstable (Shell) Fuels Stressed to Various Temperatures.

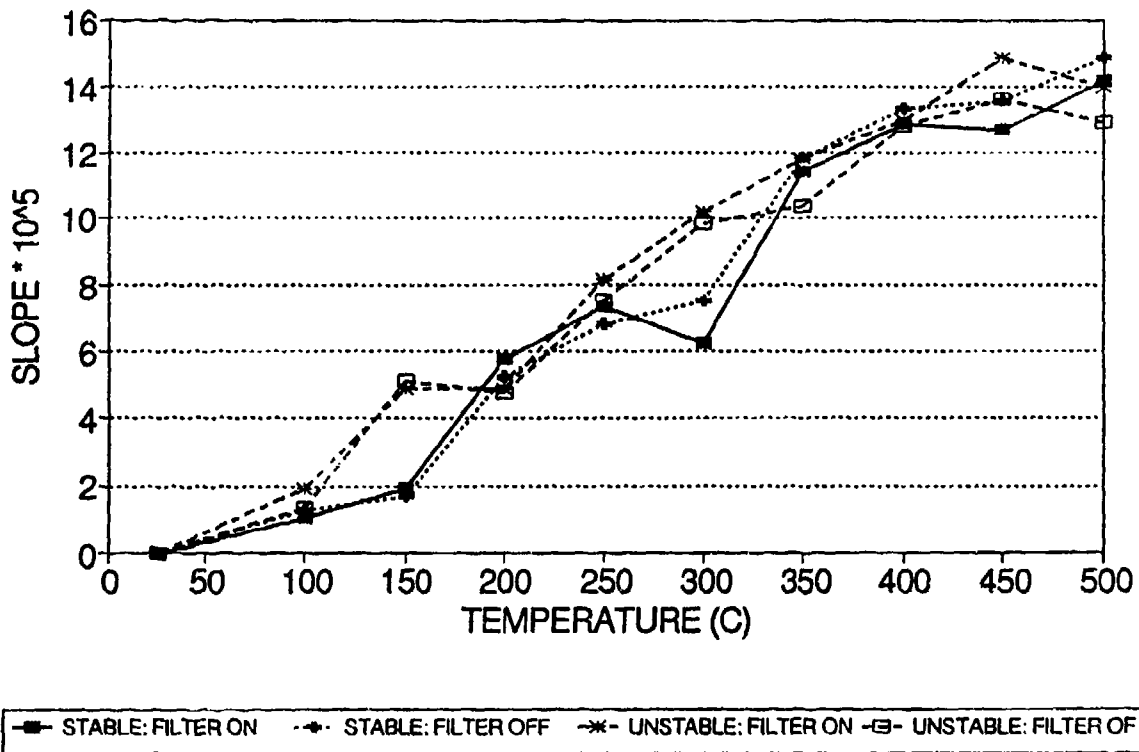


Figure 4.4-21. FT-IR/ATR Absorption Data for Slope of Baseline at 5000 cm^{-1} Absorbance from Circle Cell Subtraction Spectra for Stable (Sun) and Unstable (Shell) Fuels Stressed to Various Temperatures.

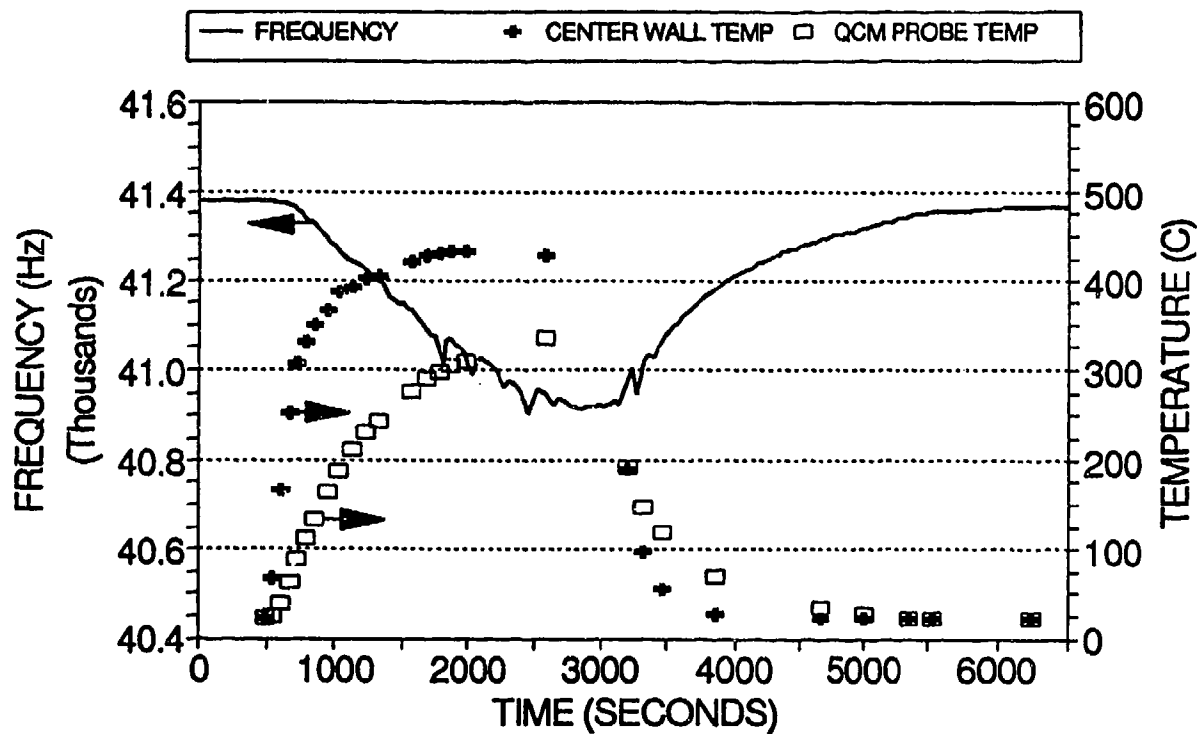


Figure 4.4-22. QCM Data from a Run with Deaerated Shell Jet-A Fuel. Note Periodic Spikes in the Frequency Once the Fuel is Above 300°C.

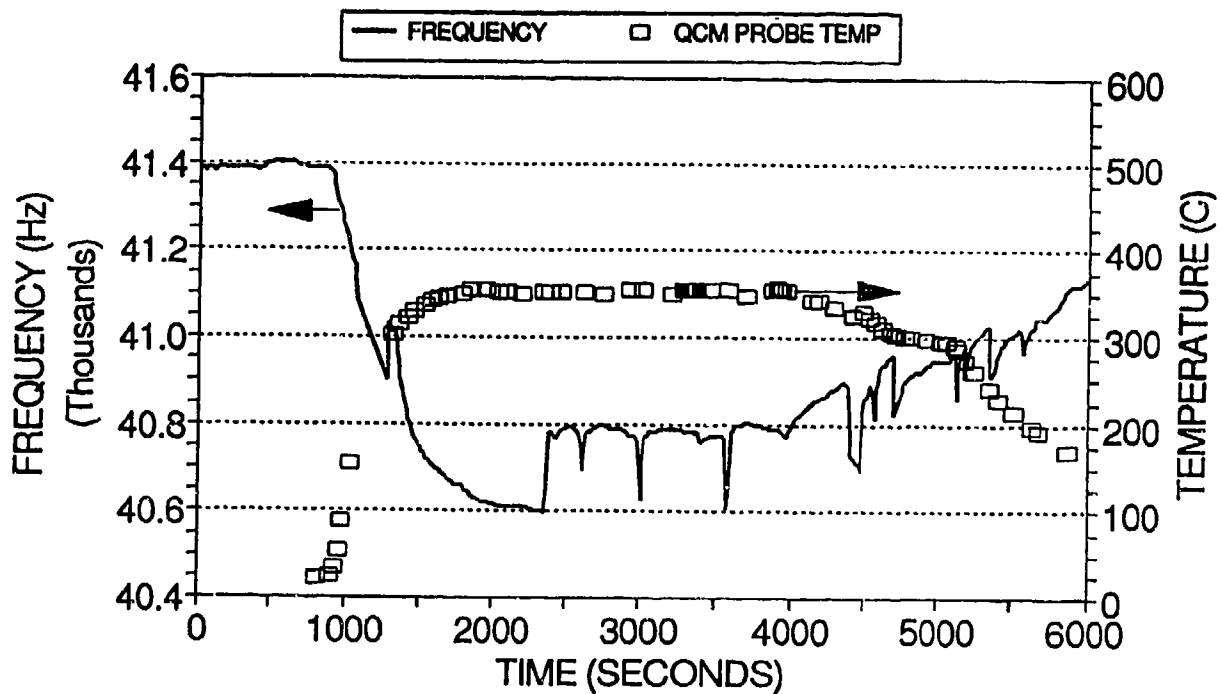


Figure 4.4-23. QCM Data from a Run with Aerated Shell Jet-A Fuel.

room temperature in contact with the fuel was 41.38 kHz and it slowly decreased during the heat-up. The lowest frequency during the run was 40.93 kHz. When the fluid was cooled, the QCM frequency increased, and the final frequency was essentially the same as the initial value (41.36 kHz). The QCM frequency displayed several spikes once the fuel was hot. These spikes suggest the formation of viscous film causing the frequency to decrease. These films, however, probably redissolved or flaked off and the frequency rose again.

Examination of the probe at the end of the run showed no visible signs of any deposit, although, there were some deposits on the region in contact with stagnant fuel and on the Cu gasket.

A similar run was conducted with aerated Shell Jet-A fuel. In this case, the QCM probe temperature was held at 350 °C for an extended period. The data from this run are displayed in Fig. 4.4-23. The initial QCM frequency was again 41.38 kHz, but the frequency during the run dropped to a substantially lower value of 40.60 kHz. After a while, the frequency increased to about 40.80 kHz, and periodically dropped to about 40.60 kHz. When the heat was turned off, the frequency increased and finally reached the same value as the initial (not shown on the figure). Examination of the probe at the end of the run showed a thin film of deposit on the probe. The fact that at room temperature the QCM frequency was the same with or without the film, strongly supports the hypothesis that the frequency change is a result of viscosity dampening due to the film and not a result of the mass change. Further proof of this conjecture can be seen in Fig. 4.4-24 which shows no change in the room temperature as a result of cleaning the probe. We suggest that at 350 °C the deposit is viscous, but at room temperature it behaves as a rigid deposit. Because the X-cut quartz crystals oscillate at a relatively low frequency (~ 40 kHz), the QCM we are using is not as sensitive to mass changes as it is to viscosity dampening.

Researchers at Sandia National Laboratories have also used a QCM to monitor film formation during thermal stressing of jet fuels (31,32). They have used AT-cut crystals which oscillate around 5 MHz. Although, they have attributed the frequency change to the mass of the film, they also observed an increase in the impedance of the system, which can only result from viscosity dampening. Thus, even in the Sandia experiment, the mass-detector is actually responding to the formation of a viscous film.

Data from a run with aerated Sun Jet A-1 fuel are shown in Fig. 4.4-25. The drop in frequency is not as large as with the Shell fuel. Figures 4.4-26 and 4.4-27 summarize the results from several runs with Shell and Sun fuels respectively. The reduction in frequency due to aeration is substantial with the Shell fuel, but with the Sun fuel there is essentially no change due to aeration. The results are consistent with the known greater thermal stability of the Sun Jet A-1 fuel and the fact that no visible deposit was observed for either the aerated or de-aerated Sun fuel. Thus, the QCM detector was able to discriminate between the two fuels. Evidently the QCM detector is responding to formation of a film on the surface of the probe. While the amount of dampening is related to the mass of the film, the relationship is not straightforward and it may be more expedient to empirically calibrate the observed frequency change against the mass of the film.

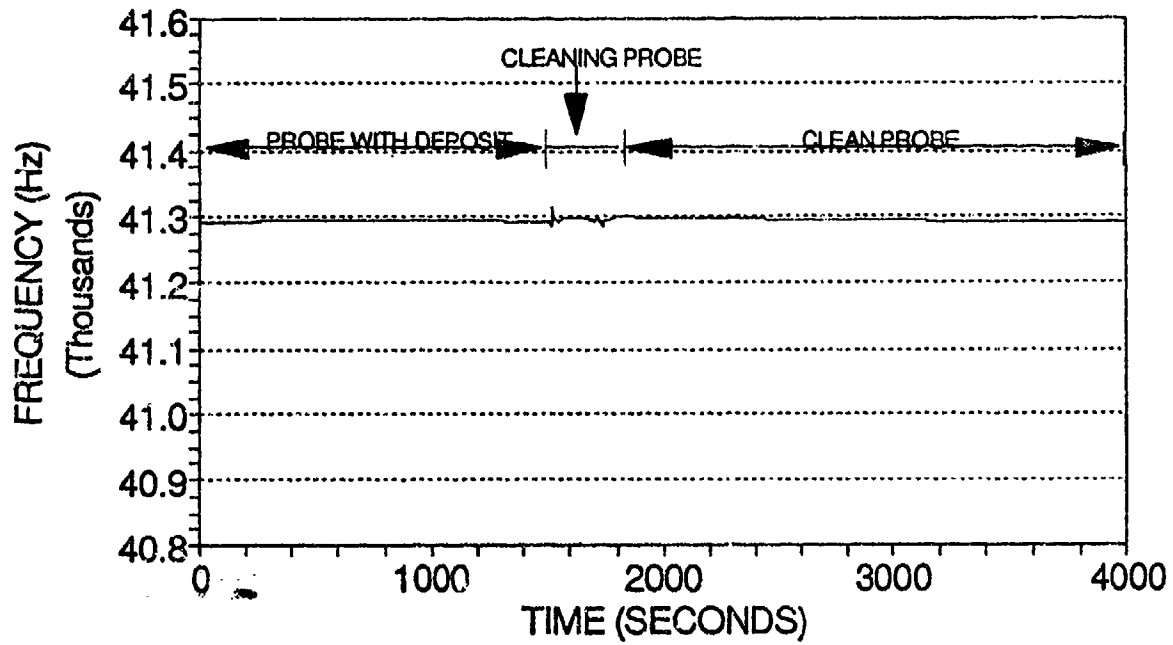


Figure 4.4-24. At Room Temperature Resonant Frequency of the QCM does not Change With or Without the Deposit.

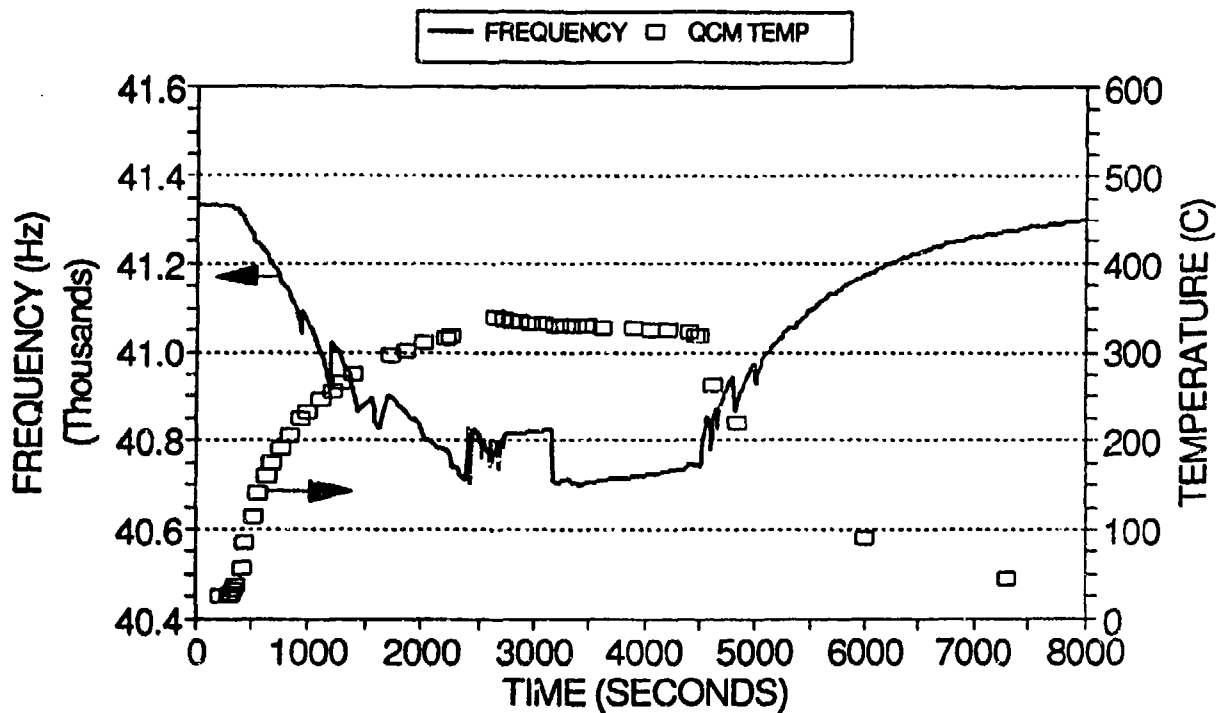


Figure 4.4-25. QCM Data from a Run with Aerated Sun Jet A-1 Fuel.

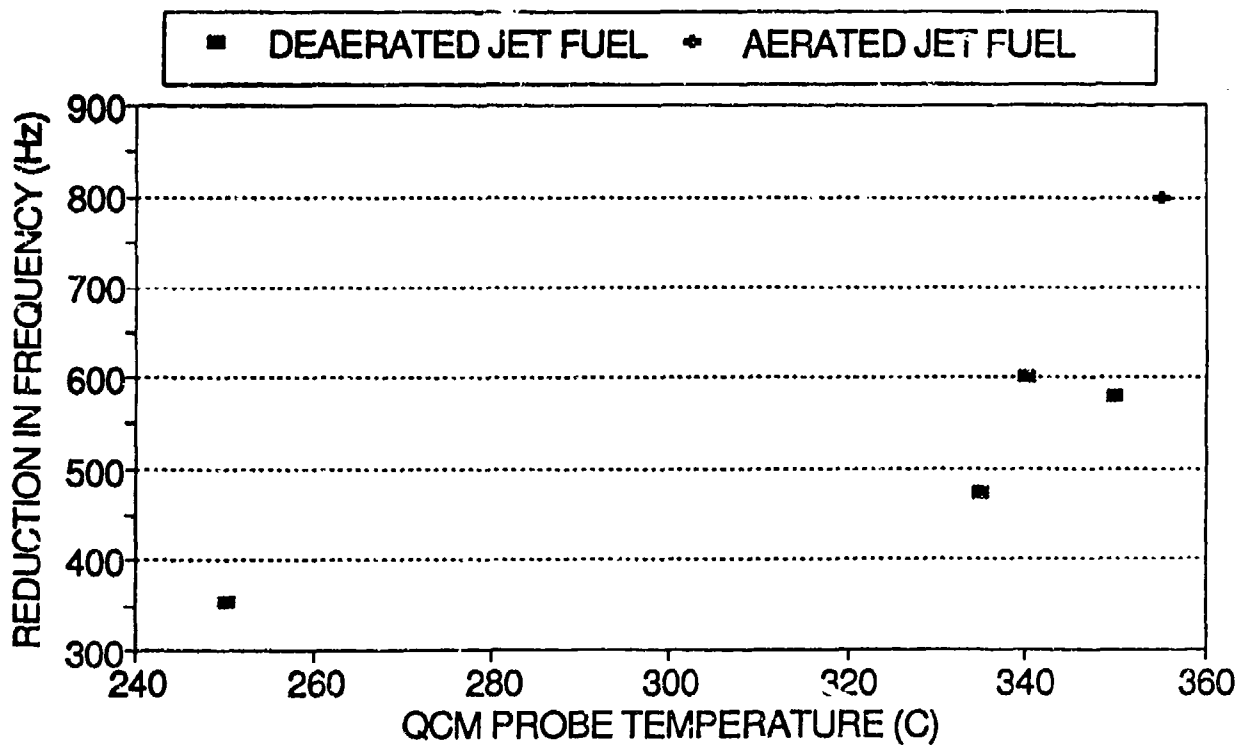


Figure 4.4-26. Reduction in Resonant Frequencies of the QCM Probe Resulting from Contact with Heated Shell Jet-A Fuel. Note Marked Effect of Aeration.

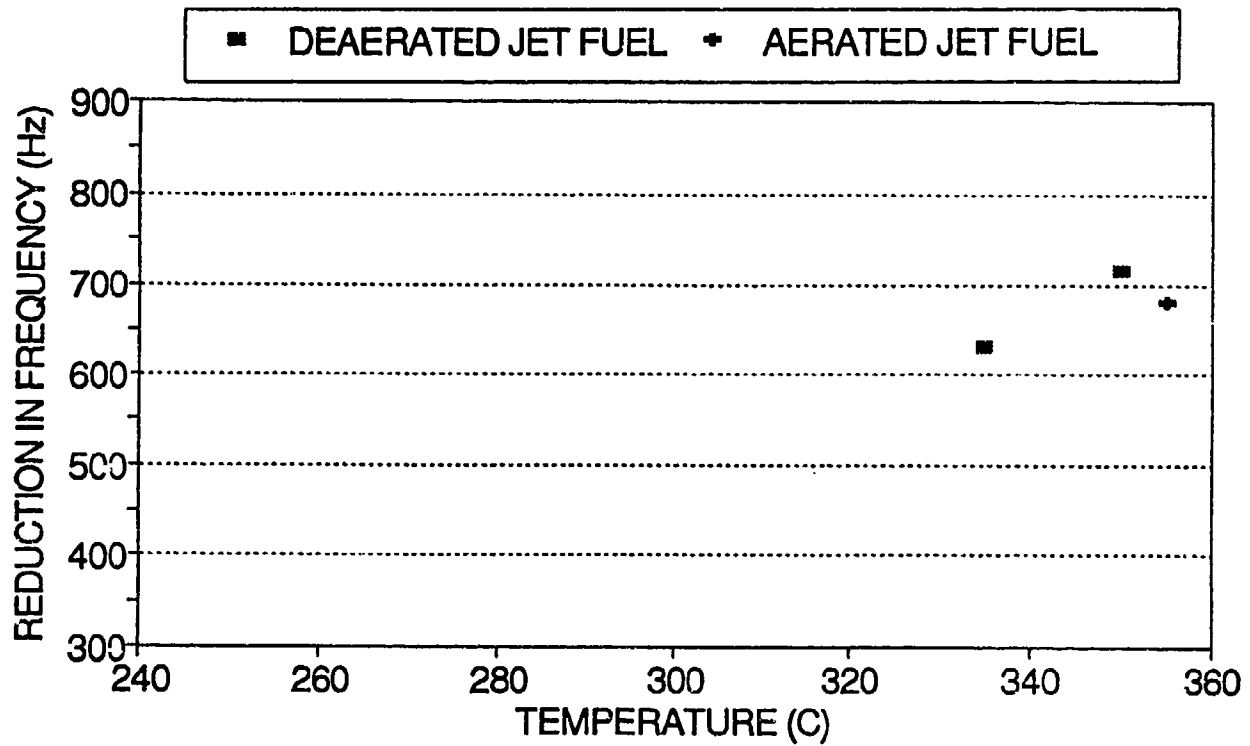


Figure 4.4-27. Reduction in Resonant Frequencies of the QCM Probe Resulting from Contact with Heated Sun Jet A-1 Fuel.

Summary

The results from the analysis of the room temperature FT-IR deposit probe absorbance spectra after thermal stressing of the Shell and Sun fuels clearly show the expected difference in stability for these two fuels. The results are not as clear for the spectra obtained at temperature, but an examination of the CH_2/CH_3 ratio shows the correct trend. This is consistent with the aliphatic nature of the initial deposits. The results from the room temperature ATR circle cell reflect changes primarily in the bulk fuel composition which are also consistent with the expected trend in stability for these two fuels. The results from the QCM tests indicate that the drop in frequency results from viscosity dampening, and not the mass, of the film. The observed greater drop in frequency for Shell Jet A as compared with the more stable Sun Jet A-1 demonstrates the feasibility of using the QCM as a thermal stability test probe.

5. CONCLUSIONS

5.1 Technical Feasibility

The Phase I program demonstrated the feasibility of using an in situ FT-IR fiber optic probe and a quartz crystal microbalance (QCM) to monitor the growth of deposits and their composition in a high-temperature, high pressure flow system. The specific accomplishments of this program can be summarized as follows:

- Designed, constructed, and tested an on-line high-temperature FT-IR probe for monitoring the amount and composition of surface deposits.
- Designed, constructed, and tested a high-temperature quartz crystal microbalance (QCM) probe for the formation and growth of a surface deposit.
- Designed, constructed, and tested a multiple path FT-IR optical bench that could sequentially monitor the fiber optic probe, an ATR circle cell, and a transmission cell.
- Modified an existing fuel stability test system to incorporate the FT-IR fiber-optic probe and the QCM probe.
- Demonstrated that both the FT-IR fiber optic probe and the QCM probe could successfully differentiate between a "stable" and an "unstable" fuel. The results from the QCM probe tests indicate that the drop in frequency for this particular probe results from viscosity dampening and not the mass of the film.
- Measured the composition of the initial deposit and its changing composition with increased thermal stressing by the FT-IR fiber optic probe. Confirmed previous work which indicated that the initial deposits are highly aliphatic.
- Measured the changes in the bulk fuel composition from thermal stressing with the ATR circle cell, which were found to be significantly different from the changes in the deposit layer composition measured by the fiber-optic probe.

5.2 Technical, Economical and Social Benefits

If carried through Phases II and III, this program will result in an instrument package, including software, for monitoring of jet fuel thermal stability. The program is designed to produce an instrument that will have direct application to process development activities for thermally stable fuels and supercritical fuels for hypersonic aircraft. However, the same instrument would have applications in a much wider market such as the production of gasoline which does not clog fuel injectors and the assessment of heat exchanger fouling in the petrochemical industry. The technology developed under this program could also lead to the development of on-line monitors of fuel stability which can be installed on board an aircraft.

5.3 Estimated Cost of Approach Relative to Benefits

The estimated cost of the combined Phase I and Phase II efforts is about \$815,000. This is relatively small when compared to the values of the aircraft that are being developed and the total value of the jet fuels that are used each year by the Department of Defense.

6. REFERENCES

1. Kendall, D.R., Mills, J.S., *Ind. Eng. Chem. Prod. Res. Dev.*, **25**, 360 (1986).
2. Hazlett, R.N., "Free Radical Reactions Related to Fuel Research," in Frontiers of Free Radical Chemistry, William A. Pryor (Ed.), Academic Press, NY, pp. 195-223 (1980).
3. Galya, L.G., Cronauer, D.C., Painter, P.C, Li, N., *Ind. Eng. Chem. Fund.*, **25**, 129 (1986).
4. Zinbo, M., Jensen, R.K., Johnson, M.D., Korak, S., *Ind. Eng. Chem. Res.*, **26**, 902 (1987).
5. Mayo, F.R., Lan, B.Y., *Ind. Eng. Chem. Res.*, **26**, 215 (1987).
6. Mayo, F.R., Lan, B.Y., *Ind. Eng. Chem. Res.*, **25**, 333 (1986).
7. Tseregounis, S.I., Spearot, J.A., Kite, D.J., *Ind. Eng. Chem. Res.*, **26**, 886 (1987).
8. Leftin, H.P., Newsome, D.S., *Ind. Eng. Chem. Res.*, **26**, 1003 (1987).
9. Taylor, W.F., *IEC Product Res. Dev.*, **8**, 375 (1969).
10. Busheva, E.M., Bepolov, I.F., *Khim. i Tecknol. Topliv i Masel*, p. 46 (September 1971).
11. Sheldon, R.A., Kochi, J.K., Metal-Catalyzed Oxidations of Organic Compounds, Academic Press, NY, (1981).
12. Naidu, S.K., Klaus, E.E., Duda, J.L., *IEC Prod. Res. Dev.*, **23**, 613 (1984).
13. Tevelde, J., Spadaccini, L.J., Szetela, E.J., Glickstein, M.R., *AGARD Conf. Proceedings*, No. 353.
14. Marteney, P.J., Spadaccini, L.J., *Journal of Eng For Gas Turbines & Power*, **108**, 648 (1986).
15. Momeny, A., "The Fuel Section of the NASA/Boeing Airframe Study," presented at the High Speed Commercial Transport Fuels Workshop, October 14-15, 1987, NASA Lewis Research Center, Cleveland, Ohio (1987).
16. Nixon, A.C., "A Study on Endothermic and High Energy Fuels for Airbreathing Engines," Report prepared for U.S. Air Force under Contract #F33615-84-C-2410, Battelle Columbus Div. (January 22, 1986).
17. Serio, M.A., Malhotra, R., Kroo, E., Deshpande, G.V., Solomon, P.R., "Thermal Stability of Aviation Fuels," Air Force Final Report under Contract No. F33615-88-C-2853 (March 1989).
18. Serio, M.A., Malhotra, R., Kroo, E., Deshpande, G.V., Solomon, P.R., *ACS Div. of Fuel Chem. Prepr.*, **34** (4), 816 (1989).
19. Deshpande, G.V., Serio, M.A., Solomon, P.R., Malhotra, R., *ACS Div. of Fuel Chem. Prepr.*, **34** (3), 955 (1989).
20. Rubey, W.A., Mazer, S.L., Taylor, P.H., Stoller, J.G., *ACS Pet. Div. Prepr.*, **32**, (2), 526 (1987).
21. Morris, R.E., Hazlett, R.N., *Energy & Fuels*, **3**, 262 (1989).
22. Grigsby, R.D., Sturm, Jr., G.P., Green J.B., Goetzinger, J.W., Kamin, R.A., *ACS Div. of Fuel Chem. Prepr.*, **34** (4), 825 (1989).
23. Roquemore, W.M., Pearce, J.A., Harrison, III, W.E., Krazinski, J.L., Vanka, S.P., *ACS Div. of Fuel Chem. Prepr.*, **34** (4), 841 (1989).
24. "Properties of Aircraft Fuels and Related Materials," United Technologies Corporation, Pratt & Whitney Topical Report No. 11 prepared for U.S. Air Force under Contract No. F33615-85-C-2508 (July 1988).
25. Barbee, J.G., Stavinoha, L.L., "Calibration of Nondestructive Birefringence Fuel Thermal Deposit Rating Device," DTIC No. AD-A206-041 (August 1988).
26. Moler, J.L., Steward, E.M., *ACS Div. of Fuel Chem. Prepr.*, **34**(4), 837 (1989).
27. Naegeli, D.W., Hill, R.H., "Laser Induced Fluorescence Detection of Gums in Jet Fuels," Final Report for Air Force WL-TR-92-2015 (May 1992).
28. Song, C., Eser, S., Schobert, H.H., Hatcher, P.G., Coleman, M.M., Peng, Y., Selvaraj, L., Parzynski, K., Bortiatynski, J., Liu, Y., Copenhagen, R.M., Arumugam, R., "Advanced Thermally Stable Jet Fuel Development Program, Annual Report, Vol. II, Compositional Factors Affecting Thermal Degradation of Jet Fuels," Final Report for Air Force WL-TR-91-2117 (May 1992).

29. Eser, S., Song, C., Copenhaver, R., Parzynski, M., ACS Div. of Petr. Chem. Prepr., **37**, (2) 493 (1992).
30. Song, C., Eser, S., Schobert, H.H., Hatcher, P.G., ACS Div. of Petr. Chem. Prepr., **37**, (2) 540 (1992).
31. Klavetter, E., Trott, W., O'Hern, T., Martin, S., "Advanced Thermally Stable, Jet Fuels Development Program, Annual Report, Vol. I., Model and Experiment System Development," Final Report for Air Force WL-TR-91-2099 (January 1992).
32. Martin, S.J., Frye, G.C., Klavetter, E.A., Ricco, A.J., ACS Div. of Petr. Chem. Prepr., **37**, (2) 457 (1992).
33. Bullock, S.P., Lewis, C., Hatchett, D.M., "The Quantitative Determination and Characterization of Aviation Fuel Thermal Stability by Quartz Crystal Microbalance (QCM) Technique," Report for the Ministry of Defence Air Systems Controllerate, D/DFS (AIR)/33/13/1 April (1992).
34. Stavinoha, L.L., Estefan, R.M., Marbach, H.W., Jr., "Development for a Laboratory Test for Multiple Injector Deposits: Approaches I and II," Department of Defense Final Report for Contract No. CM-128-85 (1-86) (September 1987).
35. Strange, H.O., "Development of a Laboratory Test for Multiple Fuel Injector Deposits - Evaluation of the Jet Fuel Thermal Oxidation Test Apparatus (JFTOT)," Department of Defense Final Report for Contract No. DAAK70-86-C-0011 (December 1987).
36. Kirklin, P.W., David, P., Aviation Fuel, Thermal Stability Requirements, ASTM Press, Philadelphia PA (1992).
37. Hazlett, R.N., Thermal Oxidation Stability of Aviation Turbine Fuels, ASTM Press, Philadelphia PA (1991).
38. Schulz, W.D., ACS Div. of Petr. Chem. Prepr., **37** (2) 383 (1992).
39. Jones, E.G., Balster, W.J., Anderson, S.D., ACS Div. of Petr. Chem. Prepr., **37** (2) 393 (1992).
40. Kauffman, R.E., Tirey, D.A., ACS Div. of Petr. Chem. Prepr., **37** (2) 412 (1992).
41. Dworzanski, J.P., Chapman, J.N., Meuzelaar, H.L.C., Lander, H.R., ACS Div. of Petr. Chem. Prepr., **37** (2) 424 (1992).
42. Acker, W.P., Hahn, R.T., Mach, T.J., ACS Div. of Petr. Chem. Prepr. **37** (2) 433 (1992).
43. Trott, W.M., O'Hern, T.J., Klavetter, E.A., ACS Div. of Petr. Chem. Prepr. **37** (2) 442 (1992).
44. Selvaraj, L., Sobkowiak, M., Coleman, M.M., ACS Div. of Petr. Chem. Prepr. **37** (2) 451 (1992).
45. Edwards, T., Anderson, S.D., ACS Div. of Petr. Chem. Prepr., **37** (2) 549 (1992).
46. Coleman, M.M., Selvaraj, L., Sobkowiak, M., Yoon, E., "Potential Stabilizers for Jet Fuels Subjected to Thermal Stress Above 400 °C," *Energy & Fuels*, **6**, 5 (1992).
47. Parker, T.E., Foutter, R.R., Rawlins, W.T., "Optical Diagnostic Methods for the Study of Fuel Fouling," ACS Div. of Ind. Eng. Chem. Res. Prepr., **31**, 2243-2251 (1992).
48. Striebich, R.C., Rubey, W.A., "A Condensed Phase Test Cell Assembly for the System for Thermal Diagnostic Studies (STDS), Final Report for Air Force WL-TR-92-2040 (August 1992).
49. Solomon, P.R., Carangelo, R.M., Hamblen, D.G., Best, P.E., Infrared Analysis of Particulates by FT-IR Emission/Transmission Spectroscopy, *Applied Spectroscopy*, **40**, (6), 746 (1986).
50. Solomon, P.R., Carangelo, R.M., Best, P.E., Markham, J.R., Hamblen, D.G., "Analysis of Particle Emittance, Composition, Size and Temperature for FT-IR Emission/ Transmission Spectroscopy," *Fuel*, **66**, 897 (1987).
51. Solomon, P.R., Chien, P.L., Carangelo, R.M., Best, P.E., Markham, J.R., "Application of FT-IR Emission/Transmission (E/T) Spectroscopy to Study Coal Combustion Phenomena," The 22d Symposium (Int) on Combustion, The Combustion Institute, Pittsburgh PA, p. 211 (1988).
52. Solomon, P.R., "On-Line Fourier Transform Infrared Spectroscopy in Coal Research," in Advances in Coal Spectroscopy (H.L.C. Meuzelaar, Ed.), Plenum Pub. Corp., pp. 341-371 (1992).

53. Best, P.E., Chien, P.L., Carangelo, R.M., Solomon, P.R., Danchak, M., Ilovici, I., "Tomographic Reconstruction of FT-IR Emission and Transmission Spectra in a Sooting Laminar Diffusion Flame: Species Concentrations and Temperatures," *Combustion and Flame*, **85**, 309-318 (1991).
54. Solomon, P.R., Best, P.E., "Fourier Transform Infrared Emission/Transmission Spectroscopy in Flames," in Combustion Measurements (N. Chigier, Ed.), Hemisphere Publishing Corp., pp. 385-344 (1991).
55. Markham, J.R., Zhang, Y.P., Carangelo, R.M., Solomon, P.R., "FT-IR Emission/Transmission Tomography of a Coal Flame," 23d Symposium (Int) on Combustion, The Combustion Institute, Orleans, France, pp. 1869-1875 (1990).
56. Markham, J.R., Solomon, P.R., Best, P.E., "An FT-IR Based Instrument for Measuring Spectral Emittance of Material at High Temperature," *Review of Scientific Instruments*, **61** (12) 3700 (1990).
57. Bates, S.C., Morrison, P.W., Jr., Solomon, P.R., Infrared Monitoring of Combustion, Proceedings from Laser Spectroscopy '91, **1434**, 28 (1991).
58. Morrison, P.W., Jr., Cosgrove, J.E., Carangelo, R.M., Carangelo, M.D., Solomon, P.R., "Fourier Transform Infrared (FT-IR) Instrumentation for Monitoring Recovery Boilers," *Tappi Journal*, **74** (12) 38 (1991).
59. Serio, M.A., Carangelo, R.M., Solomon, P.R., Markham, J.R., "An FT-IR Based Monitoring Device for NO_x, SO_x, and Particulates," Proceedings of the 8th Annual Int. Pittsburgh Coal Conference, pp. 1073-1078 (October 1991).
60. Solomon, P.R., Morrison, P.W., Jr., Serio, M.A., Carangelo, R.M., Markham, J.R., Bates, S.C., Cosgrove, J.R., "Fourier Transform Infrared Spectroscopy for Process Monitoring and Control," Proceedings of the SPIE "Process Analysis" Conf., No. 1681-35, Somerset NJ (March 1992).
61. Robinson, W.H., Smedley, S.I., Piezoelectric Method of Determining Viscosity at 40 kHz, *J. Appl. Phys.* **49**, 1070 (1978). See also Frequency of a Quartz Microbalance in Contact with a Liquid K. Keiji Kanazawa *Anal. Chem.* **57**, 1770, 1985 and Monitoring the Growth of an Oxide Film on Aluminum in Situ with the Quartz Crystal Microbalance, Mark R. Deakin, Owen R. Melroy *J. Electrochem. Soc.* **136**, 349 (1989).
62. Druy, M.A., Elandjian, L., Stevenson, W.A., SPIE 1170, *Fiber Optic Smart Structures and Skins II*, p. 150 (1989).
63. Serio, M.A., Teng, H., Knight, K., Bates, S.C., Solomon, P.R., "In-Situ FT-IR Diagnostics for Coal Liquefaction Processes," Final Report to U.S. DOE, under Contract No. DE-FG05-91ER81151 (June 1992).
64. Data from Saphikon, Inc.
65. Compton, D.C. et al., *Appl. Spectr.*, **42** (6) 972 (1988).
66. Harrick, N.J., Internal Reflection Spectroscopy, Harrick Scientific Corp., Ossining, New York, 1979, 2d printing.
67. Chang, C., Belfiore, L.A., ACS Div of Polymer Chem. Preprints, **30** (23) 325 (1989).
68. Willard, H.H., Merritt, L.L., Dean, J.A., Settle, Jr., F.A., Instrument Methods of Analysis, 6th Edition., D. Van Nostrand Publishing Company, New York NY (1981).

APPENDIX A - "Description of QCM Device"

Electronics

A simple electronics circuit was developed to operate the QCM. Shown schematically in Fig. A-1, this circuit is a simple crystal-controlled oscillator that incorporates the drive crystal of the QCM as its frequency control element. U1 functions as an open-loop oscillator, with R3 providing a very slight adjustment in the feedback. U2 is added to provide a buffered drive signal for the frequency counter. With both the sense and drive crystals disconnected from this circuit, it will free run at a much higher frequency, on the order of several hundred kHz. With both crystals properly connected, the frequency will stabilize at the resonant frequency of the crystal (about 40.168 kHz). Adjustment of R3 (located inside the control box) will have very little effect on the operating frequency, but some effect on the phase relationship between the drive and sense voltages. Normally, R3 does not need to be adjusted.

The only other instrument required to operate the QCM is a frequency counter. Any bench top counter with sufficient accuracy can be used since the signal provided by the electronics is in the form of a bipolar, +/- 5 volt square wave. Included along with the QCM and electronics box is a GT200 frequency counter board manufactured by Glide Technologies, for use with any IBM-compatible personal computer. The GT200 is fully described in the operating manual supplied with the unit, and it comes complete with the necessary software drivers and demonstration programs.

Software

In addition to the software drivers provided as part of the GT200 package, SRI has provided a data acquisition program that can be used to obtain results similar to that shown in Fig. 4.2-4. A commented source listing was also provided so that this simple program can be modified to include additional features such as the direct recording of temperatures via a suitable A/D board. The software disk includes both the original source file written in Microsoft QuickBasic Version 4.5 (but saved as an ASCII text file), as well as a compiled, stand alone version that can be operated without QuickBasic.

In the interest of providing a working software package within the time constraints, this program is quite rudimentary, and does not make use of a menu-driven user interface, nor does it provide any output options such as hardcopy plots or curve fitting. The program does generate an ASCII readable data file during the course of the measurement run that can be subsequently input by any number of commercial analysis and graphing programs. The intent was to provide a simple and reliable method to test the QCM without the need to develop any additional software. On the other hand, using the drivers and examples provided with the GT200, customized software can be written.

Operating Procedure

Operation of the QCM is very straight forward. Prior to installing the unit in the test cell, it should be tested to ensure that the crystals are oscillating properly, and that the electronics are all functional. To perform this test, it is only necessary to connect the drive and sense crystals to their respective BNC connections on the electronics box. At this point, a square wave of approximately 40 kHz should be observed at the computer BNC once power is applied to the circuit. Either the sense or drive signal can be monitored with an oscilloscope, however, the added probe capacitance may adversely affect the waveforms.

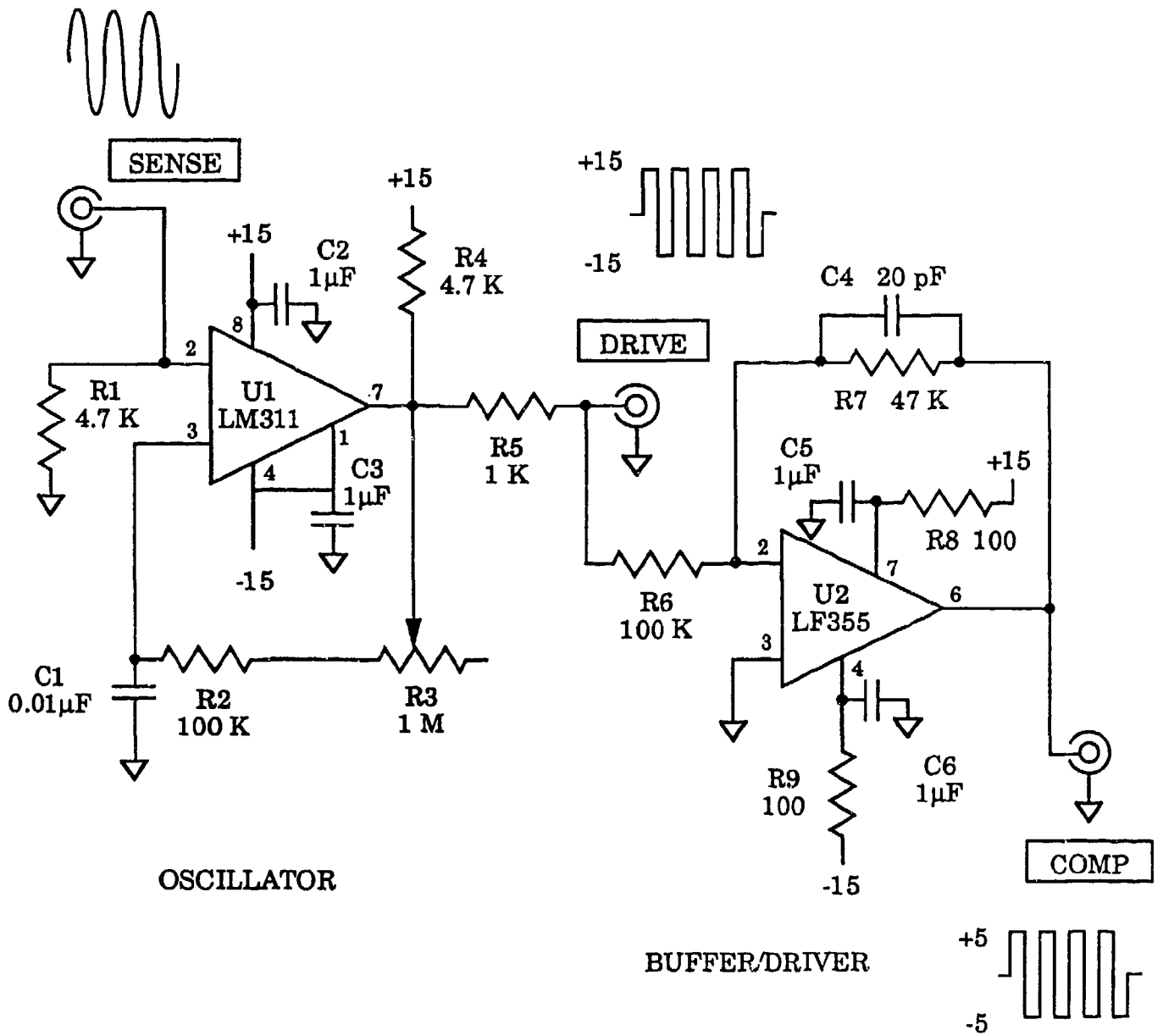


Figure A-1. Schematic of QCM Detector Drive Circuit

Once the QCM has been tested to ensure that it is functional, the unit can be installed in the test cell and retested. Using either the software provided, or custom AFR software, a frequency vs time profile can be recorded as the fuel test cell is heated. Results similar to those shown in Fig. 4.2-4 should be observed depending on the contents of the cell.

Following any test involving actual fuels, the probe assembly may be disassembled to examine the rod for deposits. Removal of the large retaining nut will allow the probe assembly to be removed from the test fixture. Replacement of the probe assembly will generally require the use of a new copper gasket.

APPENDIX B - "Raw Data from ATR Circle Cell"

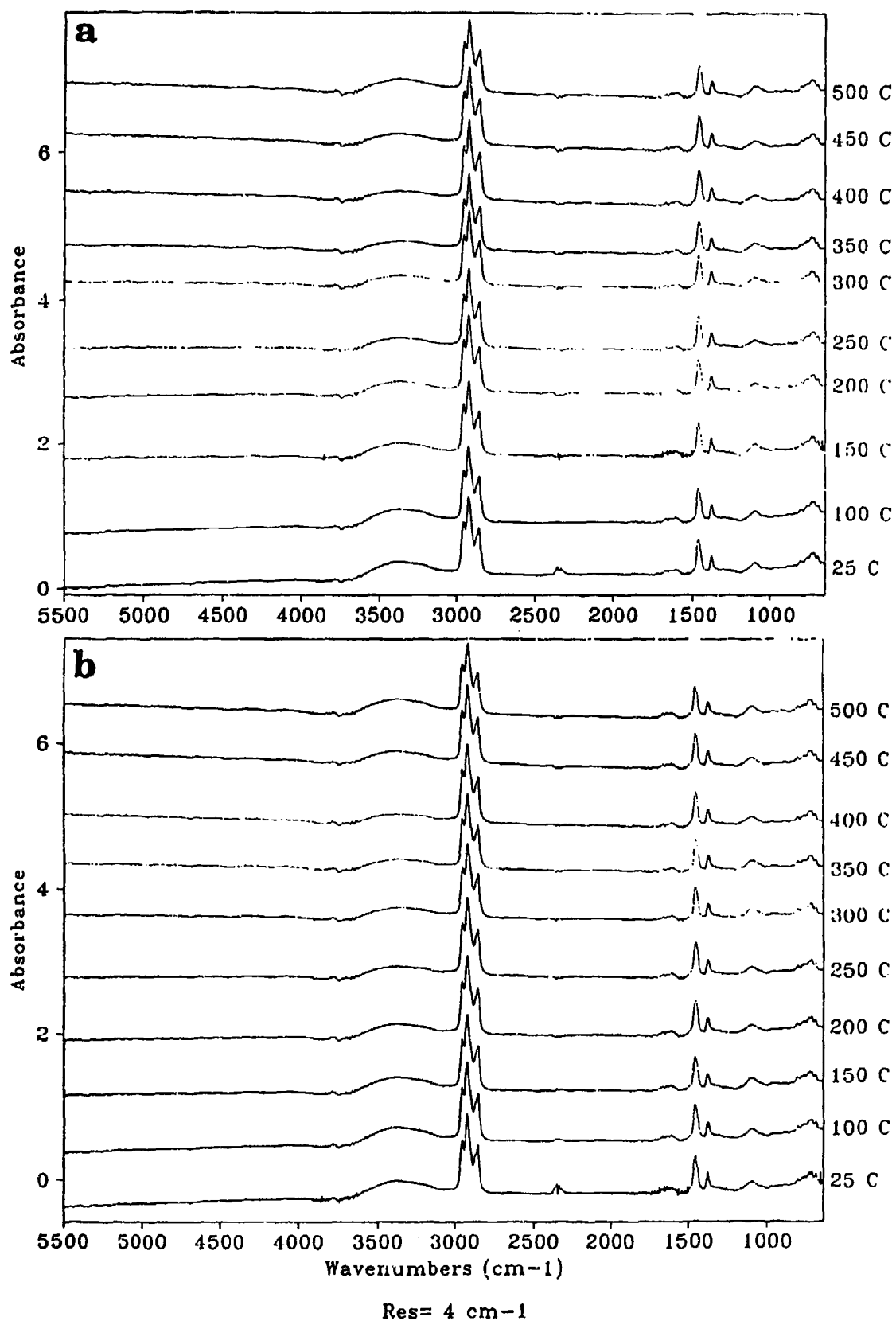
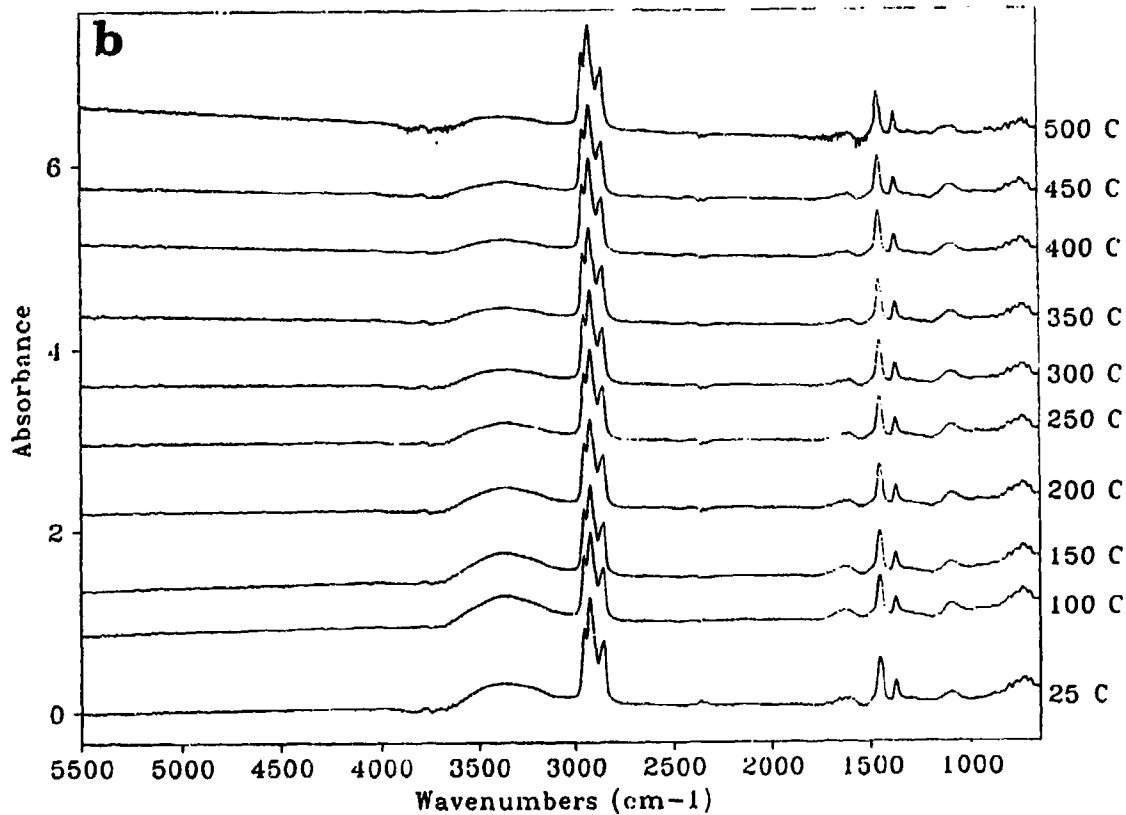
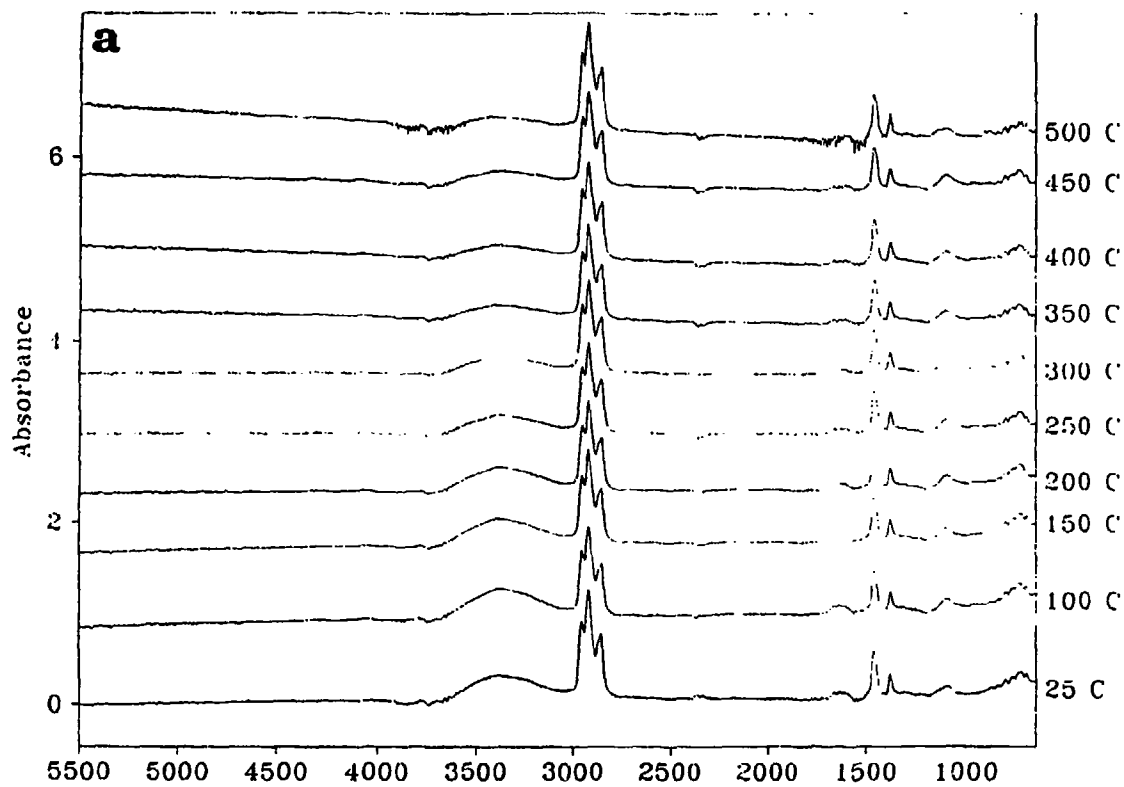
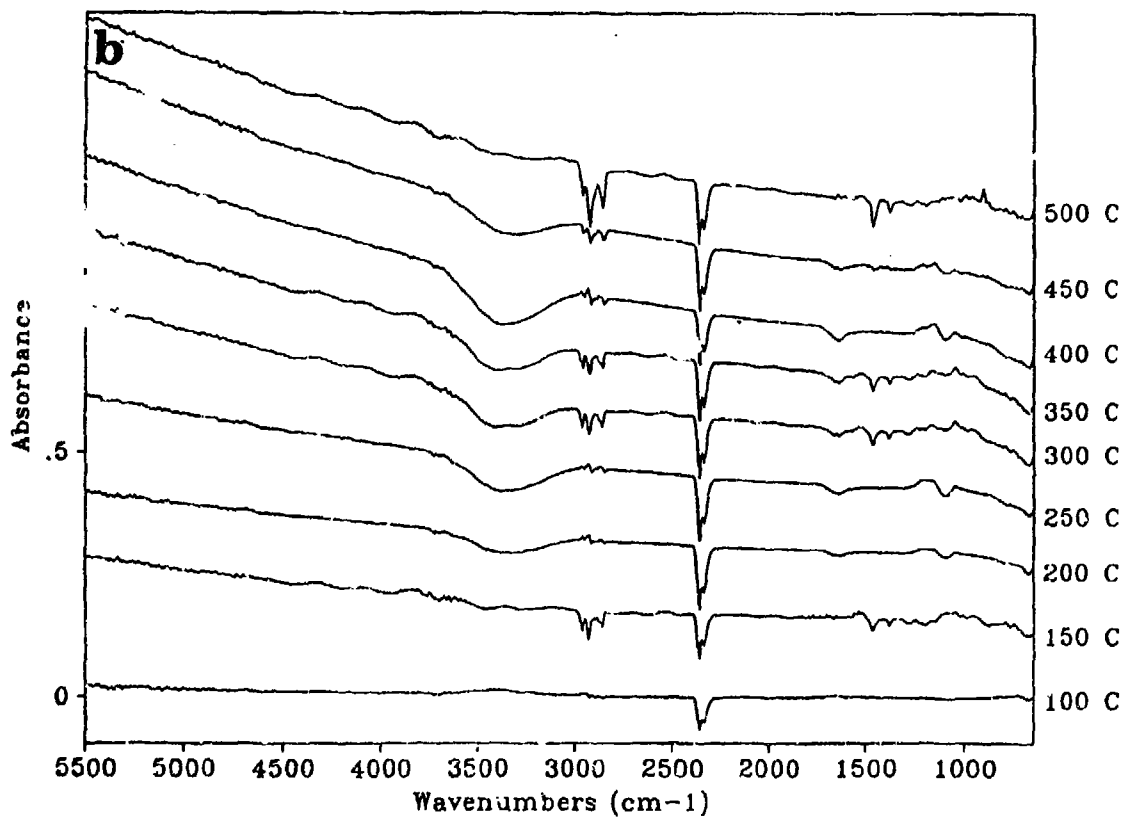
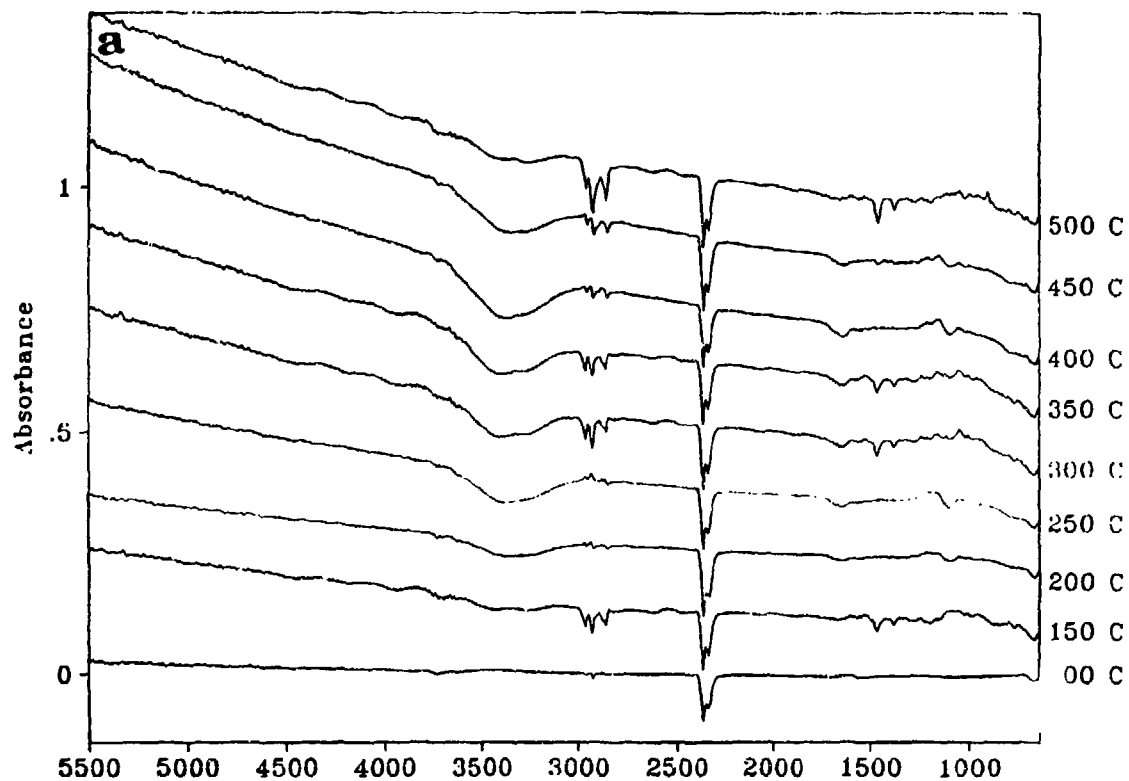


Figure B-1. Raw FT-IR/ATR Absorbance Spectra from Circle Cell for Shell Fuel Stressed to Various Temperatures. a) Filter On; b) Filter Off.



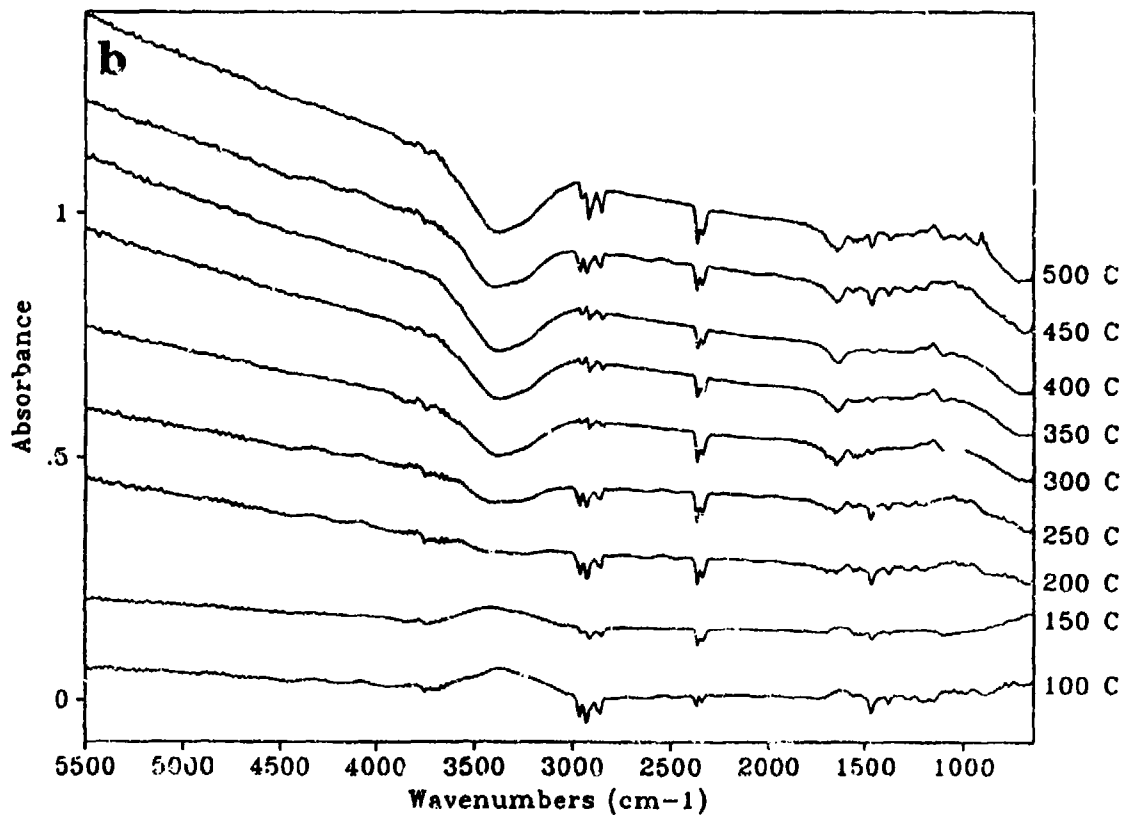
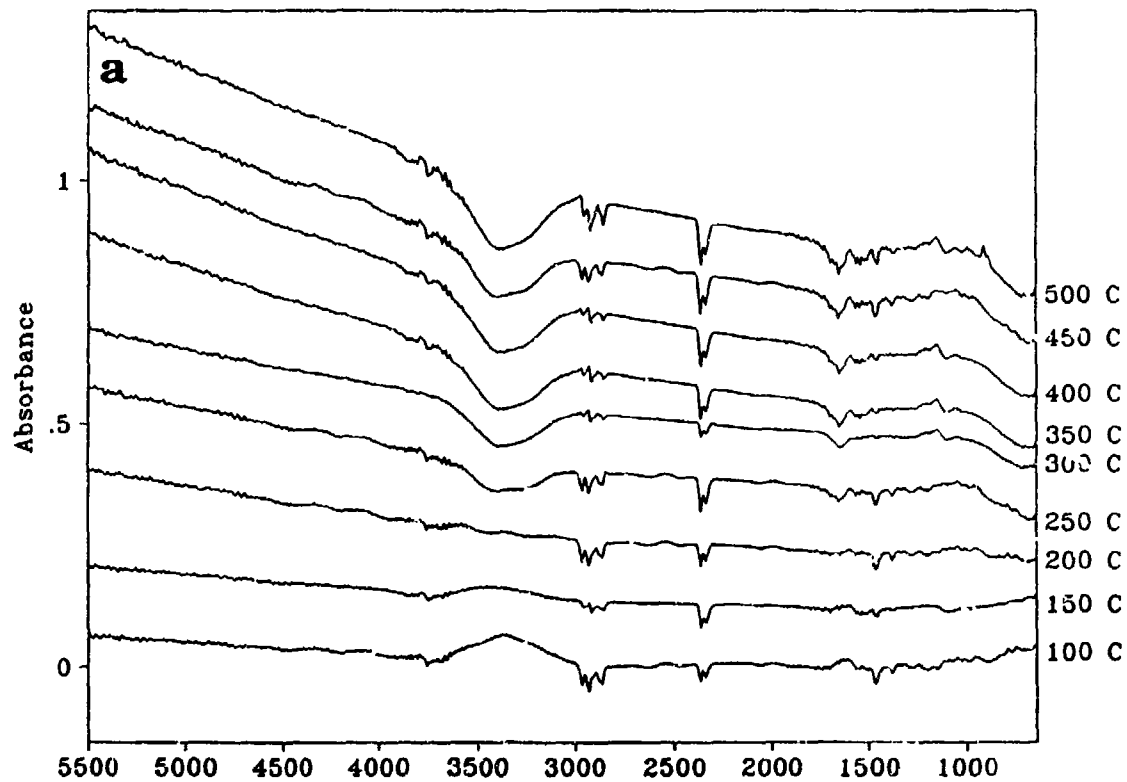
Res= 4 cm⁻¹

Figure B-2. Raw FT-R/ATR Absorbance Spectra from Circle Cell for Sun Fuel Stressed to Various Temperatures. a) Filter On; b) Filter Off.



Res= 4 cm^{-1}

Figure B-3. FT-IR/ATR Subtraction Spectra from Circle Cell for Shell Fuel Stressed to Various Temperatures. a) Filter On; b) Filter Off.



Res= 4 cm⁻¹

Figure B-4. FT-IR/ATR Subtraction Spectra from Circle Cell for Sun Fuel Stressed to Various Temperatures. a) Filter On; b) Filter Off.